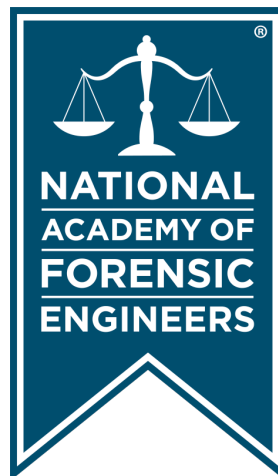


Journal of the  
**National**  
**Academy** OF  
**Forensic**  
**Engineers**<sup>®</sup>



<http://www.nafe.org>

ISSN: 2379-3252

DOI: 10.51501/jotnafe.v42i1

Vol. 42 No. 1 June 2025

# National Academy of Forensic Engineers®

## **Journal Staff**

### **Editor-in-Chief:**

David J. Icove, PhD, PE, DFE

### **Managing Editor:**

Ellen Parson

## **Technical Review Process**

The Technical Review Committee Chair chooses the reviewers for each Journal manuscript from amongst the members and affiliates of the NAFE according to their competence and the subject of the paper, and then arbitrates (as necessary) during the review process. External reviewers may also be utilized when necessary. This confidential process concludes with the acceptance of the finished paper for publication or its rejection/withdrawal. The name(s) of authors are included with their published works. However, unpublished drafts together with the names and comments of reviewers are entirely confidential during the review process and are excised upon publication of the finished paper.

# National Academy of Forensic Engineers®

## Board of Directors

### **President**

Michael Aitken, PE, DFE  
*Senior Member*

### **President-Elect**

Tonja Koob Marking, PhD, PE, DFE  
*Senior Member*

### **Senior Vice President**

Daniel Couture, PEng, DFE  
*Senior Member*

### **Vice President**

Ben Railsback, PE, DFE  
*Fellow*

### **Treasurer**

Bruce Wiers, PE, DFE  
*Senior Member*

### **Secretary**

Shawn Ray, PE, DFE  
*Senior Member*

### **Past Presidents**

Steven Pietropaolo, PE, DFE  
*Senior Member*

Joseph Leane, PE, DFE  
*Fellow*

Samuel Sudler, PE, DFE  
*Senior Member*

### **Directors at Large**

Greg Boso, PE, DFE  
*Member*

Paul Tucker, PE, DFE  
*Senior Member*

---

### **Executive Director**

Amanda Hendley

# Journal of the National Academy of Forensic Engineers®

## Editorial Board

### **Editor-in-Chief**

David J. Icove, PhD, PE, DFE  
*Fellow*

### **Associate Editor**

Paul Stephens, PE, DFE  
*Fellow*

### **Managing Editor**

Ellen Parson  
*Affiliate*

### **Associate Editor**

Michael Stichter, PhD, PE, DFE  
*Senior Member*

### **Senior Associate Editor**

Rebecca Bowman,  
Esq., PE, DFE  
*Member*

### **Associate Editor**

Paul Swanson, PE, DFE  
*Life Member*

### **Associate Editor**

Zohaib Alvi, PE  
*Member*

### **Associate Editor**

Jerry Tindal, PE, DFE  
*Senior Member*

### **Associate Editor**

Robert Peruzzi, PhD, PE, DFE  
*Member*

### **OJS Technical Editor**

Mitchell Maifeld, PE, DFE  
*Member*

### **Associate Editor**

Michael Plick, PE, DFE  
*Fellow*

### **Editor Emeritus**

Bart Kemper, PE, DFE,  
F.ASME, F.NSPE  
*Fellow*

# Submitting Proposed Papers to NAFE for Consideration

Please visit the [Journal's author page](#) for submission details.

We are looking for NAFE members who are interested in giving presentations on technical topics that will further the advancement and understanding of forensic engineering at one of the academy's biannual meetings and then developing those presentations into written manuscripts/papers, which will go through a single-blind peer review process before publication. Only papers presented at a NAFE regular technical seminar and that have received oral critique at the seminar will be accepted for review and publication. We recommend that you review the [About the Journal](#) page for the journal's section policies as well as the [Author Guidelines](#) listed on the Submissions page. Authors need to register with the Journal prior to submitting, or (if already registered) they can simply log in and begin the process. The first step is for potential authors to submit a 150-word maximum abstract for consideration at an upcoming conference into the online journal management system.

## Copies of the Journal

The Journal of the National Academy of Forensic Engineers® contains papers that have been accepted by NAFE. Members and Affiliates receive a PDF download of the Journal as part of their annual dues. All Journal papers may be individually downloaded from the [NAFE website](#). There is no charge to NAFE Members & Affiliates. A limited supply of Volume 33 and earlier hardcopy Journals (black & white) are available. The costs are as follows: \$15.00 for NAFE Members and Affiliates; \$30.00 for members of the NSPE not included in NAFE membership; \$45.00 for all others. Requests should be sent to NAFE Headquarters, 1266 W Paces Ferry Rd NW #141, Atlanta, GA 30327 or call (770) 268-0802.

## Comments by Readers

Comments by readers are invited, and, if deemed appropriate, will be published. Send to: Ellen Parson, Journal Managing Editor, 3780 SW Boulder Dr., Lee's Summit, MO 64082. Comments can also be sent via email to [journal@nafe.org](mailto:journal@nafe.org).

Material published in this Journal, including all interpretations and conclusions contained in papers, articles, and presentations, are those of the specific author or authors and do not necessarily represent the view of the National Academy of Forensic Engineers® (NAFE) or its members.

© 2025 National Academy of Forensic Engineers® (NAFE). ISSN: 2379-3252

# Table of Contents

<b>‡ Forensic Deformation Analysis of a Farm Clevis Using Photographs and Exemplar Tests</b> .....	1
<i>By Michael Stichter, PhD, PE, DFE (NAFE 1162M) and Wade Lanning, PhD</i>	
<b>ø FE Analysis of a Modular Fireplace Fire with an Improperly Constructed Hearth Extension</b> .....	11
<i>By Jerry R. Tindal, PE (NAFE 642S)</i>	
<b>‡ Forensic Analysis of an Elevated Pool Vault</b> .....	33
<i>By Brian C. Eubanks, PE, DFE (NAFE 962S), Garrett T. Ryan, PE, DFE (NAFE 1125M), and Derek T. Patoskie, PE (NAFE 1312A)</i>	
<b>υ Failure of a Climbing Treestand Due to Corrosion and Selective Leaching of Cable’s Galvanic Layer: Failure Analysis and Experimental Study</b> .....	45
<i>By Olin Parker (NAFE 1334A), Jahan Rasty, PhD, PE (NAFE 768S), and Matthew Mills, PE (NAFE 1199A)</i>	
<b>ø Using Ground Penetrating Radar Techniques in Forensic Structural Engineers</b> .....	67
<i>By Chakradhar Gondi, PE (NAFE #1329A), J. Vincent Barnes III, PE, and Michael J. Wightman</i>	
<b>§ Assessing Weather Event Damage in Forensic Engineering: Data Sources and Challenges</b> .....	77
<i>By Chad T. Williams, PE, DFE (NAFE #937M), Doug J. Heady, and Ryan L. Allen</i>	

ø Paper presented at the NAFE seminar held in January 2025 in Santa Fe.

‡ Paper presented at the NAFE seminar held in July 2024 in Ann Arbor.

υ Paper presented at the NAFE seminar held in January 2024 in Daytona Beach.

§ Paper presented at the NAFE seminar held in July 2023 in Kansas City.

# Forensic Deformation Analysis of a Farm Clevis Using Photographs and Exemplar Tests

By Michael Stichter, PhD, PE, DFE (NAFE 1162S) and Wade Lanning, PhD

## Abstract

*Photographic evidence can be a sufficient basis for a forensic failure analysis, especially when characteristic features of the failure mode are readily observed in photographs (e.g., deformation, fracture, etc.). In this case, the failed component (a farm clevis or round pin shackle) was part of equipment used to attempt to recover a vehicle mired in the mud at an above-ground mine site. The shackle failed, and the shackle pin became a projectile that penetrated the cab and injured the driver. The subject clevis was not available for physical inspection or testing. However, the condition of the subject clevis after the accident had been documented in photographs. Application of solid mechanics principles made it possible to determine the sequence of deformation steps that occurred during the failure. Additionally, comparing the deformation behavior documented in photographs of the subject clevis — and to tests of exemplars — allowed a determination of the strength of the subject clevis. Thus, investigators were able to use photographs to determine whether the shackle failed below its working load limit (WLL) or if a citation issued by the Mine Safety and Health Administration for using the subject clevis over its WLL was merited.*

## Keywords

Metal deformation, towing, extraction, heavy equipment, mining, photographs, shackle, clevis, projectile, tow rope, forensic engineering

## Introduction and Background

A piece of heavy equipment (18,000 pounds) became mired in the mud at an above-ground mine. The operator of the mired equipment requested that a bulldozer attempt to recover the mired equipment. The driver of the mired equipment connected the bulldozer to the mired equipment using a braided nylon recovery rope (rated at 130,000 pounds-force) that was connected to the bulldozer and mired equipment by a clevis on each end. Recovery ropes are designed to stretch to reduce the peak impulse when using the extracting vehicle in a jerking action. However, stretching of the rope can also store energy in the rope.

When the bulldozer pulled on the recovery rope in an attempt to recover the mired equipment, the clevis connected to the mired equipment failed and was launched by the elastic energy stored in the stretched tow rope toward the bulldozer. The clevis pin traveled toward the bulldozer cab, penetrated the steel grate on the rear window, penetrated the window, broke the headrest off the operator station, struck the operator with a glancing blow to the back of his head, and then fractured a front side window. The clevis bow also traveled toward the bulldozer, but did not

strike it — and was found on the ground some distance beyond the bulldozer. The recovery rope remained in one piece with no visible damage after use.

The Mine Safety and Health Administration (MSHA) concluded that the accident resulted both from using an under-strength (25,000 pounds-force) clevis and from using the clevis in a side-loaded configuration. The MSHA issued a citation to the mine operator, citing eCFR Title 30 Chapter I Subchapter K Part 56 Subpart M Safety Practices and Operational Procedures:

**§ 56.14205 Machinery, equipment, and tools.**  
*Machinery, equipment, and tools shall not be used beyond the design capacity intended by the manufacturer where such use may create a hazard to persons.*

The contractor and mine operator disputed this citation, claiming that the clevis failed below its rated working load limit and that it was not side-loaded. Additionally, the injured worker initiated a lawsuit against multiple parties, including the manufacturer and vendor of the failed clevis,

alleging that it failed below its rating. This prompted investigation by the involved parties as well as the MSHA.

The MSHA citation had included photographs of the



**Figure 1**

The MSHA citation included photographs of the mired equipment.



**Figure 2**

The MSHA citation included photographs of the hitch where the clevis was connected to the mired equipment (top) and the rope used to attempt to recover the mired equipment (bottom).

mired equipment, bulldozer, tow rope, and clevises (**Figures 1 through 4**). An overview of the scene is shown in **Figure 5**. Damage to the bulldozer is shown in **Figure 6**.

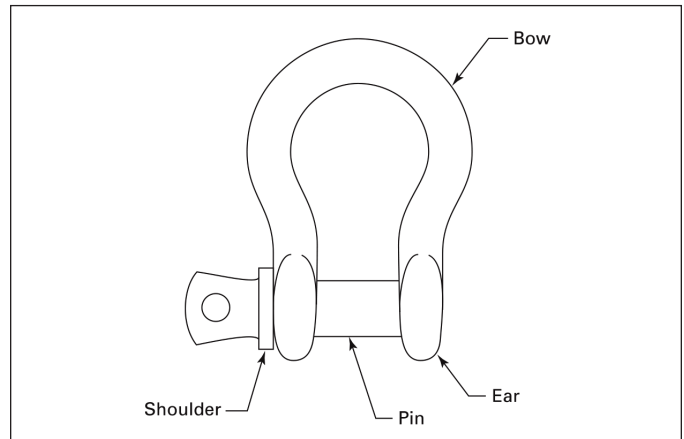


**Figure 3**

Terms for parts of a farm clevis, also known as a round pin shackle.



**Figure 4**

The MSHA citation included a photograph of the clevis and pin that were connected to the mired equipment (left) and the clevis that was connected to the bulldozer (right).



**Figure 5**

Photograph of the accident scene included in the contractor incident report. The mired equipment is mired in the mud on the right, and the CAT D8T bulldozer is positioned on the left of the image with a side-by-side UTV positioned in the foreground between the bulldozer and the mired equipment.

The locations where the clevis bow and clevis pin were found are shown in **Figure 7**. Although the exact distance that the clevis bow traveled is unknown, photographs of where it was recovered showed it embedded in soil that exhibited an impression from the bulldozer track.

Most likely, when the clevis failed and departed from the mired equipment, the clevis bow traveled past the bulldozer, landed on the ground in front of the bulldozer, and was then run over when the bulldozer continued to roll forward — after the operator was incapacitated by the head injury from the clevis pin. The clevis appeared to have sunk into the mud under the track, and did not exhibit any deformation or damage from being run over.

The MSHA responded to the claims that the subject clevis failed beneath its rating by testing similar exemplar

clevises in tension (**Figures 8 through 10**). The MSHA tests used polymer webbing to load the exemplar clevises, attempting to simulate the vehicle recovery operation. The clevises that were tested in-line (no side-loading) or with slight side-loading all withstood 60,000 pounds-force or more. The side-loaded clevises failed at 22,500 pounds-force or less. The failure mode of the subject clevis resembled the failure mode of the exemplars tested in-line, but



**Figure 6**

Photographs of the bulldozer cab included in the contractor incident report showing damage to a steel guard and the rear window (left) and fractured left front cab window (right).



**Figure 7**

Failed clevis found some distance beyond the bulldozer (left) and clevis pin found inside the bulldozer (right) from photographs included in the contractor incident report.



**Figure 8**

Exemplar clevises that were tested in-line (no side-loading).



**Figure 9**

Exemplar clevises that were tested slightly off-axis (slight side-loading).



**Figure 10**

Exemplar clevises that were tested with severe side-loading.

did not resemble the failure mode of exemplars tested in side-loading. Based on these test results, the MSHA maintained its position that the subject clevis was used over its load rating, and withdrew the claim that the subject clevis was side-loaded. **Figure 11** demonstrates the standard terminology for applied loads on a clevis.

**Deformation Failure Analysis of Clevis**

The photographs of both the subject clevis (**Figure 7**) and exemplars tested by the MSHA (**Figure 8** through **Figure 10**) can be evaluated using the principles of deformation mechanics to understand and determine how the clevis deformed and failed during the accident and the forces reached during the failure. Terms for parts of a clevis are defined in **Figure 3**.

The subject clevis was documented with multiple photographs, but the polymer recovery strap was not. Only the photographs were available for examination and analysis, and the clevis was not available for inspection and testing.

However, the photographs documented the deformation and damage to the clevis, which was sufficient to identify the location and orientation of forces and moments applied to the clevis during the failure process.

The failed component was what is referred to as a “farm clevis” or a “round pin anchor shackle” that had a non-threaded pin held in place by only a cotter pin — in this case, an R-clip. This is in contrast to shackles with screw pins or bolts, where the pin is restrained by a threaded connection. Prior studies of bolt-type<sup>1,2</sup> and screw-pin<sup>3,4</sup> shackles involved failure by fracture, by fatigue, and/or embrittlement, including a failure due to a manufacturing defect<sup>1</sup>. The subject farm clevis exhibited extensive deformation, and did not fracture.

Because of the limited ability of the cotter pin to keep the pin in place, farm clevises have less ability to resist side loading and are generally not used for lifting, as noted in ASME B30.26-2015 - Rigging Hardware, which explicitly excludes round pin shackles/farm clevises from its scope for this reason. In this analysis, the authors treated the resistance offered by the cotter pin as negligible relative to the forces required to induce plastic deformation in the bow and pin. All of the clevises discussed in this paper exhibited R-clip cotter pins that were sheared through, but none exhibited plastic damage or deformation around the ears indicative of significant load transfer from contact between the cotter pin and clevis.

For failure analysis of the subject clevis, the team applied balance of forces, balance of moments, and yield criteria: Permanent (i.e., plastic) deformation (shape change) of a metallic part indicates that it experienced a stress exceeding its yield strength, the minimum stress necessary to drive dislocation motion, causing plastic deformation. Therefore, any plastic (permanent) deformation of the clevis must have been the result of an equally balanced action/reaction force pair. The overall loading condition of the shackle was always tension between the attachment points of the tow rope and the mired equipment. The material that deformed must have been located between these attachment points such that it transmitted force from the recovery rope to the mired equipment. The absence of deformation in that portion of the clevis indicates that any load transfer through that material was beneath the yield strength of the material. Since the clevis was loaded in simple tension between the tow rope and mired equipment, the net force on the clevis will always be in tension, though the shape of the clevis (i.e., any offset between the line between the attachment points and the material participating in the load

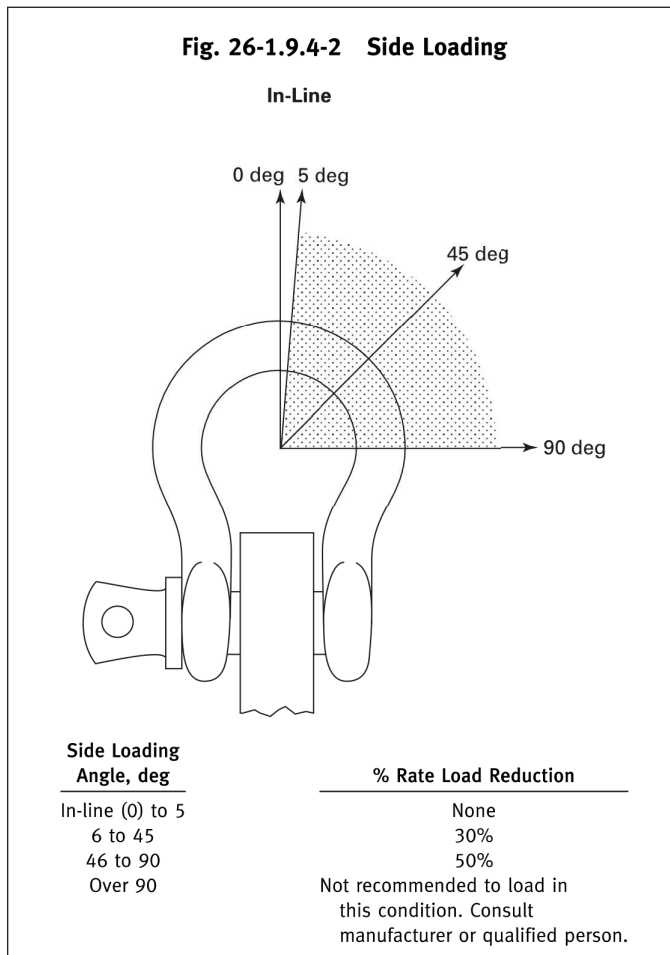


**Figure 11**

ASME B30.26-2015 provides Fig. 26-1.9.4-2, which describes side loading and corresponding WLL reduction.

transfer) can cause localized bending moments and shear stresses in addition to tension.

The side-loaded exemplar clevises — where the clevis ears were oriented transverse (90°) to the applied tensile force as shown in **Figure 11** — are straightforward to interpret. The tensile forces would be parallel or near-parallel to the pin in extreme side loading, which would result in minimal load transfer through the pin, limited to the shear strength of the cotter pin and friction between the pin and clevis ears. The pin in the side-loaded clevises exhibited no deformation because in side-loading, the pin never experienced a bending stress in excess of its yield strength. The bow of the clevis would transmit the majority of the force exerted by the tow rope and mired equipment. Thus, the bow was the part that exhibited deformation in the extreme side-loading case. The lateral offset

between the loading axis and the load-bearing clevis bow would produce a bending moment (**Figure 12**) that would cause the bow to open up when it deformed, which is what the authors observed in testing the exemplar, side-loaded clevises.

The in-line and slightly side-loaded cases, where the clevis ears were oriented longitudinal (at or nearly parallel) to the applied tensile force, followed a more complex series of deformation steps. To understand the deformation sequence, the authors identified locations where deformation was present or not present in the subject farm clevis (**Figure 13**). Notable features included: 1) The pin was bent; 2) The right side of the bow retained much of its original shape, but localized deformation appeared on the inside edge of the hole on that side; and 3) The left side of the bow was significantly deformed, and no deformation appeared in the hole on that side.

The authors anticipated that a clevis loaded in-line would be symmetrical, with load transfer through both sides of the bow and through both ears. However, the condition of the clevis after failure indicated asymmetrical loading, and more extensive deformation of the left side of the clevis.

The photographically documented deformation of the subject shackle provided the forensic team with the necessary information to determine the sequence of events involved in the shackle failure. Before the pin bent, there would be no force to cause the shackle ears to spread and the shackle bow to bend, as observed in the subject clevis.

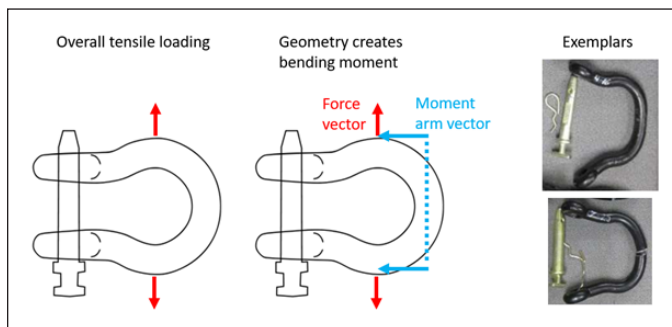


**Figure 12**

In transverse tensile loading, 90° (side loading), the overall loading condition is tensile (left). Because load transfer is primarily through the clevis bow, which is offset from the tensile axis, the bow is in bending (center). Thus, the exemplars tested in side loading exhibited bending of the bow and the ears spread apart (right).

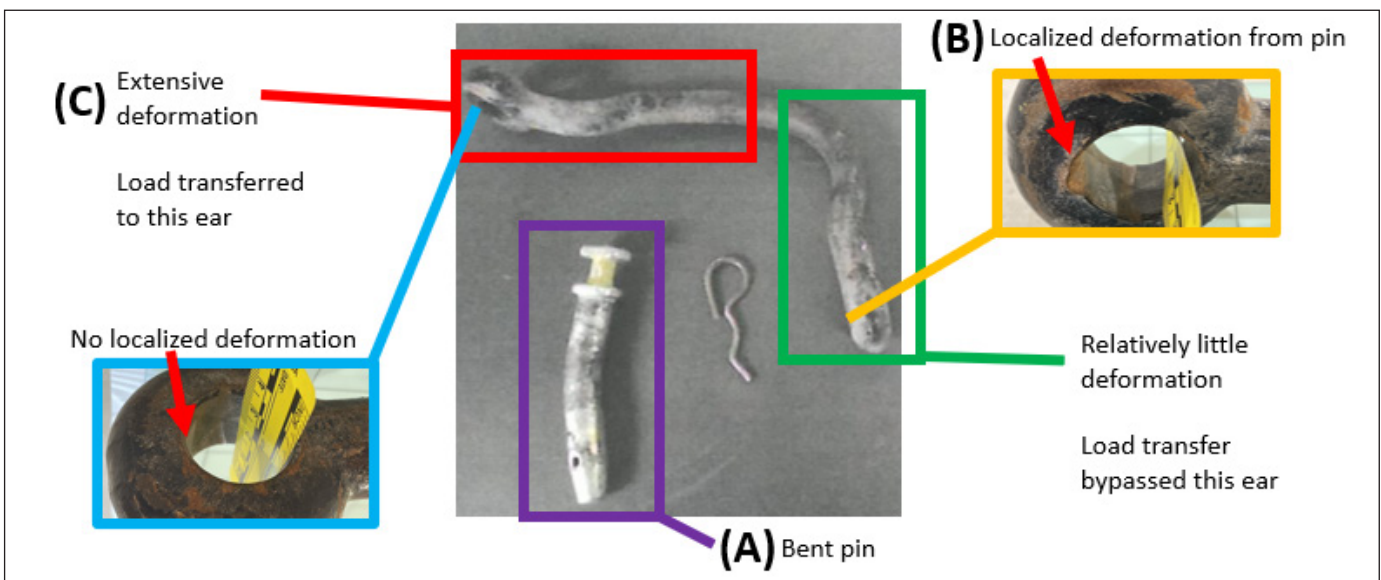


**Figure 13**

Notable areas of deformation or absence of deformation in the subject clevis.

After the pin bent, the angle of the bend would create a lateral force component that would tend to make the ears of the shackle spread apart. The bend in the pin indicated a three-point bending loading condition, which would exist while the pin was in contact with both ears, but would not exist after the pin disengaged from one or both ears. Bending of the pin after it disengaged from one ear would be a cantilever bending condition, with maximum stress in the pin at the base of the cantilever where the pin passed through one ear.

Deformation at that location was not apparent in the available photographs. Therefore, the bend in the pin occurred before the ears began to spread. Bending of the pin was the first step in the failure (Figure 13A). Before the pin bent, force between the pin and the clevis ears would have been parallel to the overall tensile forces. After the pin bent, the angle of the bend would have resulted in a horizontal component of forces between the clevis ears and pin,

and the horizontal component would have caused the clevis ears to spread apart (Figure 14). Bending of the pin would also have exerted a bending moment on the ears, which would also have caused the ears to spread apart.

Once the pin bent, there would be a driving force to make the ears of the shackle move apart. As the ears spread apart, the distance between the points of contact with the pin would increase, which would also increase the length of the moment arms of the pin in three-point bending, further increasing the driving force for bending the pin. Eventually, the ears would spread far enough so that first the cotter pin would shear, then the tip of the pin would slide out of one ear, disengaging the pin from the shackle body.

From photographs, it appeared that shearing of the cotter pin did not induce enough stress on the ear to cause visible deformation. The tip of the pin sliding out of the eye created the contact damage present on the inside of one ear (Figure 13B). Before the pin disengaged, both sides of the clevis bow and both ears would be under load — and, to the extent they deformed, would be symmetrical. After the pin disengaged, only the side of the shackle that retained the pin would be under load, and deformation would no longer be symmetrical (Figure 15).

Once the pin disengaged from one ear of the shackle, that ear would no longer participate in load transfer and would no longer deform (Figure 16). This is why the relatively undeformed side of the shackle was on the same

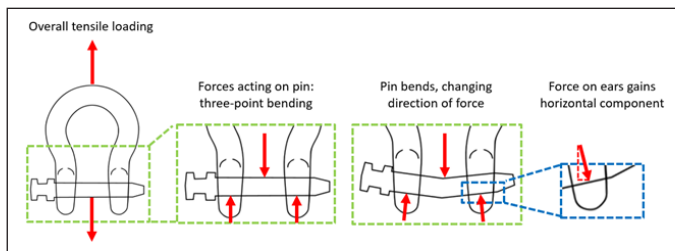


Figure 14

Longitudinal tensile loading on the clevis resulted in three-point bending of the pin. Bending deformation of the pin resulted in a horizontal force spreading the ears of the clevis apart.

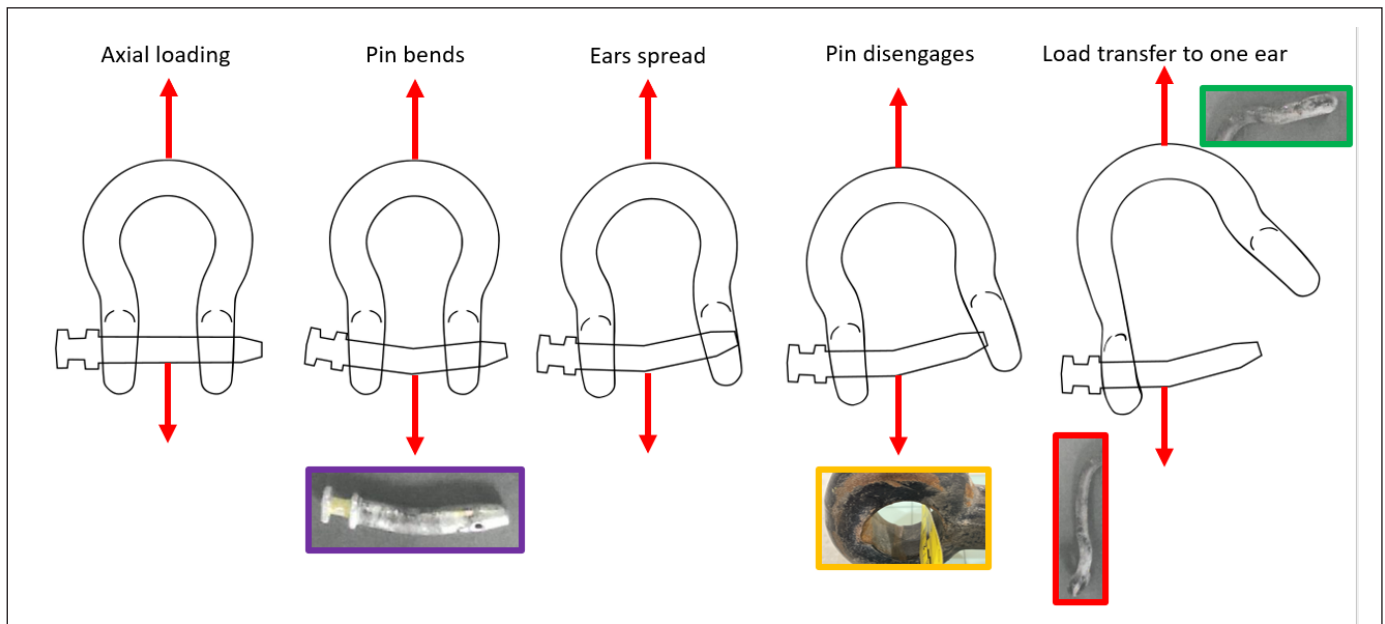
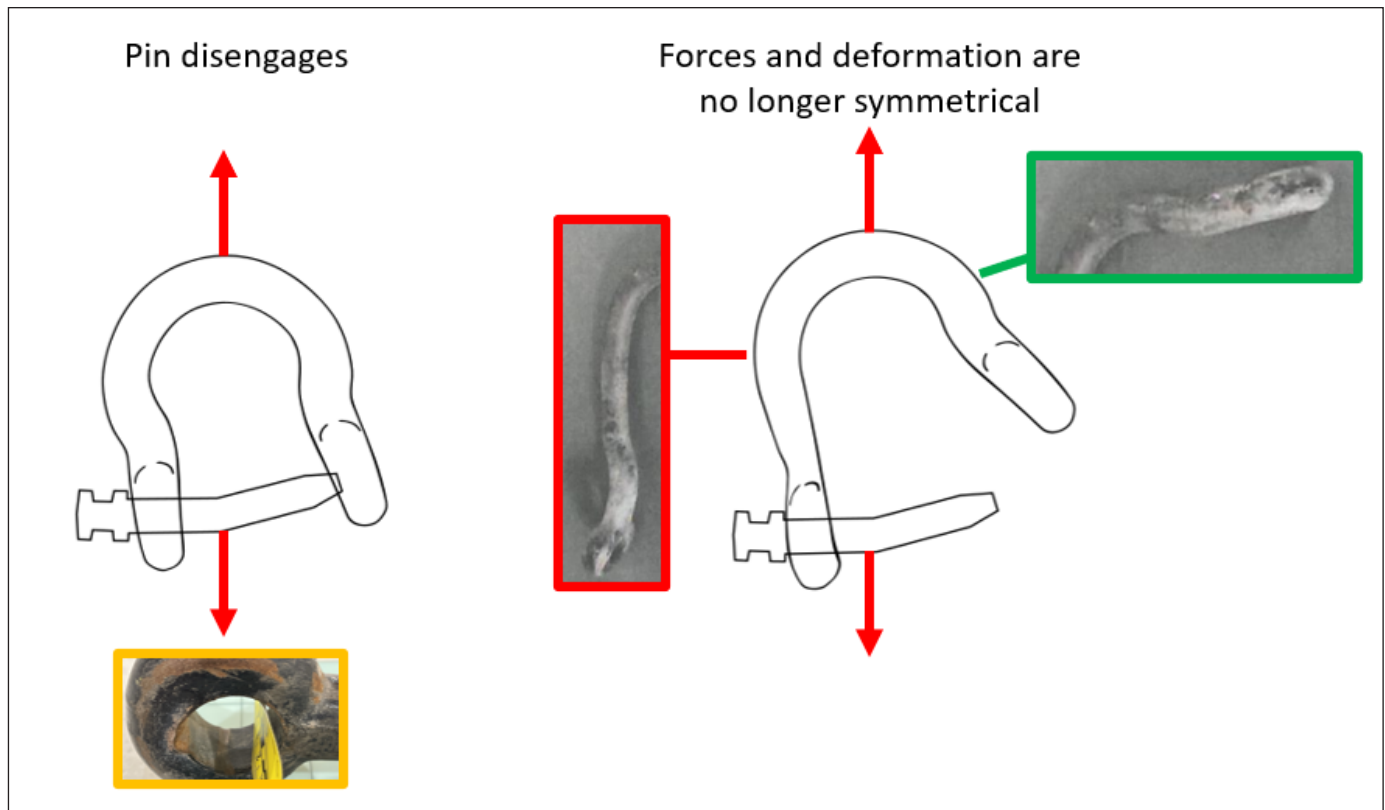


Figure 15

The shackle deformed until the pin disengaged from one ear, creating localized deformation inside the ear.



**Figure 16**

Once the pin disengaged from one ear, deformation would no longer be symmetrical. Thus, the left side of the shackle, which remained connected to the pin, deformed significantly more than the right side, which disengaged from the pin first.

side as the ear with the contact damage — because that ear disconnected from the pin first. All load transfer would be through the other ear, which would continue to deform (**Figure 13C**). Deformation would continue to change the angle of the pin relative to the tensile direction, up until the point where the pin was able to slide out of its connection point to the mired equipment (**Figure 17**). This is why the other leg was more severely deformed, and went from its original curved shape to nearly straight. Deformation of the left side of the shackle bow continued until the shackle slid off of its connection point to the mired vehicle (**Figure 17**).

The MSHA-tested shackles that were in-line or only slightly side-loaded (longitudinal loading) all had bent pins (**Figure 8** and **Figure 9**), and failed at more than twice the shackle's load rating. Bending of the pins indicates a three-point loading condition that existed before the pin disengaged from the clevis ears. Most likely, the maximum force during the test was at the yield point of the pin, which was loaded in three-point bending with relatively short moment arms.

The MSHA test was a quasi-static test with very low strain rate. The strain rate experience by the subject

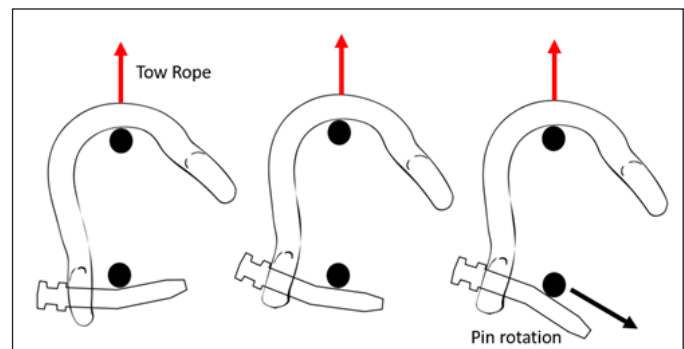


**Figure 17**

Deformation would continue until the angle of the pin allowed it to slide off of its connection point to the mired equipment.

clevis is unknown. However, yield strength and work-hardening of steel generally increase with strain rate<sup>5</sup>, so dynamic loading of the subject clevis, if it had an effect, would tend to increase the failure forces. Since the subject clevis did not fracture, the strain rate effects on impact or fracture toughness did not play a part in the failure. From that point onward, the moment arms would increase (as the ears spread apart), or the amount of material available to transfer load would dramatically decrease (when the pin disengaged from one ear).

The subject clevis also had a bent pin, and the ear that retained the pin was significantly more deformed than the other ear (**Figure 7** and **Figure 13**). Similarities between post-failure conditions of the subject clevis and one of the exemplars (**Figure 18**) indicated that they followed a similar series of deformation steps. Thus, the subject clevis failed by the same sequence of deformation and load transfer as the exemplars — and with similar forces in excess of the clevis' rating. The MSHA was correct to cite the mine operator for using the clevis above its rating.

As a matter of practice when recovering mired equipment, it is generally not advisable to select recovery straps, shackles, etc., based on the weight of the mired equipment or an estimate of the force needed to recover it. The risk of an error in such an estimate is high (consider fluid dynamics, soil properties, unknown buried obstructions, etc.), and risks failure of the tow strap or shackles if the estimate is incorrect. Best practice is to select recovery straps, shackles, etc., based on the towing equipment — in this case, the bulldozer that was attempting to recover the mired vehicle.

The subject bulldozer, like most similar equipment, had instructions to this effect in its manual. The bulldozer's manual recommended choosing recovery straps, shackles, etc., rated for at least 150% the weight of the towing vehicle. The best practice in this case would have been to use the 85,000 pounds-weight of the bulldozer to select a tow strap and shackles rated for at least 127,500 pounds-force. This way, if the force to recover the mired vehicle was higher than expected, the bulldozer would be more likely to spin its treads than break the towing equipment. Using the subject shackle (with its 25,000 pounds-force working load limit) went against the bulldozer manual's instructions and would foreseeably result in overloading and breaking the shackle.

The MSHA was also correct to withdraw its conclusion regarding suspected side-loading of the clevis — or at least severe side-loading (transverse tension). In severe side-loading, the pin would carry little to no load because the applied force would tend to make the ears spread apart, moving parallel to the pin. In this case, most of the load would be borne by the bow of the clevis with a bending moment roughly equal to the radius of the bow.

The authors would expect the side-loaded clevis to be much weaker than in-line loading. Rather than distributing the stress across both ears, only the bow would carry the load. Rather than bending the pin with a very short moment arm, the bow would be bent using a longer moment

arm. Thus, the MSHA's report that the exemplars tested in extreme side-loading (**Figure 10**) failed at a force beneath the clevis' rating was predictable. Since there was no deformation of the pin in severe side loading (but there was deformation of the pin in the subject shackle), the logical finding is that the subject shackle was not severely side-loaded.

The most significant difference between the exemplar and subject clevises (**Figure 18**) was that the exemplars fractured. This fracture may be due to the testing equipment used with the exemplars. The quasi-static test conducted by MSHA involved less dynamic loading, and therefore less likelihood that the clevis could disconnect from the load frame in the manner that the subject clevis disconnected from the mired vehicle. Thus, the MSHA exemplar continued to be loaded until final fracture, while the subject clevis disconnected from the mired vehicle before it could fracture.

Differences among the deformations exhibited by different clevises were most likely due to the distribution of external forces acting upon the clevises. There were two clevises in use at the time of the accident — one connected to the bulldozer and one connected to the mired vehicle (**Figure 4**). Even though the clevises were identical to one another and were subjected to the same total amount of force, the clevis connected to the bulldozer exhibited only slight spreading of its ears; it was significantly less deformed than the clevis connected to the mired vehicle.

The difference in deformation is due to the difference in how those forces were applied. The more extensively deformed clevis was connected with its pin passing through a ring-shaped hitch on the mired vehicle (**Figure 2**), while

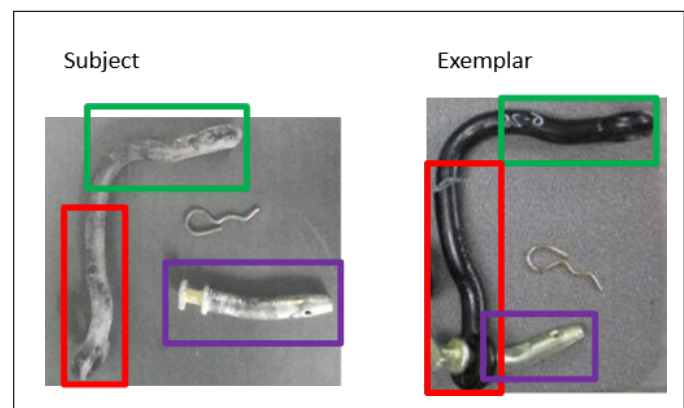


**Figure 18**

Similarities between the subject clevis and exemplar clevis indicate that they followed a similar sequence of deformation steps and that the subject clevis failed at a similar force to the exemplar clevis.

the less deformed clevis was connected with its pin passing through a bracket on the bulldozer. The ring on the mired vehicle (with its round shape) would tend to concentrate stress at the center of the pin, inducing a three-point bending condition. The bracket on the bulldozer would distribute the stress more evenly across its pin. Nevertheless, the presence of some permanent deformation (however slight) on this other clevis indicates that it had also exceeded its elastic limit. The failed clevis was essentially loaded in three-point bending while the clevis connected to the bulldozer was in double-shear loading. Thus, even though both clevises were subjected to the same force, the clevis with a more concentrated force acting on its pin exhibited more extensive deformation and failed first.

### Summary

Analysis of artifacts present in photographs as well as the testing performed by the MSHA was used to determine the failure mode and the applied forces to the clevis that caused it to fail. The locations on the shackle where deformation was present (or not present) provided the evidence necessary to infer the sequence of deformation steps leading up to failure. The photographs also provided enough documentation of the failure mode to rule out a manufacturing defect as a cause of failure. The cause of failure were longitudinal (not side-loaded) tensile forces in excess of the clevis's working load limit and elastic limit.

### Conclusion

Basic principles of solid mechanics, such as balance of forces (Newton's Third Law) and yield criteria, can be used to analyze deformation of a failed component and determine how the failure initiated and evolved. This, combined with testing that replicates similar deformation, can also be used to determine the failure strength of the component.

In this case, investigators determined that a clevis failed by longitudinal tension (in-line or mild side-loading) and that the failure occurred in a sequence of steps: 1) pin bending; 2) clevis ears spreading; 3) pin disengagement from one ear; 4) continued deformation of the other ear; and 5) pin disengagement from the mired vehicle, releasing the clevis such that both the pin and clevis became projectiles moving toward the bulldozer cab. By comparison to exemplars, investigators determined that the failure occurred at a force greater than the working load limit of the clevis.

### References

1. D. P. Couture, "Forensic Engineering Investigation of a High-Voltage Transmission Line Anchor Shackle Failure," *Journal of the National Academy of Forensic Engineers*, vol. 39, no. 1, pp. 35-46, 2022. Online]. Available: <https://doi.org/10.51501/jotnafe.v39i1.65>.
2. S. Lee, I. Jeon, and D.-C. Baek, "Deviation based fault detection method for shackles under variable loading," *Journal of Mechanical Science and Technology*, vol. 32, no. 2, pp. 753-760, 2018. Online]. Available: <https://doi.org/10.1007/s12206-018-0124-2>.
3. S. Weller, P. Thies, T. Gordelier, and L. Johanning, "Reducing Reliability Uncertainties for Marine Renewable Energy," *Journal of Marine Science and Engineering*, vol. 3, pp. 1349-1361, 2015. Online]. Available: <https://doi.org/10.3390/jmse3041349>.
4. R. R. Gaji and M. T. Telsang, "FEA Based Analysis of Shackle For Offshore Application," *International Journal of Mechanical and Industrial Engineering*, vol. 3, no. 3, Article 2, 2014. Online]. Available: <https://doi.org/10.47893/IJ-MIE.2014.1146>.
5. B. L. Boyce, T. B. Crenshaw, and M. F. Dilmore, "The Strain-Rate Sensitivity of High-Strength High-Toughness Steels," Sandia Report, SAND2007-0036, 2007.



# FE Analysis of a Modular Fireplace Fire with an Improperly Constructed Hearth Extension

By Jerry R. Tindal, PE (NAFE 642S)

## Abstract

*A fire originated beneath a modular fireplace hearth in a newly constructed home, which then spread into the adjacent chase and attic spaces, resulting in the destruction of the residence. The fireplace was installed on a CMU block riser positioned on a wooden subfloor in violation of the manufacturer's installation instructions. Scene investigators concluded based on fire patterns and witness observations that the fire originated beneath the fireplace hearth and that the first fuel ignited was wood construction in proximity to the hearth. The author was contacted 3.5 years after the fire during ongoing litigation to review and analyze the available information and determine the cause of the fire. This paper examines the cause of the fire based on forensic engineering analysis and testing. Incorporation of analysis of previous similar cases and testing data as well as new testing data are utilized to reinforce the author's cause determination.*

## Keywords

Modular fireplace, hearth extension, wood burning, chimney, low-temperature ignition, smoldering, clearances, fire investigation, methodology, reconstruction, testing, chase, combustible concealed space, conduction, convection, radiant, heat transfer, NFPA 921, NFPA 211, UL 127, International Residential Code, forensic engineering

## Background

The home in question was a newly constructed (less than 7 months old) two-story wood-framed structure of approximately 8,000 square feet containing two modular fireplaces. Identical in make and model, the fireplaces were installed on the first floor back-to-back to one another, utilizing a common fireplace and chimney chase enclosure. One of the fireplaces faced into the living room (living room fireplace); the second faced into a covered screened-in porch (porch fireplace). The chase enclosure was wood-framed, wood-sheathed with oriented strand board (OSB), and bisected the south exterior wall of the home. The OSB was covered with metal lathe, a mortar base (scratch) coating, and finally a stone veneer set in mortar. The chase formed a combustible vertical concealed space on the interior side that was sealed on the exterior (living room) side with masonry (mortar and stone veneer).

Sometime around 5 p.m. the evening prior to the incident, the homeowners built a fire in the living room fireplace and maintained an active fire (fuel continuously being added to and flaming) up until between 10 and 10:30 pm. When they retired to bed between 11 and 11:30 p.m.,

the fire had burned down to hot and simmering coals with no visible flames. The porch fireplace had not been used the evening prior to the incident. Monitored smoke alarms alerted the homeowners and the fire department to the house fire around 5:55 a.m. (6.5 to 7.0 hours after they went to bed). The homeowners opened their closed bedroom door and observed smoke inside the living room but no flames. They exited the home and observed flames at the junction between the roof and stone veneered chase. After verifying the fire department had been notified, they made multiple trips back into the home to save family photographs/property and never observed any flames inside the home. As they stood outside during firefighter operations, they observed the chase collapse into the structure as the compromised wood floor beneath gave way. No other sections of the home collapsed. As a result of the fire and structural damage, the home ultimately had to be demolished.

The living room fireplace was installed on top of a nominally 8-inch concrete masonry unit (CMU) block riser that was built on and supported by a wood-framed and decked floor. The installation method violated the

manufacturer's installation instructions related to installing the fireplace on wooden floors and will be discussed in further detail later. Based on an examination of the scene, fire patterns, and subsequent chase collapse due to a compromised supporting floor (as observed by witnesses), scene investigators for the property insurer concluded that the area of fire origin was beneath the hearth of the fireplace. The investigators further concluded that the first fuel ignited was wood construction in proximity to the hearth.

Based on the thickness of the masonry riser materials provided, defendant parties were skeptical that sufficient heat would be transferred from the hearth through the baseplate and riser to ignite the wooden floor. After unsuccessful mediation attempts, the personal attorneys representing the homeowner assigned the author to review and analyze the available information and determine the cause of the fire.

**Figures 1 and 2** depict views of the home and chase area on the south side of the home prior to and after the fire. **Figures 3 and 4** depict the living room and porch fireplaces prior to the fire.

### Forensic Engineering Investigation and Findings

Based on a review of the initial discovery documents provided and the author's previous experience, the author concluded that it was unlikely that sufficient heat transfer occurred through the combined hearth, base plate of the fireplace, and CMU riser to ignite the wood floor. As

discussed below, given the history and actual use conditions of the fireplace in combination with the hearth, base plate, and riser construction, it was unlikely sufficient heat would be transferred to ignite the floor — albeit such configuration still created a substantial fire hazard.

The homeowners (an older couple with no children living in the home) had moved into their new home in early spring and did not begin using the fireplaces until the first week in October. The incident fire that destroyed



**Figure 2**

A view of the south side of the home after the fire with the remains of the stone veneered chimney and fireplace chase. The fire department utilized a track hoe during overhaul operations, making reconstruction more difficult.



**Figure 1**

A view of the south side of the home prior to the fire with the stone veneered chimney and fireplace chase bisecting the wall between the living room and covered porch. The first observed flames were at the juncture of the roof and chimney chase (circled in yellow but on the opposing side).



**Figure 3**

A view of the finished living room fireplace and stone veneered chase enclosure prior to the fire.



**Figure 4**  
A view of the porch fireplace and stone veneered chase enclosure prior to the fire.

the home occurred in the first week of December, providing a use period of approximately eight weeks. The homeowners testified that the living room fireplace had been used approximately five to 10 times — each time for a period of 5 to 6 hours (including the evening before the incident). The porch fireplace had also been used five to 10 times, although each time for a period of only 2 to 3 hours. Therefore, the fireplaces had each been used only once or twice a week for relatively short periods of time during each use.

### Historical Testing and Results — Prior Cases #1 and #2

Approximately nine years prior to the author's involvement with the subject case, he constructed, instrumented, and tested a similar modular fireplace for another case (Prior Case #1). The fireplace was installed on an open back CMU riser with a hollow center. During that testing, the author thermocouple instrumented the interior top surface (floor) of the hearth as well as the exterior (bottom) surface of the base plate directly beneath the

hearth thermocouple. These thermocouples were placed simply for the benefit of collecting the empirical data (for potential future use) and were unrelated to any question involved in the case. Testing with active burn times of 5 to 6 hours (substantially like the subject case of this paper) was performed. **Figure 5** depicts some of the data collected from the testing. While the temperature of the hearth surface interior reached and exceeded 1,100°F for an extended period, the exterior surface of the base plate directly beneath only reached approximately 276°F after 5 hours and 45 minutes. The temperature of the exterior surface of the base plate continued to very slowly climb when the testing was terminated.

The exterior surface of the base plate was open to the air and therefore subject to natural convective cooling as it was installed on an open back hollow CMU riser. The insulating effect of a wooden floor against the bottom of the base plate was not evaluated. However, in yet another separate case (Prior Case #2) several years later involving a similar modular fireplace installed directly on a wooden floor with no CMU riser, the author contracted with a Fire Dynamics Simulator (FDS) modeler and professional fire protection engineer to construct a model and evaluate the heat transfer effect of the previously tested fireplace being installed on a wooden floor. The modeler utilized the empirical hearth interior surface temperature data obtained in the actual testing and used FDS to model the conduction heat transfer through the hearth refractory and base plate into the contacting wood flooring. **Figure 6** depicts the results of the modeling, which indicates a maximum temperature at the interface of the base plate and wood floor of approximately 300°F after approximately 5 hours and 45 minutes.

### Past to Current Case Fireplace Construction Differences

A more substantial difference existed between the subject fireplace in this paper and the tested fireplace (Prior Case #1) and modeled fireplace (Prior Case #2). The tested and modeled fireplaces had a combined hearth refractory and base plate thickness of only approximately 5¼ inches. The combined hearth refractory, base plate, and solid-filled CMU riser thickness for the subject fireplace was much greater (at approximately 14¼ inches). An additional 9 inches of masonry was between the hearth surface and the wood floor — and would provide an increase in the overall thermal resistance to heat transfer. Therefore, it would produce even lower temperatures than the modeled 300°F (Case #2) obtained in the absence of the riser over the same period of burn time.

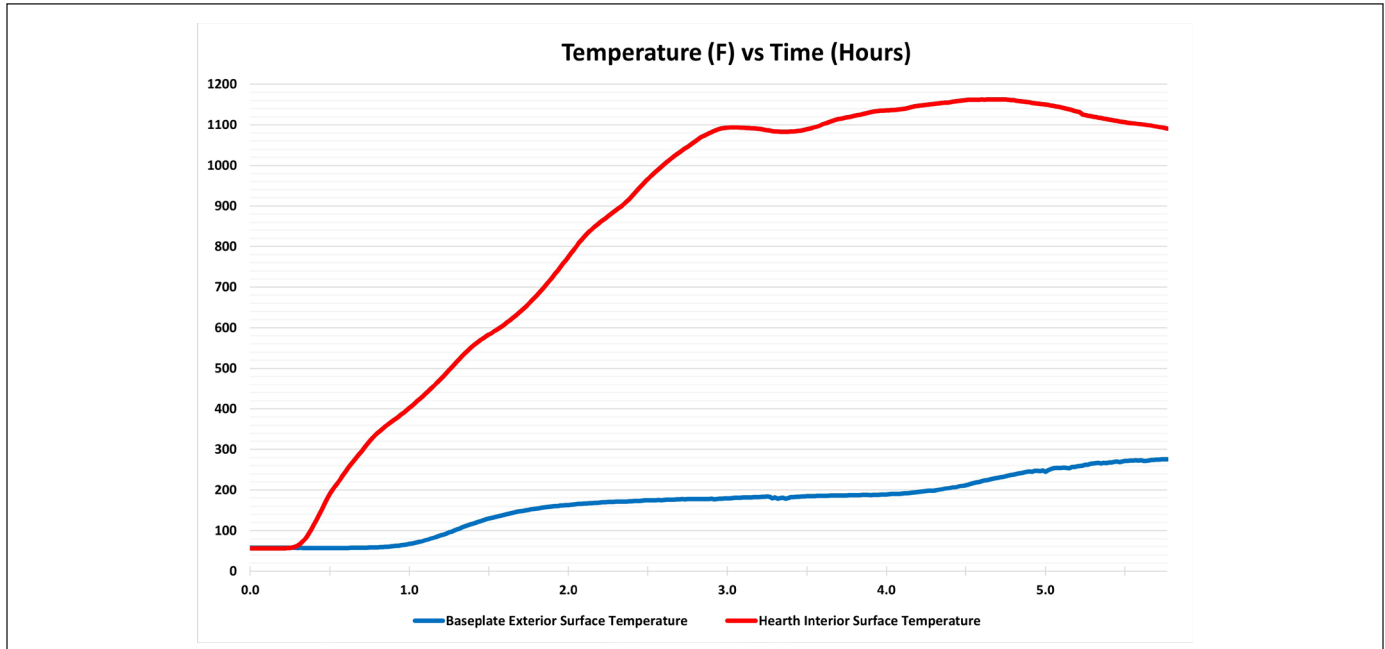


Figure 5

Prior Case#1 temperature results for the hearth interior surface temperature and the base plate exterior surface temperature for a burn test of approximately 5 hours and 45 minutes. Combined hearth refractory and base plate thickness of 5¼ inches. The exterior surface of the base plate was open to ambient air of 77°F average temperature. The exterior base plate surface temperature reached approximately 276°F after 5 hours and 45 minutes.

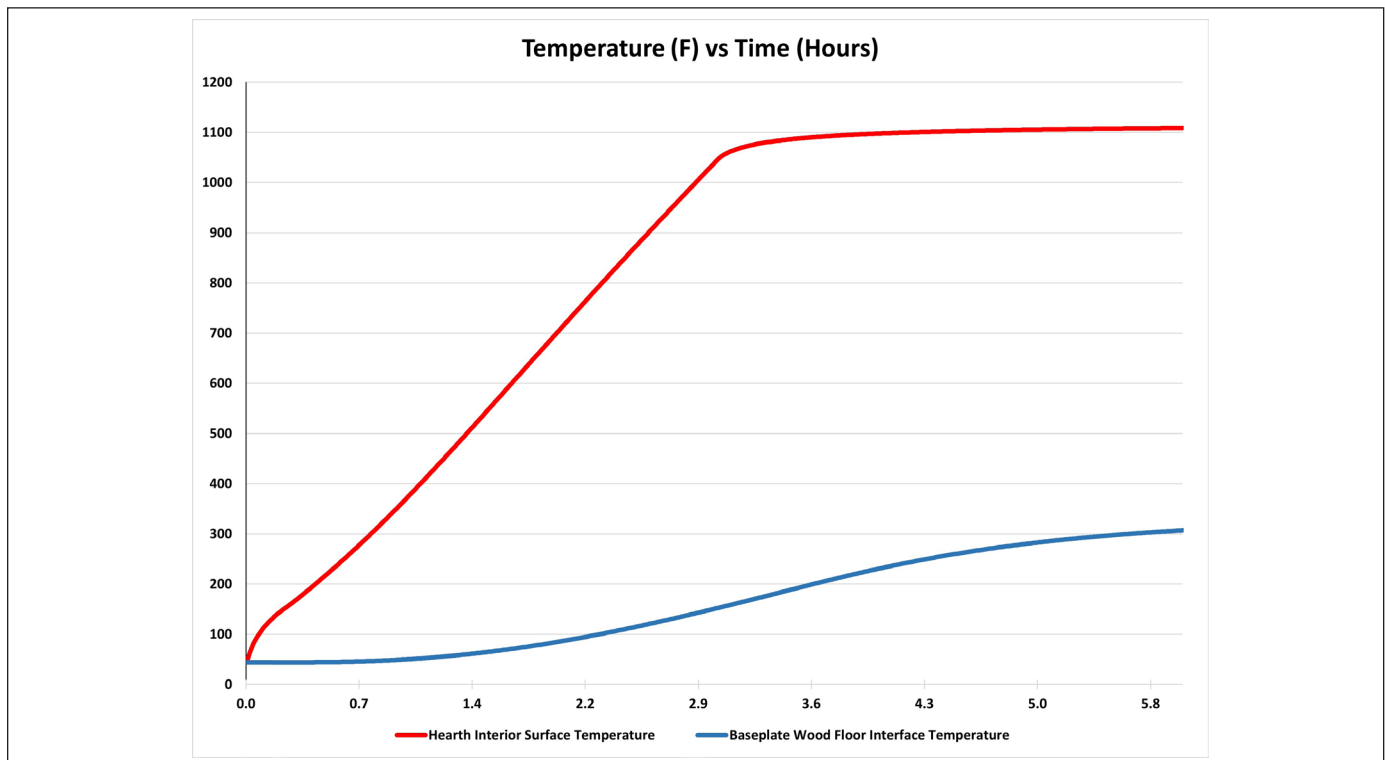


Figure 6

Prior Case #2 FDS modeled temperature results for the hearth interior surface temperature and the base plate exterior surface wood floor surface interface temperature for a burn test of approximately 5 hours and 45 minutes. A combined hearth refractory and base plate thickness of 5¼ inches. Models the exterior of fireplace and base plate sitting on a wood floor surface. The exterior base plate and wood floor interface temperature reached approximately 300°F after 5 hours and 45 minutes.

### Historical Testing and Results — Prior Case #3

Additional testing data was reviewed and considered for yet another prior case involving a similar modular fireplace that the author constructed, instrumented, and tested<sup>1</sup>. While no thermocouples were installed beneath the base plate, the rear wall exterior surface of the firebox where interfaced with contacting wood studs was instrumented. The rear wall of the firebox varied in combined refractory and modular block thickness ranging from 7¼ inch at the hearth surface level up to 11¼ inch (still 3 inches less than 14¼ inches) at the top of the firebox. Although the case only involved active burn testing of 3 to 4 hours, after the case concluded, the author performed active burn tests for approximately 12 hours for the benefit of data collection (again for potential future use). Temperatures at the 7¼-inch thickness at the hearth level and 11¼-inch thickness at the top of the firebox reached approximately 205°F and 182°F, respectively, after approximately 5 hours and 45 minutes. The temperature differences illustrate the reduction in temperatures achieved due to increased masonry thicknesses. It should be noted that the blocks utilized in

the modular fireplace construction are proprietary blends of lightweight masonry containing air voids and volcanic pumice aggregate; therefore, they would have a lower thermal conductivity than the dense concrete blocks and (Type S) mortar fill that was used to construct the riser<sup>2-8</sup>. Nevertheless, there will be a substantial reduction in the heat transfer rate — and subsequently the wood floor temperature — due to the overall increase in masonry thickness (i.e., 5¼ inches versus to 14¼ inches).

Again, it should also be reiterated that as fuel continues to be added to the fireplace for extended burn times, the temperatures in the masonry will continue to rise, creating an imminent fire hazard to wood materials in contact or close proximity to the masonry riser surfaces. **Figure 7** depicts some data collected from the testing for a period of up to approximately 7 hours.

### Initial Conclusions

Temperature ranges exceeding 170°F, the safe temperature limit of Underwriter's Laboratories (UL)<sup>9,10</sup>,

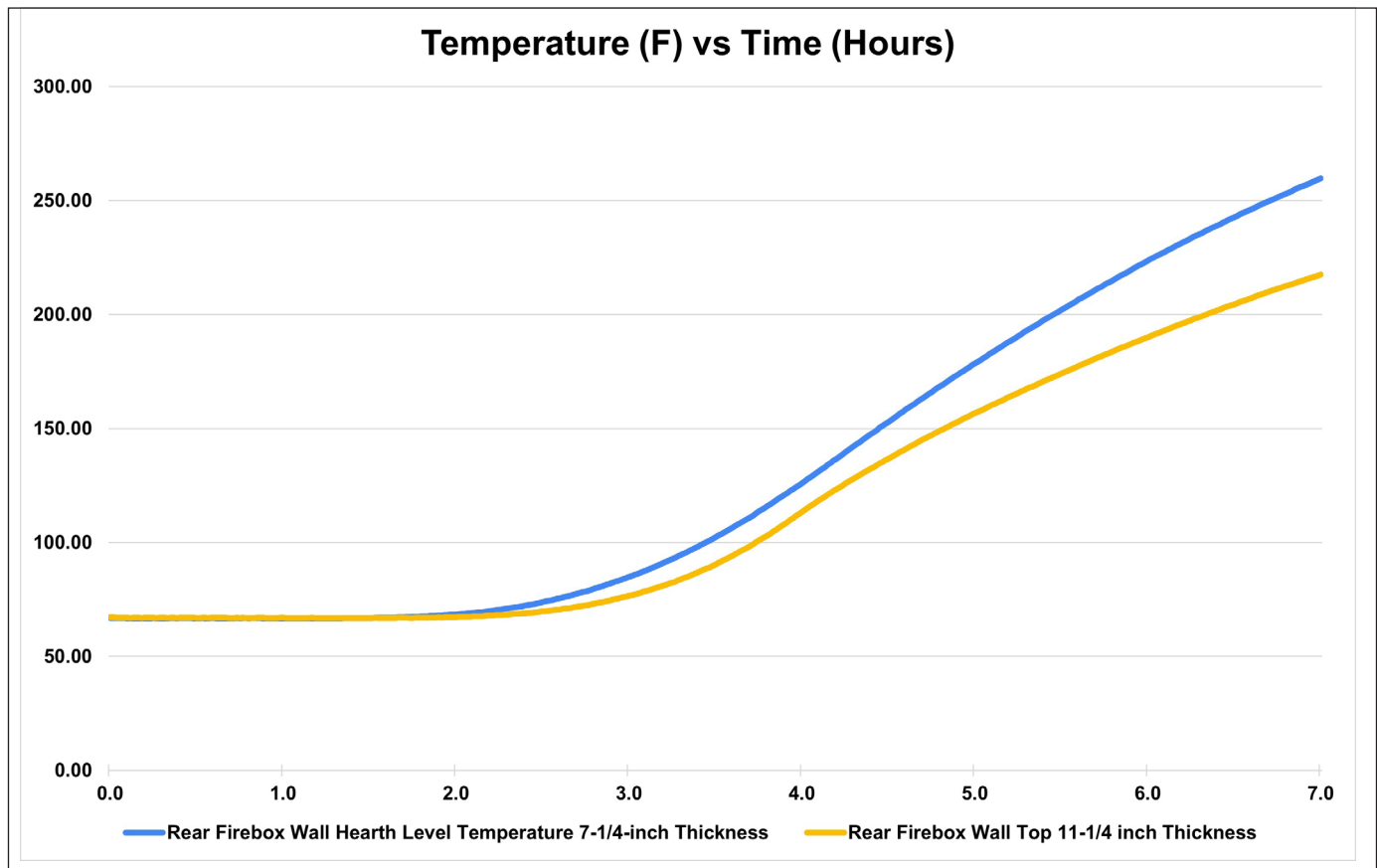


**Figure 7**

Prior Case #3 temperature results for the rear firebox wall and wood stud interface after approximately 7 hours of active burn testing. Note temperatures continue to climb as the fire is fed and the active burn time continues. Temperatures at the 7¼-inch thickness at the heart level and 11¼-inch thickness at the top of the firebox at the interfaces with the contacting wood studs reached approximately 205°F and 182°F, respectively after approximately 5 hours and 45 minutes.

represent a substantial fire hazard<sup>11</sup>; however, over a generally longer exposure time<sup>9,11,12</sup> than experienced in the subject case of five to 10 total burns at 5 to 6 hours each and temperatures considerably less than 300°F.

For the limited use history of the subject fireplace of this paper — and for the relatively short periods of time of each use — it was concluded there was insufficient heat transfer to ignite the wooden floor beneath the masonry riser. However, it should be noted that either a prolonged use (months or years of “short” burns) or extended use times (periods of longer burning) do represent a fire hazard as stated. This is further clarified by the fact that temperatures continue to climb in the masonry — and at the exterior surfaces of the masonry — as active burn times within the firebox continue. A fireplace should be able to operate continuously without the concern of igniting wood construction around the fireplace or chimney.

### **Additional Analysis — Construction Progress Photographs**

After presenting these conclusions to the homeowner’s attorneys, the author requested if any additional discovery, particularly pre-fire construction photographs, were available. Hundreds of pre-fire photographs were then provided to include daily construction progress photographs. After analyzing the photographs, multiple violations of the manufacturer’s installation instructions and the (applicable) 2015 edition of the International Residential Code (IRC) clearances to combustibles and hearth extension construction requirements were discovered and evaluated for both the living room and the porch fireplaces. Discussion will be primarily (though not exclusively) limited to the living room fireplace because the porch fireplace was not in use at the time — and not the cause of the incident fire. However, the installation issues of the same model fireplace on the porch reflected a consistency in the lack of understanding of the proper installation requirements and a lack of an appreciation for the imminent fire hazards created by both. Therefore, some references will also be made to the porch fireplace installation and hearth extension construction.

IRC<sup>13</sup> Chapter 10 Sections *R1004 Factory-Built Fireplaces* and *R1005 Factory-Built Chimneys* provide that:

***R1004.1 General.*** *Factory-built fireplaces shall be listed and labeled and shall be installed in accordance with the conditions of the listing. Factory-built fireplaces shall be tested in accordance with UL 127.*

***R1005.1 Listing.*** *Factory-built chimneys shall be*

*listed and labeled and shall be installed and terminated in accordance with the manufacturer’s instructions.*

Prefabricated fireplaces and chimneys are required to be installed in accordance with the manufacturer’s installation instructions. Subsequently, a violation of the manufacturer’s installation instructions violates the building code. The manufacturer’s installation instructions are an integral part of the fireplace listing and are used as a reference during examination and testing of factory-built fireplaces by testing laboratories<sup>10,14</sup>. Fireplace and chimney systems are assembled and constructed by testing laboratories using the manufacturer’s installation instructions, including the manufacturer’s specified minimum clearances to combustibles. The test assemblies are instrumented with thermocouples to verify maximum safe temperatures are not exceeded during operational testing.

Prefabricated masonry modular fireplaces that do not have factory-built and tested hearth extensions are required to comply with IRC Chapter 10 Section R1001.9, which provides [underlined emphasis added]:

***R1001.9 Hearth and hearth extension.*** *Masonry fireplace hearths and hearth extensions shall be constructed of concrete or masonry, supported by noncombustible materials, and reinforced to carry their own weight and all imposed loads. Combustible material shall not remain against the underside of hearths and hearth extensions after construction.*

The building code commentaries associated with hearth and hearth extensions provide additional insight:

*The hearth includes both the floor of the firebox and the projection in front of it<sup>15</sup>.*

*Combustible forms and centers could ignite from exposure to heat from the adjacent fire place....these and other similar concealed, combustible components must be removed<sup>16</sup>.*

**Figure 8** is an annotated excerpt of IRC Figure R1001.1 that illustrates the proper construction of hearth and hearth extensions for masonry fireplaces. There should be no combustible materials, including wood framing or sheathing, within or beneath the hearth or hearth extension.

Industry standard NFPA 211, *Standard for Chimneys, Fireplaces, Vents, and Solid Fuel-Burning Appliances*, 2019 Chapter 11 Fireplaces<sup>17</sup>, reflects similar provisions:

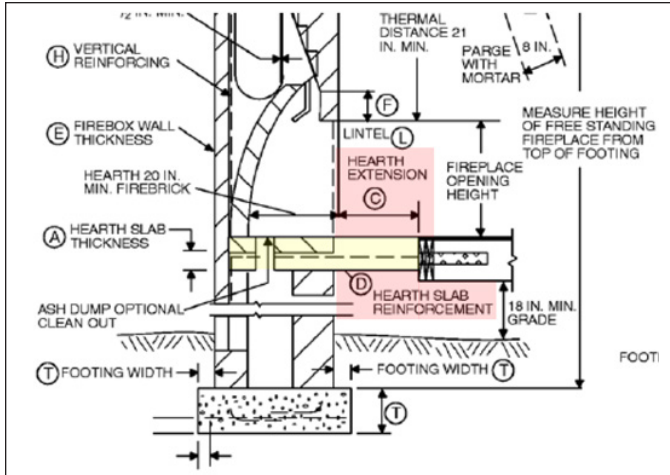


**Figure 8**

Annotated excerpt of IRC Figure R1001.1, illustrating the proper construction of hearth and hearth extensions for masonry fireplaces.

*11.1 Factory-built fireplaces shall be listed and installed in accordance with the terms of the listing.*

*11.2 Hearth extensions shall be provided in accordance with the manufacturer's instructions or be of masonry or noncombustible construction in accordance with Section 11.3.*

**11.3 Hearth Extensions**

*11.3.1 Masonry fireplaces shall have hearth extensions of brick, concrete, stone, tile, or other approved noncombustible material wholly supported by and integral with the chimney structure, and a minimum 4 in. (102 mm) clearance shall be maintained directly below the underside.*

*11.3.1.1 Support for the hearth shall be provided by a structural slab or corbeled brickwork.*

*11.3.1.2 Wooden forms used during the construction of the hearth and hearth extension shall be removed when the construction is completed.*

Finally, the provisions of the IRC and NFPA 211 regarding hearth and hearth extensions are also provided and illustrated in the manufacturer's installation instructions and will be referenced. **Figures 9 and 10** depict annotated pre-fire construction photographs of the living room fireplace prior to the enclosure and finishing of the chase.

The manufacturer's installation instructions provide for only one listed and tested system for the installation of the fireplace on a combustible floor that was not implemented



**Figure 9**

A view of the living room fireplace prior to chase enclosure. Notes: 1) wood floor; 2) CMU riser; 3) base plate; and 4) hearth refractory brick.



**Figure 10**

Another view of the living room fireplace with fiberglass batt insulation prior to chase enclosure. Notes: 1) wood floor; 2) CMU riser; 3) base plate; 4) hearth refractory brick; 5) radius throat front (RTF) block component; and 6) insulated air clearance spaces around the firebox (in blue font).

As a result, the installation violated the manufacturer’s installation instructions and subsequently the building code. The fireplace was installed on an unlisted, untested, and unapproved solid-filled CMU riser supported by a wooden floor that was previously discussed in this paper.

The fireplace further incorporated a masonry block chimney system as opposed to a lightweight listed metal chimney system for installations to be performed on wooden floors. The fireplace, hearth extension, and chimney system were required by the installation instructions and code to be installed on a concrete slab supported by a CMU riser footing with no combustible materials within or beneath. **Figure 11** depicts an annotated excerpt from the manufacturer’s installation instructions for installation of the fireplace where a crawl space with a combustible floor is involved (as in the subject case).

The installation manual further provides in reference to the concrete slab and drawing and in concert with the IRC and NFPA 211 that:

*The fireplace must sit on a concrete pad or slab... This pad or slab should provide for the noncombustible hearth extension substrate needed to support the code required noncombustible hearth extension finish materials.*

*Concrete Pad Supported by Masonry (CMU) Tower (Figure 4.2): Typically used when the fireplace is placed over a ... crawl space. The noncombustible pad is best made from a 6” thick concrete slab with #4 rebar... poured on top of corrugated metal. Concrete pad must be supported by a full masonry tower with no combustible underpinnings...*

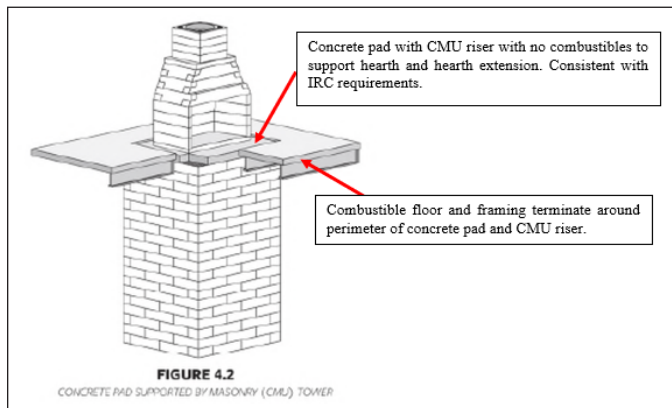


**Figure 11**

Concrete pad and foundation support structure drawing excerpted from the manufacturer’s installation instructions where the fireplace is to be installed in a home with a combustible floor and with a crawl space.

**Figure 12** incorporates side by side comparative photographs taken from nearly the same perspective and angle of the fireplace and chase enclosure with the OSB and then after/during the installation of the hearth extension, mortar and stone veneer. **Figure 13** is **Figure 12** again but with annotations to illustrate some of the features discussed.

The A and B lines approximately define the rectangular firebox opening and illustrate the very close proximity of the OSB to the opening edges. A/B (and other) ratios within the two photographs are equivalent. The light green dash-dot line across the windowsills provides a frame of reference to the top of the firebox. The Radius Throat Front (RTF) block (previously referenced in **Figure 10**) of the firebox begins at the top edge of the firebox opening and runs vertically up  $9\frac{3}{16}$  inches toward the green dash-dot line. As seen in **Figure 10** and again in **Figure 14**, the RTF block forms a trapezoid shape (front face) with interlocking side blocks. The RTF block is clearly covered by the OSB depicted in **Figure 13**. OSB also extends over to the sides of the firebox near the opening edge. The area near the top of the hearth, extending down to the floor and running across the width of the firebox, is clearly



**Figure 12**

Photographs from near the same perspective/viewpoint and angle of the chase with OSB and then with the stone veneer and hearth extension in place. The stone finish in the right-side image defines the top edge of the firebox opening, which is consistent with the top edge of the OSB above the firebox opening in the left-side image.



**Figure 13**

Annotations added to the photographs of Figure 12.

covered by OSB in the left-side image and then the masonry hearth extension in the right-side image.

The construction superintendent, who was present daily and took all photographs during the building of the home, had already been deposed; however, he was not questioned relative to the photographs contained in **Figure 12**. Furthermore, no subcontractors had been questioned relative to the photographs (they had simply been overlooked in the several years of discovery). Therefore, the author requested if testimony could be obtained from the superintendent regarding his observations of the placement of OSB around the opening of the firebox. As a result, affidavit testimony was obtained, and the supervisor testified that the OSB was installed no more than 1.5 inches from the opening edges of the firebox.

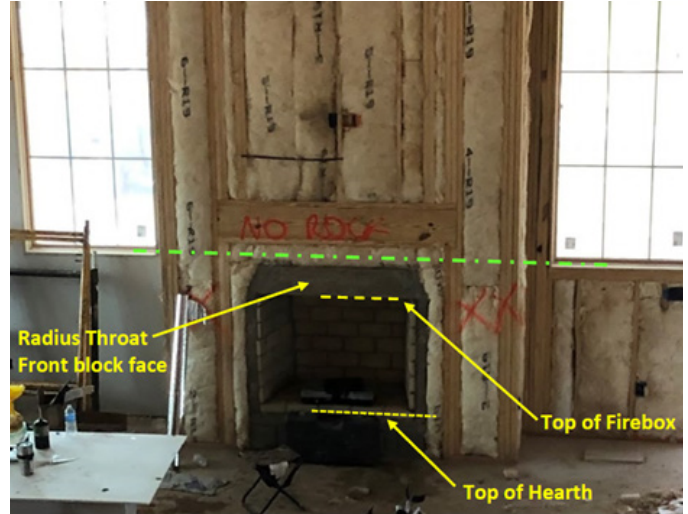


**Figure 14**  
An annotated photograph of the living room fireplace prior to OSB and stone veneer enclosure.

**Figure 15** is an excerpt from installation instructions

This fireplace is designed to be installed so a 3” ledge is left on top of the radius throat front. This ledge allows space for a framing header to maintain the required 1” clearance and at the same time align flush with the room face of the firebox.

**▲ WARNING**

Failure to maintain stated minimum clearance to combustibles on page 12 may result in a fire or explosion, causing property damage, personal injury, or loss of life.

**3-inch recessed ledge designed into the firebox for purposes of maintaining clearances to combustibles**

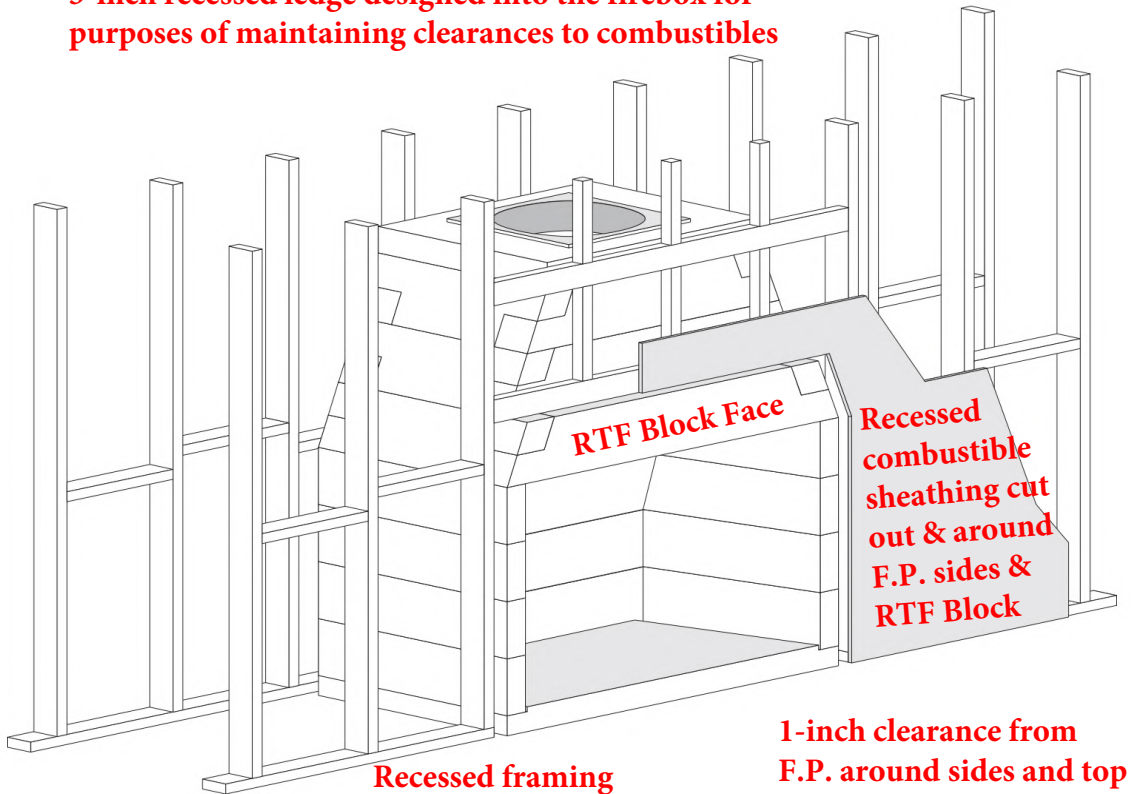


**Figure 15**  
An excerpted and annotated view of an isometric drawing and the instructions above the drawing from the manufacturer’s installation instructions.

illustrating and describing the fireplace design for framing and combustible sheathing installation around the firebox for the purposes of maintaining required clearances to combustibles. The fireplace is designed with a 3-inch ledge over the top of the RTF block to allow framing and combustible sheathing to be recessed and brought flush with the front vertical face of the firebox. For the case in question, OSB was installed across the face of the RTF block as well as the faces of the sides of the firebox and base plate. The OSB further projected beyond the vertical face of the firebox opening, creating a “trim” around the opening. **Figure 16** is another excerpted and annotated drawing from the manufacturer’s installation instructions that depicts the proper construction around the firebox above the opening to maintain clearances to combustibles.

The OSB should not be in contact with any portion of the face of the RTF block (in this case, the OSB covers approximately 8 vertical inches of the face and runs across the entire width of the block). Instead, the OSB should be above the top of the RTF block with a minimum of 1-inch vertical clearance. Furthermore, the OSB should not project beyond the vertical face of the RTF block, as such projection creates a combustible trim above the face opening of the firebox. Based on the manufacturer’s installation instructions, such trim projection would require a minimum

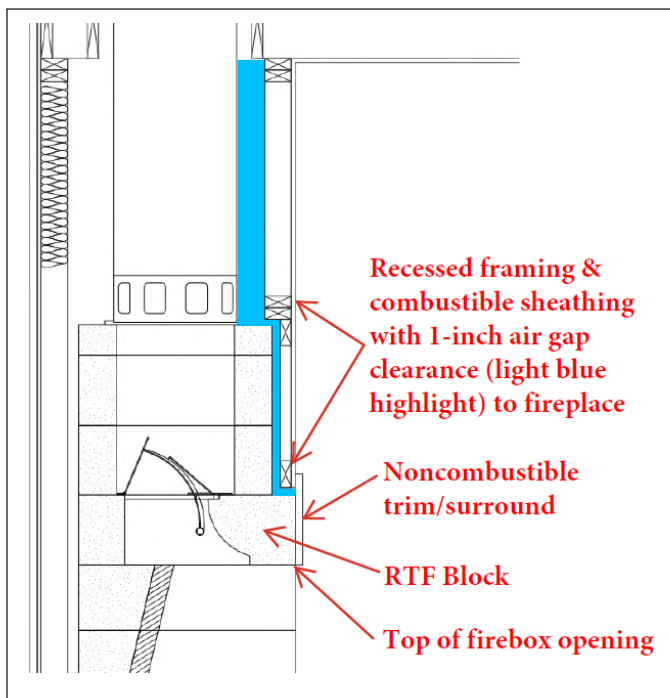


**Figure 16**

An excerpted and annotated profile drawing from the manufacturer’s installation instructions pertaining to the combustible framing and sheathing around the top of the firebox. Note also the required cooling air spaces which are annotated in blue.

of 12 inches clearance. Covering such projecting trim with mortar and/or stone veneer does not render it noncombustible and does not prevent exposure to the substantial heat emanating from the top of the firebox opening; it merely conceals it, creating a hidden fire hazard.

The OSB on the sides is required to have 1-inch horizontal clearance to the sides of the firebox and is required to be recessed flush with the front vertical face. The OSB on the sides overlaps the vertical front face of the sides of the firebox and also projects beyond the vertical face, forming a “trim.” No OSB or other combustible construction is permitted within or beneath the hearth and hearth extension. Yet, the OSB that was routed across the bottom opening of the firebox is sandwiched beneath and between the masonry joint formed by the hearth and hearth extension.

It should be noted also that a faulty or missing seal between the hearth and hearth extension could allow penetrating embers at that location to precipitate a fire. NFPA 211 Section 11.2.1.5 requires that joints be fully sealed. However, in this case: (1) the homeowners reported no cracking in or between the hearth or hearth extension; (2) the available photographs indicated no cracking in or between the (relatively new) hearth or hearth extension; and (3) the masons who constructed the unit stipulated all potential voids and joints were solid filled. Direct examination of the fireplace joints could not be made post-incident due to the level of destruction during collapse.

As previously observed in **Figures 10** and **14**, fiberglass batt insulation was installed in the air clearance spaces between the firebox and the wall framing in violation of the manufacturer’s installation instructions. The instructions state that (in multiple locations of the manual) no insulation is to be placed in the air clearance spaces around the fireplace. Insulating air clearance spaces around the perimeter of the firebox will result in higher operating temperatures of those faces and, in particular, any combustibles in (improper) contact with or in close proximity to them.

While the installation violations of the OSB across the top and sides of the firebox are clear fire hazards, the scene investigators concluded that the origin of the fire was beneath the firebox hearth due to the extensive fire damage to the floor and floor system beneath. The floor system beneath the firebox and hearth extension was consumed and compromised during the fire event, resulting in the collapse of the chase enclosure. Floor systems beneath

masonry are often protected<sup>18</sup> from fire exposure and remain in good condition after extinguishment when a fire originates elsewhere.

The hearth, hearth extension, and the joint between the two are subject to substantial radiant heat transfer from the fireplace opening and subsequently substantially elevated temperatures. *Kirk's Fire Investigation*<sup>19</sup> notes that radiant heat fluxes of 20KW/m<sup>2</sup>, producing equilibrium surface temperatures of approximately 500°F can be experienced at the face of the fireplace; and radiant heat fluxes of up to 30KW/m<sup>2</sup>, producing equilibrium surface temperatures of up to approximately 800°F can be experienced in the interior of the fireplace.

As previously noted, the author has instrumented the

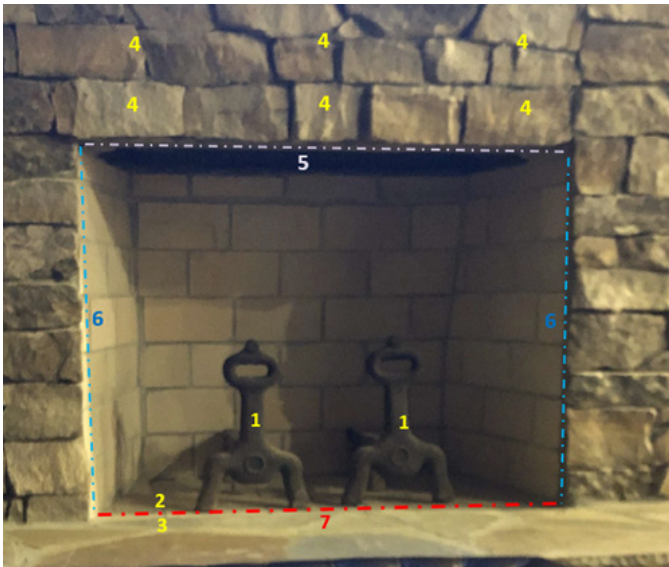


**Figure 17**

A view of the finished fireplace opening and hearth extension in front of the fireplace. Notes: 1) andirons (used to support logs during fireplace use); 2) fireplace hearth (note proximity of mortar joint 7, red dash-dot line); 3) fireplace (flush) hearth extension; 4) stone/mortar covering OSB running across and in direct contact with the face of the RTF block and with air/clearance spaces above the RTF block packed with fiberglass insulation; 5) mortar joint covering the edge of the OSB sheathing projecting beyond and around the perimeter face of the fireplace opening (trim projection); and sandwiched between the stone veneer and the RTF block face along the top of the firebox opening; 6) mortar joint covering the edge of the OSB sheathing projecting beyond and around the perimeter face of the fireplace opening on the sides (trim projection) and sandwiched between the stone veneer and firebox side faces. Blue dash-dot line. The OSB is also in direct contact with the vertical front face of the firebox sidewall; and 7) mortar joint covering the edge of the OSB sheathing projecting beyond and around the perimeter face of the fireplace opening and sandwiched between the hearth and hearth extension. Red dash-dot line. Subject to intense radiant, conduction and convection heat transfer processes during operation of the fireplace.

Red dash-dot line. Subject to intense radiant, conduction and convection heat transfer processes during operation of the fireplace.

top surface of the hearth floor of a modular wood-burning fireplace and recorded operational temperatures. Temperatures in excess of 1,100°F are established and maintained on the floor due to the continuous accumulation of hot and burning embers. The accumulated burning embers on the surface result in conduction and convection heat transfer processes directly impinging on and heating the hearth floor. The hearth extension is as the name indicates: an extension of the hearth. Hot and burning embers and ash commonly accumulate not just on the hearth floor but also up to and including the joint between the hearth and hearth extension (and sometimes beyond). **Figure 17** depicts a summary of the features of the as-built fireplace and the discussed concealed fire hazards. **Figure 18** depicts the subject fireplace in operation.

During operation — and for an extended period after operation of the fireplace — conduction heat transfer will occur from the vertical front face of the hearth refractory brick and base plate into the OSB in direct contact with the base plate. Heat will also directly transfer via conduction from the top of the mortar joint above and into the OSB. Heat will further be transferred via conduction into the vertical face of the OSB from the hearth extension side.

### Analysis Pursuant to Past Testing & Investigations

As part of his investigation, the author continued reviewing past case file materials as well as testing and data



**Figure 18**

A view of the subject fireplace in use (on a different occasion) sometime prior to the incident. Note the spark screen forms a trapezoid projection (yellow outline) out into the hearth extension. Also note the hot burning coals and ash accumulating beneath the burning logs and andirons on the hearth surface.

involving incidents where modular masonry fireplace installation defects caused structural fires. In addition, the author performed laboratory supplemental new testing utilizing a modular fireplace that he had constructed for another case years before of the same make and by the same manufacturer. The new testing will be discussed in a later section.

Prior Case #4 involved a modular masonry fireplace that was enclosed in a wood-framed and wood-sheathed chase and finished on the exterior with masonry stucco. The fireplace was installed on a concrete block (CMU) riser set on a concrete slab foundation. The fireplace incorporated an adjacent wood framed and sheathed hearth extension covered with metal lathe and then stucco. The stucco covering created a hearth extension flush with the fireplace hearth. Fire investigators examined and reconstructed the scene and concluded that the fire originated within the wood-framed and sheathed hearth extension, spread into the connected chase enclosure, and then spread vertically up the interior of the chase and into the rest of the home. As a result, the home was destroyed.

The fireplace was part of a rental beach residence used for short-term vacations. The complete history of the fireplace is unknown — though it was thought to be infrequent because of the transient nature of the property. On the date of the incident, the home was being rented for a wedding. Around 4:30 p.m., a fire was built in the fireplace, and the fireplace was operated up until around 9:30 or 10 p.m. (5 to 5.5 hours), at which time there were only hot embers and ashes remaining on the hearth. Guests left the fireplace/patio area around 11:30 p.m. Sometime after 5 a.m. (approximately 7 hours after active burning in the fireplace ceased), a guest woke up to use the bathroom, smelled smoke, and searched for/discovered a fire at the



**Figure 19**

Prior Case #4. A view of the fireplace during excavation and reconstruction at the fire scene.

wall common to the fireplace chase enclosure. The 911 call occurred at 5:36 a.m.

Based on the scene and reconstruction data obtained by the fire investigators, an exemplar modular fireplace, chase, and hearth extension were constructed, instrumented with thermocouples, and tested. Testing was conducted with the hearth extension wood framing against the base plate of the firebox and approximately 1.5 inches below the hearth surface and mortar covering the hearth extension surface. Based on the testing, temperatures obtained (up to approximately 650°F) were more than sufficient to initiate thermal decomposition, charring, and smoldering ignition of the wood substrate of the hearth extension<sup>11,18,20</sup>.

It should be noted that the engineer performing the testing on multiple occasions pushed embers and ash away from the masonry joint between the hearth and the hearth extension toward the back of the firebox. Variations in temperature would (and did) occur, depending upon where hot ashes and embers accumulated relative to the joint — and particularly where they accumulate relative to the thermocouples that were imbedded beneath the joint. The temperatures measured were not necessarily the hottest points along the joint. **Figures 19** through **21** depict



**Figure 20**

Prior Case #4. A view of the fireplace, chase, and hearth extension during laboratory reconstruction (per data from the fire investigators scene exam) and instrumentation prior to covering the hearth extension and surround with masonry. Notes: 1) wood framed hearth extension covered with plywood, felt paper and metal lathe prior to covering with masonry mortar; 2) hearth refractory; and 3) joint between hearth and hearth extension.



**Figure 21**

Prior Case #4. Joint between the hearth and hearth extension (fitted with new wood after a prior test run) prior to thermocouple instrumentation, filling and covering with masonry. The wood framing is beneath the hearth refractory brick surface (approximately 1.5 inches) and in contact with the base plate. The joint as well as the surface of the hearth extension were filled and covered with masonry to make it flush with the hearth.

the fireplace at the scene and reconstructed fireplace for testing purposes. **Figure 22** depicts a data plot from the testing.

Prior Case # 5 involved a modular fireplace and chase

enclosure built into the exterior wall of a home. The fireplace was installed on a double layer of concrete CMU blocks resting on a concrete slab. The fireplace incorporated a wood-framed and wood-sheathed chase enclosure with brick veneer finish. OSB wrapped the entire face perimeter of the fireplace (substantially similar to the subject fireplace of this paper). OSB was sandwiched/embedded between the base plate of the firebox and the masonry hearth extension (also substantially similar to the subject fireplace of this paper).

Fire investigators and engineers (including the author) examined the scene and delayered the fireplace brick veneer. It was concluded that the fire originated within the OSB sandwiched between the fireplace base plate (beneath the hearth) and the masonry hearth extension. The OSB was ignited via smoldering ignition. Once sufficient degradation occurred to the embedded OSB structure and sufficient oxygen pathways were available, the smoldering fire transitioned to flaming combustion and spread into the chase enclosure, vertically up the interior of the chase, and then into the rest of the home. As a result, the home was completely destroyed.

The new home had been completed in May of 2010 and occupied by the owners around that time. The fireplace had only been used approximately six to seven times

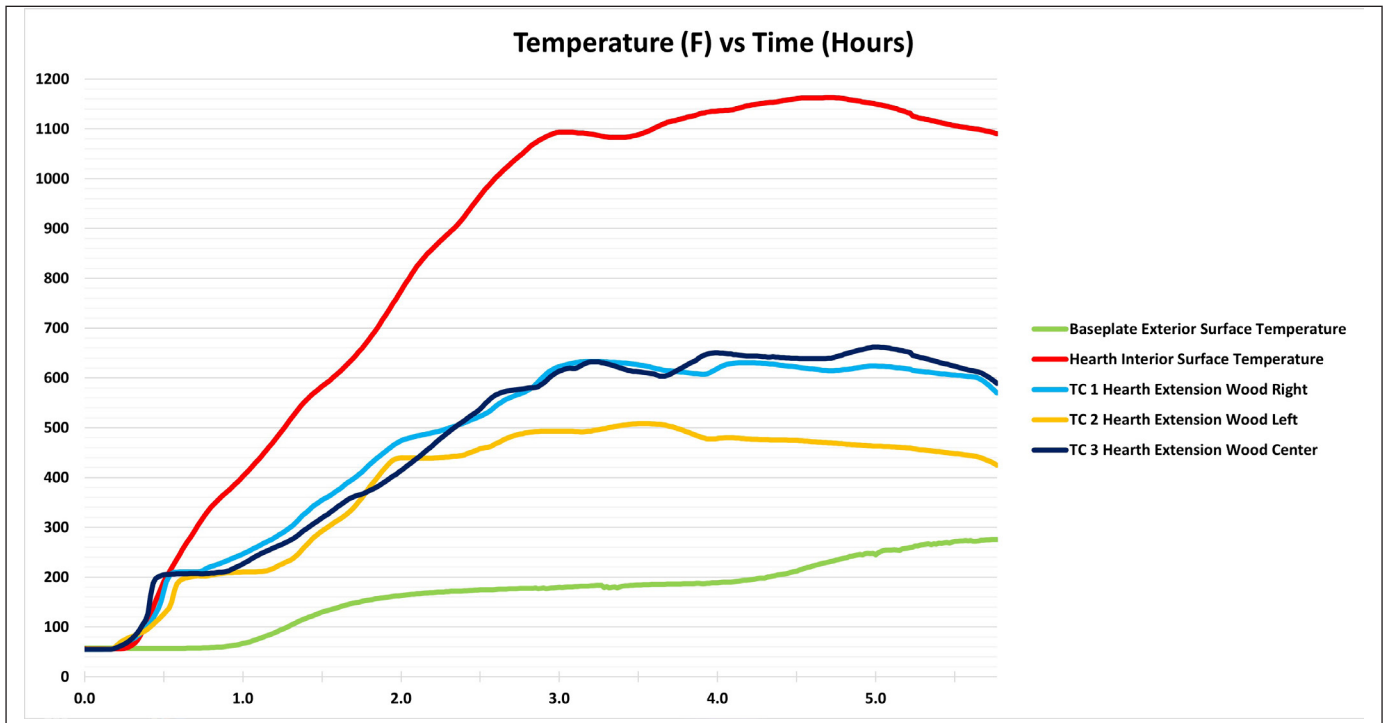


**Figure 22**

Prior Case #4. Data plot of thermocouple temperatures on the wood approximately 1.5 inches below the mortar joint between the hearth and the hearth extension. Also included are the hearth interior surface temperature and the exterior bottom surface of the base plate.

prior to the incident fire. On the date of the incident in early October of 2010, a fire was built in the fireplace around 10:15 a.m. and maintained up until around 6:45 p.m. (approximately 8.5 hours into the fireplace operation), at which time the wife discovered smoke in the home. Looking from a window, the homeowners saw smoke coming from around the flashing of the chimney. **Figures 23 through 26** depict the delayering of the brick veneer and origin of the fire.

### Supplemental New Testing for the Subject Case

In addition to the past case file testing and material reviews, the author performed demonstrative (supplemental new) testing to illustrate the nature of the fire hazard created by installing wood within the hearth and hearth extension structure. Testing data was already available for wood located 1.5 inches beneath the surface of the hearth. It should be noted that the superintendent for the subject case of this paper testified the OSB was within 1.5 inches of the opening of the firebox. To expand upon the available existing data, the new testing for the subject case fireplace doubled the distance to the OSB to a depth of 3 inches. In addition, OSB at a depth of 2.5 inches was included in the same testing to illustrate/contrast differential heat transfer under the same conditions. A small to modest active fire was maintained in the fireplace over the approximate same period of time for the subject case.

The testing results were generally consistent with what would be expected to occur based on the fireplace



**Figure 23**

Prior Case #5. A view of the modular fireplace during delayering of the brick veneer.

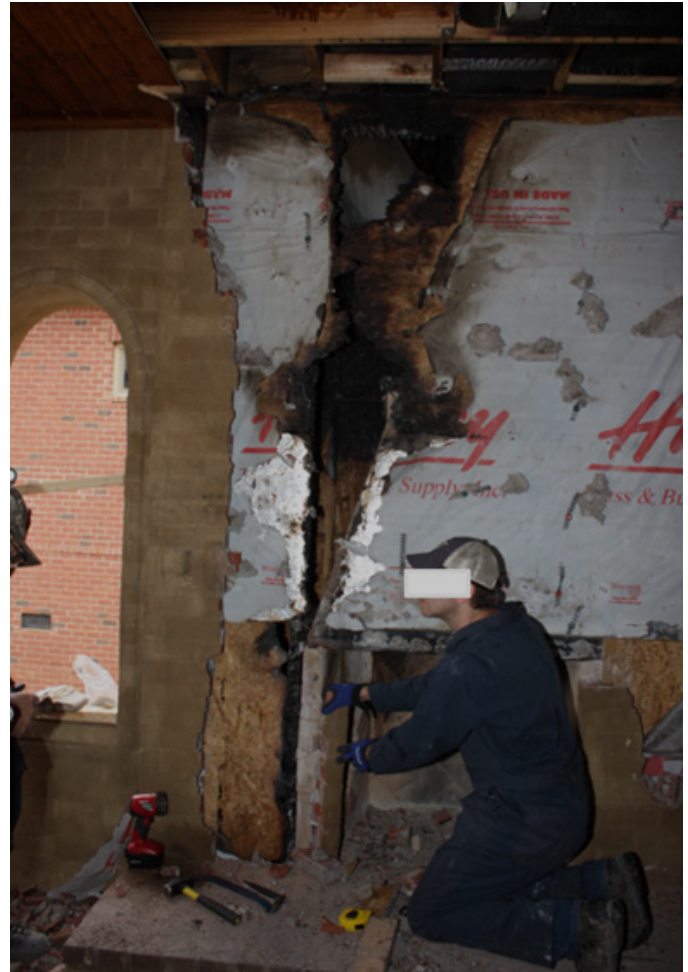


**Figure 24**

Prior Case #5. Another view of the fireplace during progressive delayering. Fire spread from near the base of the fireplace and up the wall and into the attic.



**Figure 25**

Prior Case #5. A view with the hearth extension masonry removed, exposing the joint between the hearth and the hearth extension. The yellow arrows indicate the OSB remains and burned-away portions of the OSB that was sandwiched between the hearth and the hearth extension. The fire spread until reaching the left side of the fireplace where the interior side of the OSB ran vertically up the chase.



**Figure 26**

Prior Case #5. The OSB had been installed approximately 1.5 inches below the surface of the hearth.

face radiant heat exposure data previously referenced in *Kirk's Fire Investigation* (i.e., up to around 500°F). It should be noted, however, that radiant heat transfer is not the only heat transfer process taking place, particularly at the hearth floor surface as previously discussed.

Convection and conduction heat transfer processes are operative on the hearth surface due to the accumulation of burning embers, log fragments, and hot ashes on that surface over the course of the active/flaming fire — and then even well after the active/flaming fire is out (i.e., smoldering embers beneath insulative ash cover). Depending on how/where the hot embers and burning collapsing logs fall as fuel consumption takes place will substantially impact temperatures on, near and within the masonry joint between the hearth and hearth extension. In general, the test fires were monitored to keep any burning logs or large burning embers that collapsed directly off of the joint, although such a scenario is certainly foreseeable and even likely.

As noted, the tests involved a maintained small to modest fire in the fireplace. It is also certainly foreseeable that a larger fire could be built and maintained that would more rapidly elevate the observed temperatures both in rate and magnitude within the joint and subsequently the wood. So, variability in fire size — as well as different distributions of natural falls of burning logs and embers from the andirons within the fireplace — can result in temperatures even more elevated than those obtained in the present tests. Nevertheless, the temperatures that were obtained in the testing were much more than sufficient to ignite the embedded wood. In any case, as discussed, the codes and standards prohibit any wood in the structures of a hearth and hearth extension because it is well understood that given sufficient foreseeable conditions and time, igni-

tion of that wood will occur.

The previously constructed lab fireplace<sup>1</sup> utilized was installed on a raised concrete slab and has a full masonry hearth extension. The joint between the hearth and the hearth extension was sawn out with a masonry saw. One-half-inch OSB sheathing board was step cut and instrumented with thermocouples and installed in the joint against the base plate below and along the full opening of the fireplace. Thermocouples were placed on the top horizontal edge of the OSB at intervals of approximately every 2 inches. Half of the OSB strip was installed 2.5 inches below the hearth surface. The other half of the OSB strip was stepped down and installed 3 inches below the hearth surface. The joint cavity balance was backfilled with Type S mortar.

Two similar operational tests were performed, each with active burns over a period of approximately 4.5 and 5.25 hours. A small to moderate fire was maintained in the fireplace by periodically adding wood as the logs in the fireplace were consumed. Temperatures obtained during the first test for the 2.5-inch and 3-inch depths below the hearth extension reached a range of approximately 360°F in approximately 3.5 and 4.5 hours. Temperatures continued steadily rising thereafter for another approximately 3.5 hours to peak temperatures of nearly 500°F and 460°F (well after active/fuel fed burning had ceased). Temperatures did not drop below 360°F for another approximately 4 hours after peak or approximately 6.5 hours after the fire in the fireplace was down to glowing embers. The temperatures obtained were much more than sufficient<sup>11,18,20</sup> to thermally decompose, char, and ignite the OSB to self-sustained smoldering combustion, which is further discussed later.

**Figures 27 through 30** generally depict the fireplace setup and burn testing. **Figures 31 and 32** depict the data plots of testing results from the first test. The results are similar for the second test, which are depicted in **Figures 33 and 34**. Note that the data logger was shut off approximately 7 hours after active burning ceased in the second test. The data logger was allowed to run longer after test one, and the data reflects the long period of time that it takes the masonry to cool back down to ambient temperatures. **Figure 35** depicts hot glowing embers that were hidden by ash and uncovered approximately 7 hours after the active fire ceased in the fireplace during the second test.

## Analysis and Discussion

Although analysis of the area of origin was not within the scope of the author's assignment, the data he reviewed

in this case was consistent with the area of origin being beneath the living room fireplace, specifically beneath the hearth and hearth extension masonry joint. The area of most extensive damage occurred to the enclosed chase structure. The homeowners reported there was no visible fire in the living spaces of the home (including the living

room), as they made multiple trips into and out of the home while attempting to save family photographs. The chase structure also collapsed during the incident as observed by the homeowners consistent with structural compromise of the floor while the remainder of the house structure remained standing.

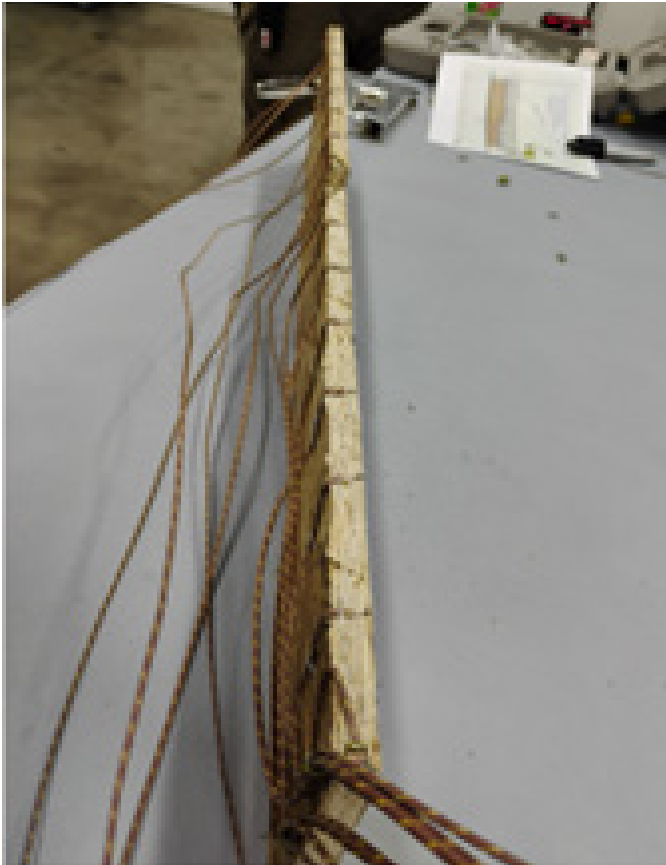


**Figure 27**

A view of the thermocouple instrumented stepped OSB sheathing installed in the joint between the hearth and hearth extension.



**Figure 28**

A view of the thermocouple instrumented joint between the hearth and the hearth extension after installation of the OSB.



**Figure 29**

A view of the equipment and fireplace setup.



**Figure 30**

A view of the small to modest fire maintained in the fireplace during testing.

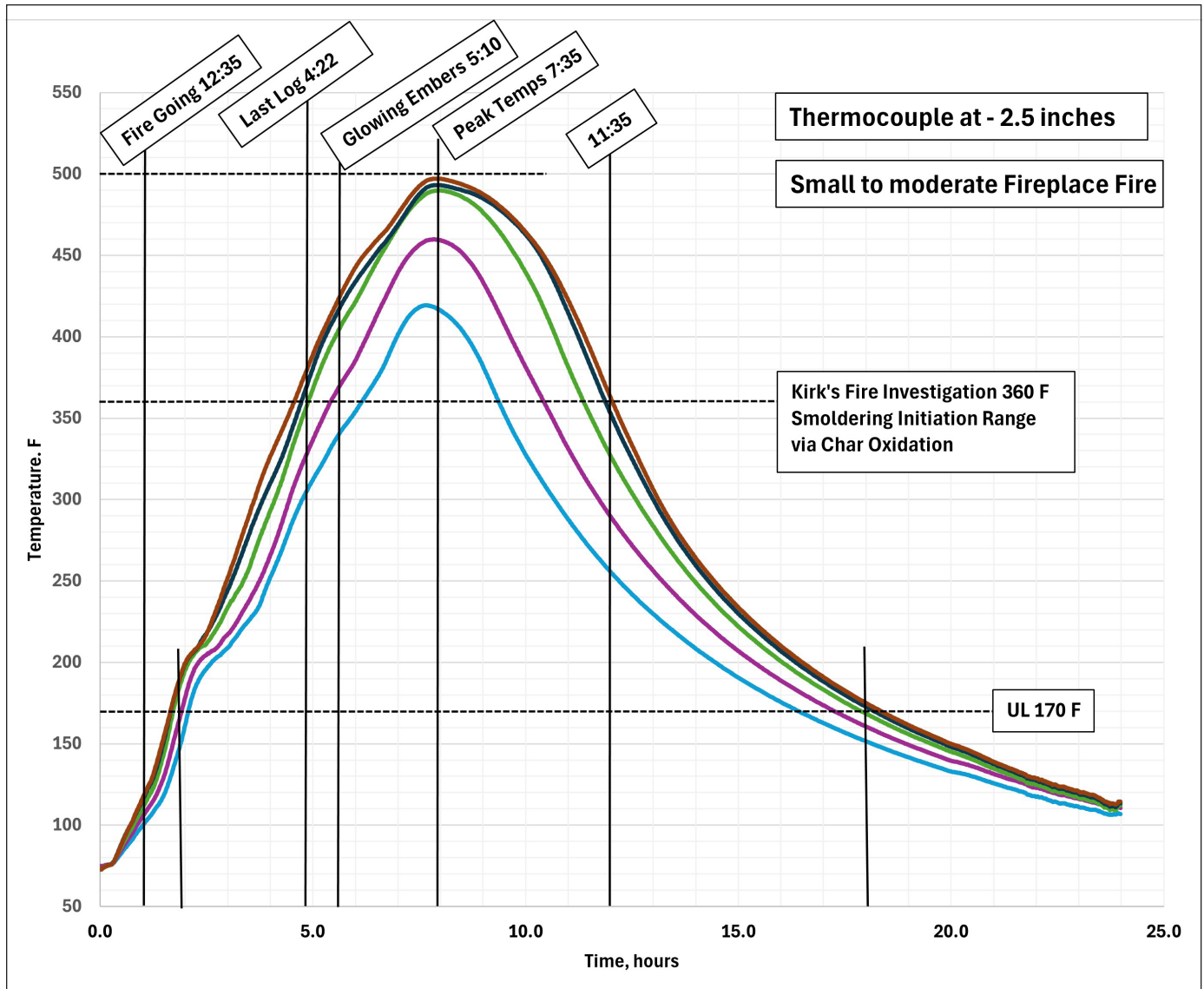


Figure 31

A view of thermocouple data at 2.5 inches depth from Test 1.

The chase was of combustible construction on the interior with masonry and stone on the exterior, creating a substantially sealed/isolated combustible concealed space through which a smoldering fire could initiate, transition to flaming, become well developed, and spread before ultimate discovery. The OSB sandwiched between the hearth and hearth extension masonry joint was in very close proximity to the hottest part of the fireplace: the hearth floor. The hearth floor is the hottest part of the fireplace and remains the hottest part the longest due to: (1) high operational temperatures transmitting energy via radiation, conduction and convection into the hearth and hearth extension masonry; and (2) the accumulation of sustained glowing/ slow smoldering embers protected by ash cover. Just as the insulative hearth ashes contained glowing em-

bers some 7 hours after cessation of flaming fire in the fireplace, thermally damaged, charred, and smoldering OSB sandwiched within the hot masonry joint would also be sustained. Once the OSB was sufficiently thermally and physically degraded and oxygen channels opened up, the smoldering fire transitioned to flaming and spread through the chase interior and then into the remainder of the home.

Temperatures in the demonstration testing reached 460°F/500°F (3 inch / 2.5 inch) in test one and 475°F/508°F (3 inch / 2.5 inch) in test two. Temperatures at 1.5-in depths would therefore be even higher for the testing undertaken utilizing a small to moderate fire and controlling large ember and log collapse migration onto the joint. The temperatures obtained reached and exceeded common

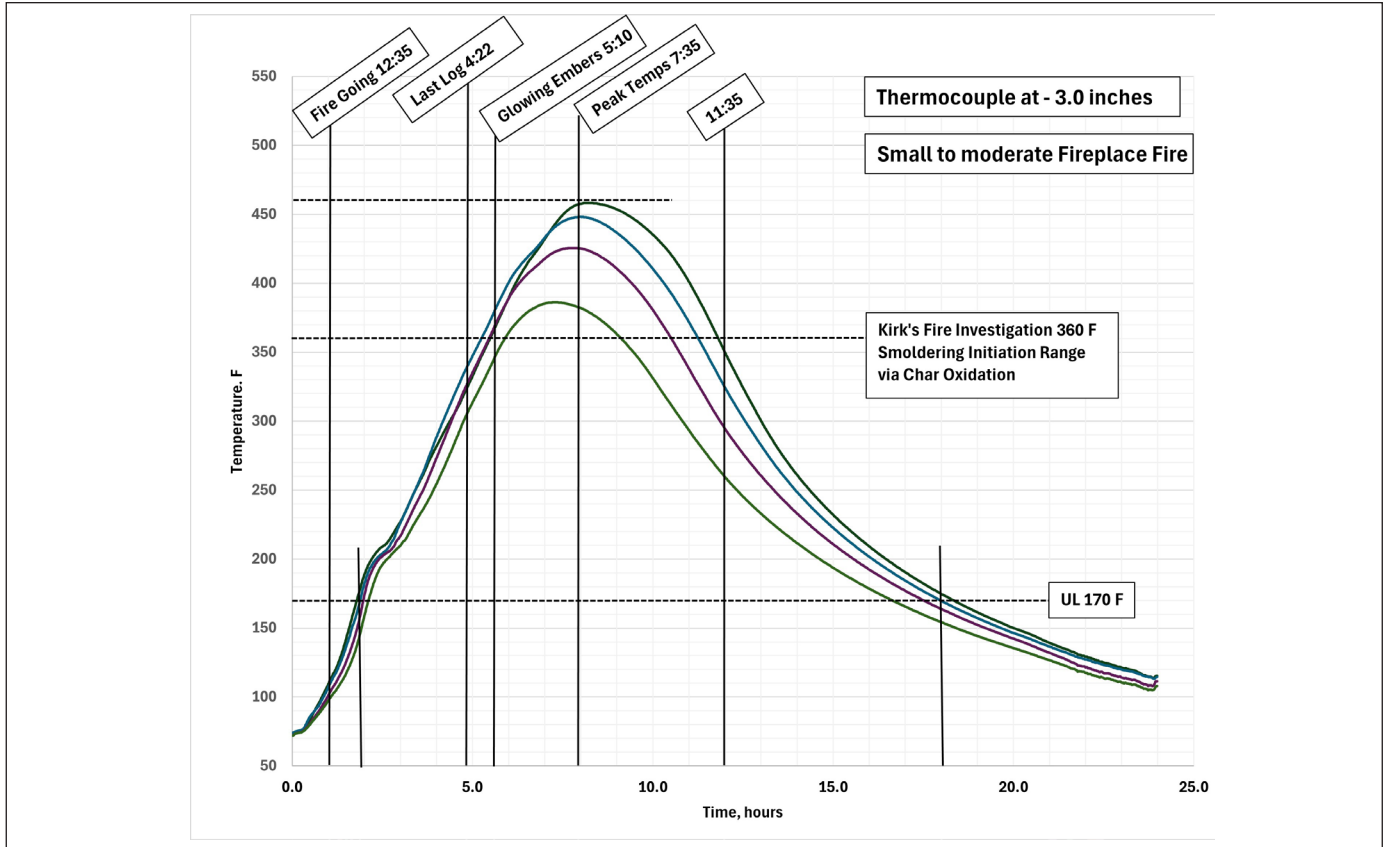


Figure 32  
A view of thermocouple data at 3.0 inches depth from Test 1.

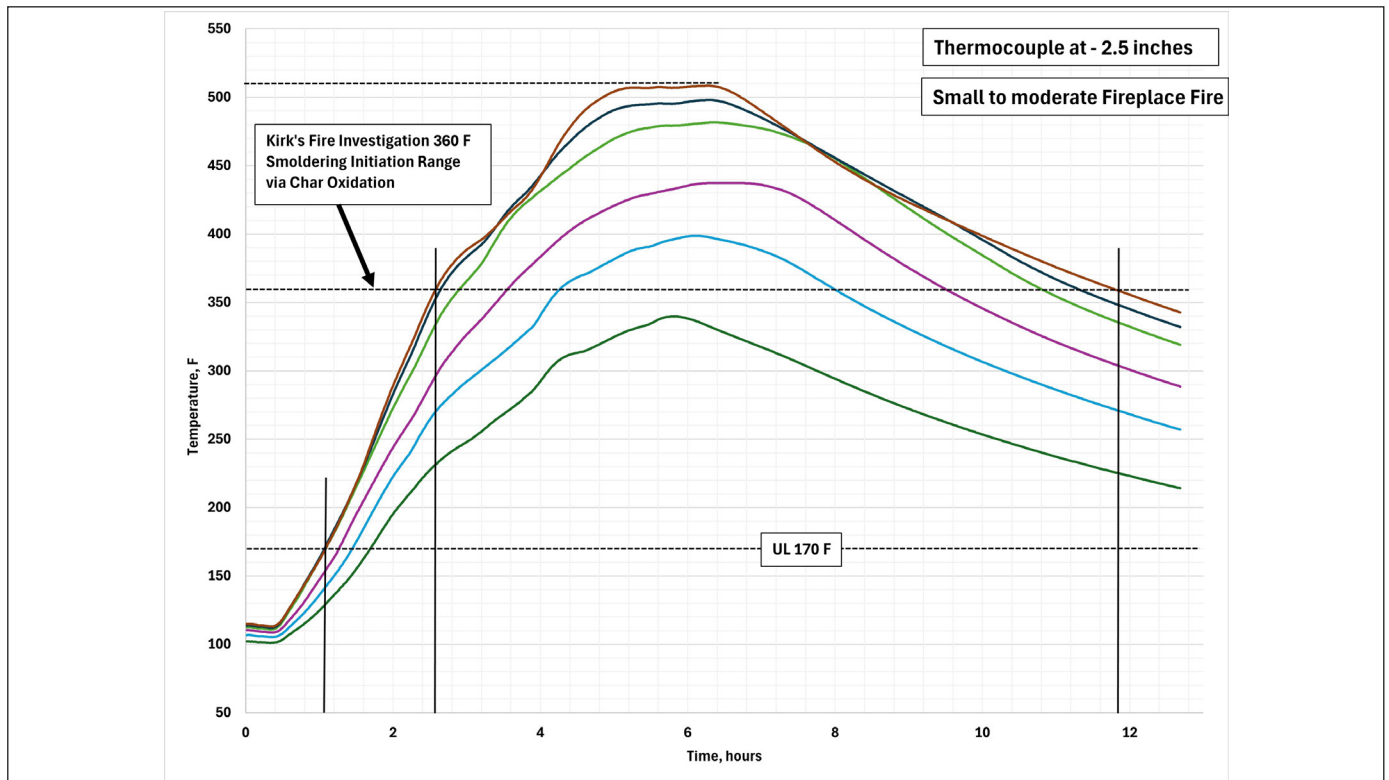
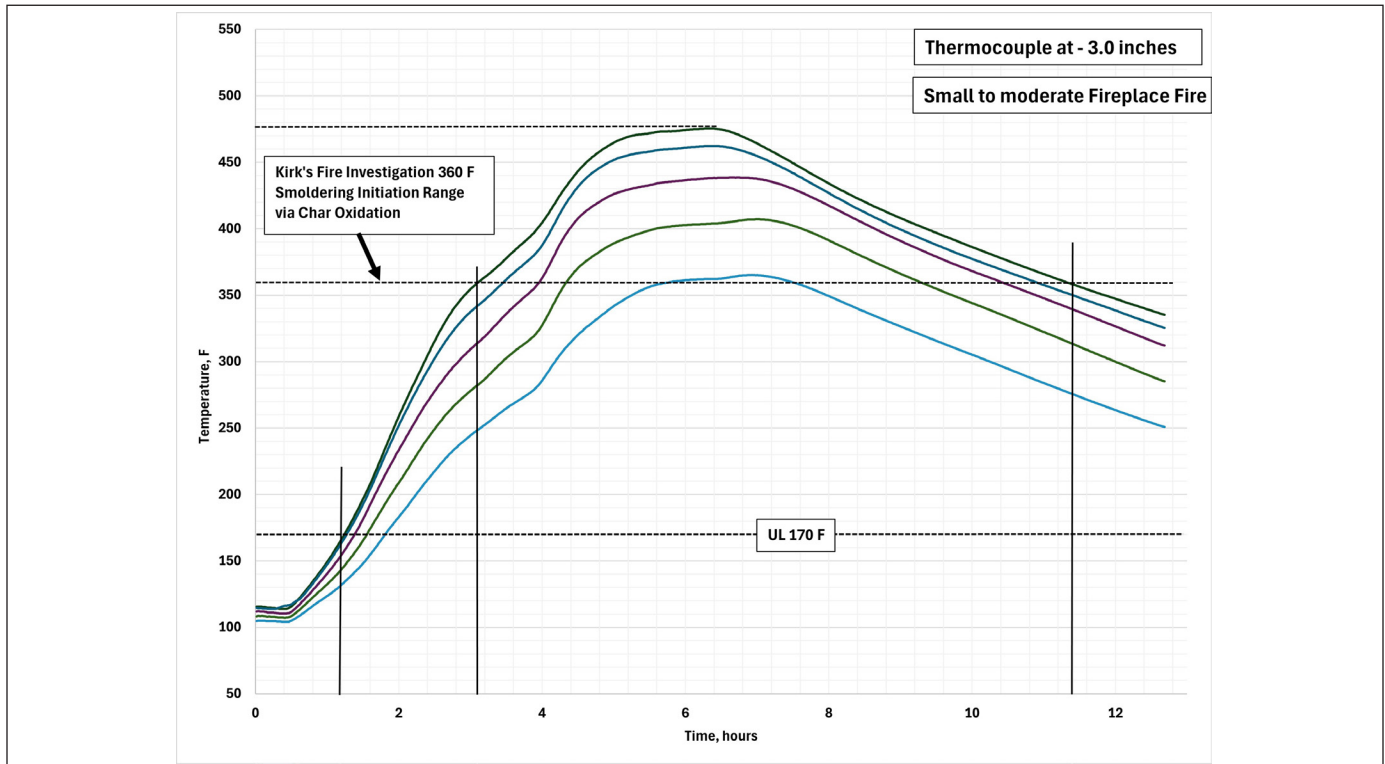


Figure 33  
A view of thermocouple data at 2.5 inches depth from Test 2.



**Figure 34**  
A view of thermocouple data at 3.0 inches depth from Test 2.

temperature ranges associated with the ignition of wood (392°F to 480°F)<sup>18,20</sup>.

Of additional interest in this case is that temperatures exceeding 360°F are also attained and maintained for extended periods of time. The OSB is embedded in hot masonry, concealed, and therefore in an oxygen limited and insulated environment. As a result, the installation configuration also represents a substantial smoldering ignition fire hazard. *Kirk's Fire Investigation 8th Edition* notes in discussing smoldering ignition:

*At temperatures above 180°C (360°F), the pyrolysis of all three major constituents (i.e. cellulose, hemicellulose, and lignin) reaches its maximum rate, leaving a smaller percentage (10 to 20 percent by weight) as char. If the heat being accumulated by the char is retained, and there is an adequate supply of oxygen, the temperature of the mass can rise to the point at which combustion can take place....The retention of heat depends on the amount of thermal insulation available and the amount of heat that is being lost to convective and conductive processes. If there is too much insulation, the supply of oxygen becomes inadequate to sustain*



**Figure 35**  
A view of hot glowing embers hidden in the ash and uncovered 7 hours after active burning ceased in the fireplace.

*combustion, although smoldering combustion can take place at very low oxygen levels....*

The OSB embedded in the masonry joint would be subject to substantial pyrolysis, char formation, and smoldering ignition with sustained combustion likely every time the fireplace was used. In uses of the fireplace prior to the night of the incident, insufficient oxygen (due to the embedded nature) and eventual heat dissipation (after the masonry mass cooled down) would cause the charred and smoldering OSB to self-extinguish until the next use of the fireplace when the process of pyrolysis, char formation, and smoldering ignition with sustained combustion would repeat itself. Once the OSB underwent sufficient thermal and physical degradation and sufficient oxygen channels and pathways opened up along and within the OSB, the smoldering combustion could then transition into flaming combustion.

A smoldering fire in the masonry embedded OSB may initiate at any time during operation of the fireplace and continue to smolder for an extended period of time (many hours), well after the active fire in the fireplace has ceased. For example, approximately 7 hours after active (flaming) fire had ceased in the second burn test, ashes within the firebox were stirred, and substantial glowing/smoldering embers were still present (**Figure 34**) though not visible or otherwise detected until the ash was moved around. Ash covering the embers had functioned to insulate and sustain slow smoldering combustion (with a low heat release rate) without the production of any detectable smoke. In like manner, charred and smoldering wood embedded within the hot masonry joint would continue to smolder in a manner even less detectable due to the masonry embedded concealed nature. Not until the smoldering combustion transitioned into flaming combustion (not a predictable event<sup>18</sup>) within the chase would the fire likely become detectable. *Kirk's Fire Investigation 8th Edition* [pp. 258] notes:

*... Due to the low heat release rate (HRR) and slow combustion and the insulative properties of ashes and the charred wood, the embers are undetected when removed. ... Wood or charcoal embers, insulated by ashes, can continue to smolder for 3 or 4 days under the right conditions and can result in ignition after being removed.*

*Kirk's Fire Investigation 8th Edition* [pp 79-80] also notes that:

*Investigators tend to associate the time of discovery with the time of first ignition. This assumption may introduce serious errors into the fire analysis. Due to its slow output of heat and smoke, smoldering may proceed for an extended period of time without being noticed. When the combustion transitions to flame, it is almost certain to be discovered quickly.*

The cause of the fire was the defective installation of the living room fireplace by integrating wood OSB into the structure of the required non-combustible hearth and hearth extension in violation of the manufacturer's installation instructions, the IRC, and nationally recognized standard NFPA 211.

The porch fireplace contained similar multiple violations related to clearances to combustibles — two of which are mentioned here. The porch fireplace was installed directly on top of the wood floor with no CMU riser. The porch fireplace was installed with a wood-framed and sheathed hearth extension in direct contact with the base plate of the firebox. The relatively infrequent use (five to 10 times) and much less operational times (2 to 3 hours) with each use is the likely reason a structural fire had not yet resulted from using the porch fireplace.

The installation of the living room fireplace as well as the porch fireplace included multiple violations of the manufacturer's installation instructions as well as the IRC and NFPA 211, which created conditions that would result in an imminent fire.

## Conclusions

In this paper, the use of testing and analysis from prior or similar cases was used to evaluate and support the fire cause in the present case. Additional testing and analysis was implemented to illustrate to (and enhance the understanding of) various involved parties as it relates to heat transfer into masonry hearth and hearth extensions and how fires may smolder undetected for extended periods of time before transitioning to flaming combustion.

## References:

1. J. Tindal, "Forensic engineering analysis of modular woodburning fireplace fire with gas log lighter in determining fire's cause," *Journal of the National Academy of Forensic Engineers*, vol. 38, no. 2, pp. 33-52, Dec. 2021.

2. *Guide to Thermal Properties of Concrete and Masonry Systems*, ACI/TMS 122R-14, Farmington Hills, MI: American Concrete Institute, 2014.
3. Amerimix, "Mortar Types: Know Your Mix," Amerimix Technical Documents. [Online]. Available: <https://tinyurl.com/mrxfkj34>. [Accessed: Oct. 14, 2024].
4. Lignacite, "An Introduction to Dense Concrete Blocks: Their Properties, Benefits and Uses." [Online]. Available: <https://tinyurl.com/5h54vtpw>. [Accessed: Oct. 14, 2024].
5. Lignacite, "The Thermal Performance of Concrete: An Introduction." [Online]. Available: <https://tinyurl.com/2ps669xk>. [Accessed: Oct. 14, 2024].
6. Sakrete, "Mortar Mix Type S data sheet." [Online]. Available: <https://tinyurl.com/yh6jvk98>. [Accessed: Oct. 14, 2024].
7. Carmelo, "Carmelo Mix Type S data sheet." [Online]. Available: <https://tinyurl.com/3vdrv8ec>. [Accessed: Oct. 14, 2024].
8. J. P. Holman, *Heat Transfer*, 7th ed. New York, NY, USA: McGraw-Hill, Inc., 1990.
9. D. J. Icove and G. A. Haynes, *Kirk's Fire Investigation*, 8th ed. New York, NY, USA: Pearson, 2018.
10. *UL 127 Standard for Factory-Built Fireplaces*, Northbrook, IL: Underwriters Laboratories, 2015.
11. V. Babrauskas, B. Gray, and M. Janssens, "Prudent Practices for the Design and Installation of Heat-Producing Devices Near Wood Materials," *Fire Mater*, no. 31, pp. 125-135, 2007.
12. J. Tindal and J. Warren, "Forensic engineering analysis of low temperature ignition of wood," *Journal of the National Academy of Forensic Engineers*, vol. 26, no. 1, pp. 85-103, Jun. 2009.
13. *International Residential Code*, ICC, Club Hills, IL, 2015.
14. *Hearth Design Specialist*, 1st ed. Arlington, VA: National Fireplace Institute and Hearth, Patio and Barbecue Educational Foundation, 2020.
15. *International Residential Code Commentary*, ICC, Club Hills, IL, 2015.
16. *International Building Code Commentary*, ICC, Club Hills, IL, 2009.
17. *Standard for Chimneys, Fireplaces, Vents, and Solid Fuel-Burning Appliances*, NFPA 211, 2019.
18. *Guide for Fire and Explosion Investigations*, NFPA 921, 2024.
19. J. D. DeHaan and D. J. Icove, *Kirk's Fire Investigation*, 7th ed. New York, NY, USA: Pearson, 2012.
20. V. Babrauskas, "Ignition of Wood: A Review of the State of the Art," *Interflam*, pp. 71-88, 2001.



# Forensic Analysis of an Elevated Pool Vault

By Brian C. Eubanks, PE, DFE (NAFE 962S), Garrett T. Ryan, PE, DFE (NAFE 1125M), and Derek T. Patoskie, PE (NAFE 1312A)

## Abstract

*Distress observed in the plaster lining and gunite/shotcrete of a pool structure located within a podium slab on the third floor of an eight-story student housing building located in central Texas was determined to be causally related to the gunite/shotcrete mix. The gunite/shotcrete mix combined high alkali Portland cement with siliceous aggregates sufficient to generate alkali-silica reaction (ASR). Additional construction deficiencies associated with the thickness of the pool shell and the clear cover over the steel reinforcement were determined to have exacerbated the distress in the structure. Upon demolition of the pool structure, design deficiencies were subsequently identified in the recessed concrete vault that supported the pool structure. The identified design deficiencies included inaccurate structural design and analysis with finite element modeling software, inconsistencies in the thickness of the floor slab, omission of a shear key at the abutment/connection of the floor slab and the vault walls, and an inadequate amount of bonded, non-prestressed reinforcement in the floor slab. These deficiencies culminated in the demolition and reconstruction of the vault. This paper will explore the different parties involved in the design and construction of the project, the errors that resulted in deficient conditions, and the positions maintained by the different forensic engineering consultants representing the various parties.*

## Keywords

Analysis, alkali-silica, ASR, building code, construction, case study, craze cracks, defect, deficiency, demolition, forensic engineering, evaluation, finite element, ground-penetrating radar, GPR, gunite, Portland cement, investigation, map cracks, methodology, non-prestressed reinforcement, performance, petrography, plaster, podium slab, pool, reaction, shear key, shotcrete, siliceous aggregates, slab, specification, variances, vault

## Introduction and Background

A building located in central Texas was comprised of a five-story wood-framed superstructure (i.e., the framed portion of the building above the foundation) intended for multi-family residential/student housing. The wood-framed superstructure was constructed on a concrete podium slab above a three-story parking garage (one story below-grade) with retail and leasing space at the ground level.

A pool structure (pool vault and pool shell) was located in the plaza deck portion of the podium slab on the third floor of the subject building. According to the structural engineering plans for the subject building, the plaza deck portion of the third-floor podium slab was designed with a rectangular, recessed concrete vault, herein referred to as the “pool vault.” The pool vault extended downward into the second-story area below to accommodate the pool shell, which was designed by another engineering firm.

The pool shell was designed as a gunite/shotcrete shell that was constructed over the underlying pool vault. The general terminology and cross section of the subject pool structure is illustrated in **Figure 1**.

The authors served as a consultant for the general contractor and were tasked with determining the probable cause(s) of distress in the pool structure and providing recommendations for remedial measures, if applicable.

## Pool Shell Evaluation

In order to provide an opinion regarding the probable cause(s) of distress in the pool shell, the authors reviewed the architectural/engineering documents for the subject building and pool structure, performed visual observations of the pool and adjacent deck surfaces, performed a relative elevation survey of the pool coping, observed ground-penetrating radar (GPR) surveys, obtained concrete cores for laboratory testing, and analyzed the

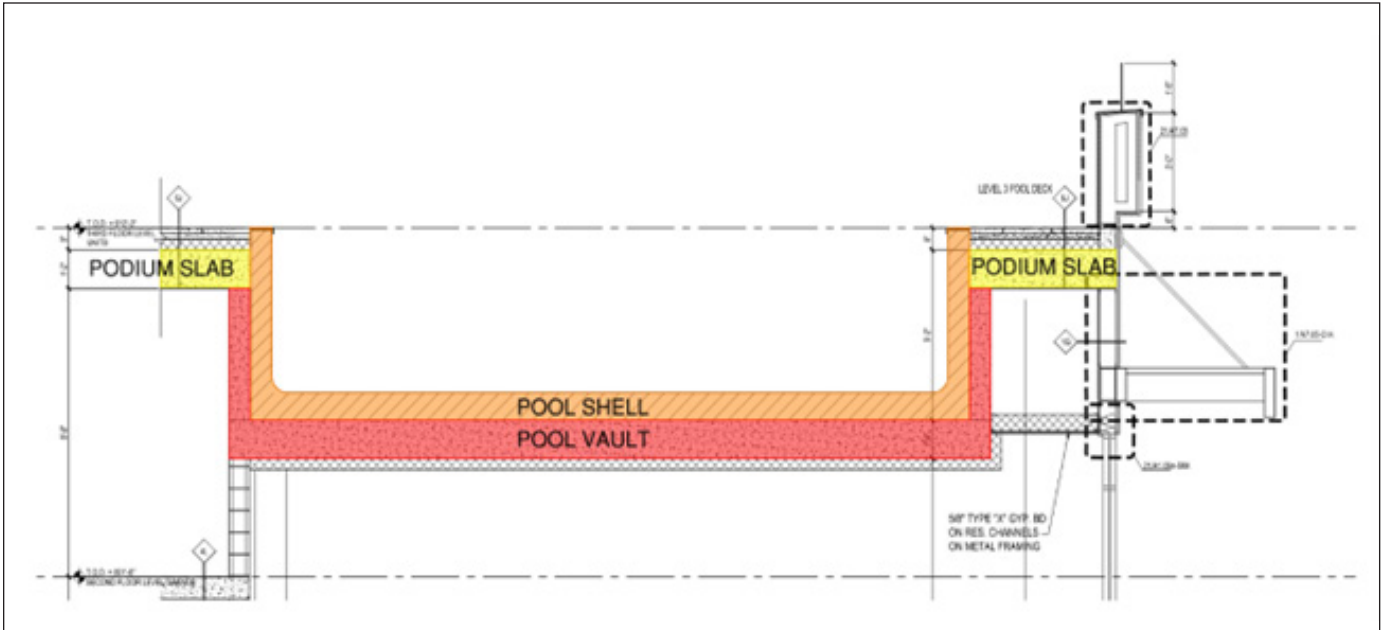


**Figure 1**  
Terminology and cross section of the subject pool structure.

collected information. A general photograph of the pool and adjacent deck surfaces is shown in **Figure 2**.

At the time of the initial site visit, concrete cracks were observed outside portions of the north, east, and south perimeters of the pool vault walls that ranged from hairline (0.003 inches) to approximately 0.020 inches in width. Cracks and/or mortar separations were also observed in the cast stone coping around the perimeter of the pool that ranged from hairline to approximately  $\frac{3}{16}$  (0.1875) of an inch in width. Further, cracks in the plaster lining of the pool were observed that typically ranged from hairline to approximately 0.060 inches in width,

with the largest crack measured at  $\frac{1}{8}$  (0.125) of an inch in width. The cracks observed in the plaster lining of the pool were oriented horizontal, vertical, and diagonal, and most of the cracks appeared to exhibit a pattern consistent with craze cracks or map cracks, as defined in ACI 201.1R-08 and illustrated in **Figure 3**<sup>1</sup>.

Utilizing a Zip Level Pro-2000, a relative elevation survey was performed on the cast stone coping around the perimeter of the pool in order to investigate the possibility of post-construction differential movement. The relative elevation survey indicated that the coping around the perimeter of the pool exhibited an overall levelness variance on the order of 1.2 inches. The relative elevation survey



**Figure 2**  
General view of the subject pool and adjacent deck surfaces.



**Figure 3**  
Cracks observed in the plaster lining of the pool shell.



**Figure 4**

GPR survey performed on the floor of the pool shell.

did not exhibit any salient pattern or trend associated with the levelness of the coping nor any anomalous elevations indicative of structural movement.

GPR surveys were performed within the pool structure to evaluate the placement of steel reinforcement within the floor and walls of the pool shell, as illustrated in **Figure 4**. The GPR surveys performed on the floor of the pool shell did not detect any salient signs of steel reinforcement; however, it should be noted that the presence of cracks and/or moisture may have limited the effectiveness of the surveys<sup>2</sup>. A GPR survey performed on one wall of the pool shell detected the presence of steel reinforcement spaced at approximately 12 inches on center horizontally and vertically. The same GPR survey also indicated an average gunite/shotcrete cover of approximately 3½ inches (horizontal bars) to 3¾ inches (vertical bars). A GPR survey performed on another wall of the pool shell detected the presence of steel reinforcement spaced at approximately 9 to 14 inches on center vertically and approximately 12 inches on center horizontally. The same GPR survey also indicated an average gunite/shotcrete cover of approximately 5¼ inches (horizontal bars) to 5¾ inches (vertical bars).

Selective demolition was performed within the pool shell, as illustrated in **Figure 5**, in order to determine whether the cracks observed in the plaster lining continued into the gunite/shotcrete and to verify the locations of the steel reinforcement indicated in the previous GPR surveys. An exploratory opening located near the central portion of the pool shell extended into the gunite/shotcrete, and it was intended to locate the steel reinforcement in the floor of the pool shell; however, no steel reinforcement was encountered at this location.

Gunite/shotcrete core samples were obtained from various locations within the floor and the walls of the pool shell in order to evaluate the compressive strength of the gunite/shotcrete. The structural engineering plans for the

pool shell did not specify a compressive strength for the gunite/shotcrete; however, according to the American Shotcrete Association, in conjunction with the authors' experience in the design, construction, and forensic investigation of pool shells, the average compressive strength of the tested cores (5,515 pounds per square inch - psi) exceeded typical industry strength specifications of around 4,000 psi for most pool structures of similar construction<sup>3</sup>.

Additional gunite/shotcrete core samples were obtained for petrographic examination. Concrete/gunite/shotcrete petrography is the examination of prepared samples under microscopes that use reflected light, transmitted light, and/or electron beams to identify basic components of the sampled material, study cracks/microcracks, and identify secondary deposits that form when the material deteriorates. Petrography can be utilized to evaluate proportioning of the concrete/gunite/shotcrete mix (i.e., percentages of aggregates, cementitious materials, water, voids, etc.) as well as evaluate mixing/consolidation, finishing operations, curing, cracking, and causes of low strength. In addition, petrography can be utilized to visually identify mechanisms affecting durability, such as freeze-thaw damage, alkali-aggregate reactions, chemical attack, and more<sup>4</sup>.

Through petrographic examination, it was determined that all of the applicable gunite/shotcrete core samples contained macro-cracks, microcracking, and abundant evidence of alkali-silica reaction (ASR) that radiated from chert (hard, fine-grained sedimentary rock) aggregates, cracked chert aggregates, partially-consumed chert aggregates, and/or desiccated alkali-silica gel within voids as illustrated in **Figure 6**.



**Figure 5**

Selective demolition performed within the horizontal floor surface of the pool shell.

## Alkali-Silica Reaction (ASR)

ASR is a chemical reaction that can occur in cementitious mixtures (e.g., concrete, gunite, shotcrete, etc.) between chemical compounds found in Portland cement (alkalis) and silica found in many common aggregates. The alkalis of concern (primarily sodium and potassium hydroxides) form alkali hydroxides as they dissolve in water, which increases the pH of the concrete mixture. Siliceous components of aggregates, such as quartz, cristobalite, tridymite, chalcedony, chert, opal, and acidic volcanic glass, dissolve at higher pH levels (typically above 13) to form a hygroscopic gel that swells and increases in volume as it absorbs moisture. As the gel expands, it exerts internal pressures that can lead to cracking when the internal pressures exceed the tensile strength of the hardened/cured cementitious mixture. Cracking may appear more prominent near the surface as a result of alkalis migrating upward/outward with the bleed water. ASR cracks typically appear as craze cracks or map cracks near the surface of the concrete/gunite/shotcrete<sup>5</sup>.

As previously stated, most of the cracks observed in the plaster lining of the pool appeared to exhibit a pattern consistent with craze cracks or map cracks, which is consistent with distress patterns causally related to ASR. As a result, the authors determined that the distress observed in the plaster lining and gunite/shotcrete of the pool shell was causally related to ASR. In addition, the distress related to ASR was exacerbated by construction deficiencies associated with the thickness of the pool shell and the depth of gunite/shotcrete cover over the reinforcement steel, which likely increased the volume of reactive materials available for ASR to occur and located the tensile reinforcement



**Figure 6**

Desiccated alkali-silica gel adjacent to a chert aggregate viewed under microscope.

further away from the surface of the structure, reducing its effectiveness to resist surface cracking.

Curative treatments for structures affected by ASR are not easily performed, if at all possible. Isolated repairs of damaged sections are possible; however, ASR can be expected to continue in non-repaired portions of the affected structure. Due to the presence of desiccated alkali-silica gel within voids, as identified in the gunite/shotcrete core samples, it was expected that the distress would likely continue to manifest as the desiccated alkali-silica gel experienced additional hydration and expansion. In some cases, the rate of ASR can be retarded through the application of a waterproofing membrane, which can reduce the volume of water available to fuel the expansion of the alkali-silica gel; however, this treatment was not practical for a pool structure due to the likelihood of contact between the gunite/shotcrete and moisture from the pool water<sup>6</sup>.

While curative treatments for structures affected by ASR are not easily performed, if at all possible, preventive measures can be taken prior to construction in order to mitigate the likelihood of ASR occurring. Such preventive measures can include project-specific specifications that limit the amount of Portland cement in an attempt to reduce the alkalinity of the concrete mix, specifications for a low-alkali proprietary cement product, and/or specifications for performing aggregate testing to identify and limit the amount of silica within the concrete mixture.

## Pool Shell Demolition

Based upon the magnitude of distress causally related to ASR within the pool shell — in conjunction with the likelihood for such distress to continue — it was recommended by the authors, as well as various other consulting firms (including the owner's consultant), that the pool shell be removed and replaced.

During demolition of the pool shell, cracks were observed at various locations in the concrete support structure underlying the pool shell. Of particular concern was a horizontal crack that exhibited lateral displacement located in the outside face of the vault wall near the abutment of the vault wall and the vault floor as shown in **Figure 7**.

Investigations of the observed cracks in the pool vault were subsequently performed by a consultant for the building owner, which ultimately led to allegations of deficiencies related to the design and construction of the pool vault.



**Figure 7**

Horizontal crack exhibiting lateral displacement near the abutment of the vault wall and the vault floor.

### Pool Vault Evaluation

In order to provide an opinion regarding the probable cause(s) of distress in the pool vault, the authors reviewed the architectural/engineering documents for the subject building and pool structure, performed visual observations of the pool vault, observed GPR surveys, observed selective demolition of the pool structure, reviewed investigation reports issued by other consultants involved in this forensic investigation, and analyzed the collected information considered to be relevant to the evaluation.

The evaluation of the pool vault began with an attempt to compare the measurable aspects of the as-built pool vault with the original design specifications for the pool vault. It was found that the structural engineering plans provided by the structural engineer of record (SEOR) lacked sufficient instruction for the construction of the pool vault as well as the integration of the pool vault with the podium slab.

The structural engineering plans provided by the SEOR did not include any specifications, sections, and/or details associated with the abutment/connection of the third-floor podium slab to the walls of the pool vault. In addition, the structural engineering plans did not include any specifications, sections, and/or details associated with the abutment/connection of the walls of the pool vault to

the floor of the pool vault. Further, the structural engineering plans did not include any specifications regarding the thickness and/or steel reinforcement for the walls of the pool vault. The omission of such information was recognized by the general contractor and/or its subcontractors during the original construction, and a request for information (RFI) was subsequently submitted for clarification.

The SEOR responded to the RFI with specifications for mats of vertical and horizontal reinforcement bars to be installed in the walls and floor of the pool vault. The response was void of information regarding specific sections or details that were missing from the structural engineering plans. Ultimately, the pool vault was inspected by a third-party representative prior to concrete placement during the original construction, and, according to inspection reports, the pool vault was apparently found to be compliant with the presumed intent of the SEOR.

The authors and other consultants agreed to perform independent structural analyses of the as-built structure. The structural analyses would evaluate the expected capacity of the structure as-designed, as well as the actual capacity of the structure as-built, with respect to the loads required by the applicable building code. The presence/absence of steel reinforcement, as well as the length of corner bars/hooks (if present), could not be reliably determined through construction-phase photographs, construction-era documentation, and/or non-destructive evaluation. Due to the aforementioned unknowns, structural analyses could not be performed without acquiring additional information about the as-built structure.

As a result, all consultants collectively agreed that selective demolition was warranted in isolated areas of interest, and the demolition would progress as necessary until the as-built construction of the pool vault could be determined with a reasonable degree of certainty to allow for structural analyses of the as-built structure. Ultimately, the selective demolition progressed until it was determined that corner bars/hooks were omitted from the as-built structure. Independent structural analyses performed by each consultant, considering the omission of corner bars/hooks, indicated that the concrete pool vault was not structurally adequate to support the required design loads of the superstructure, and the concrete pool vault was subsequently demolished in its entirety, as illustrated in **Figure 8**.

The owner's consultant concluded the concrete pool vault was not structurally adequate to support the required



**Figure 8**

Selective demolition of the pool vault.

design loads of the superstructure, and the observed cracks in the pool vault were due to a combination of “poor construction and non-code-compliant structural engineering design.” The owner’s consultant issued a Certificate of Merit against the SEOR, and legal counsel for the SEOR subsequently retained a consultant of its own to evaluate the claims made against the SEOR by the owner’s consultant.

**Alleged Design Deficiencies**

The owner’s consultant performed a structural analysis of the as-designed pool vault utilizing RAM Concept by Bentley Systems, Inc. (RAM)<sup>7</sup>. The consultant acknowledged that the concrete pool vault could have been designed to act as a composite structure (i.e., the walls and slab of the vault work in tandem in the transfer of loads).

Alternatively, it could have been designed for the floor slab of the pool vault to transfer loads to supporting columns without additional support from the walls of the concrete pool vault.

An illustration depicting the difference between composite action and non-composite action is provided in **Figure 9**. Regardless of the intent for the design by the SEOR (composite structure vs. non-composite structure), a general contractor and/or its subcontractor would not ordinarily possess the knowledge, education, and/or training necessary to identify and comprehend the intent of the SEOR with respect to the potential need for composite action between the walls of the concrete pool vault and the adjacent floor slabs.

The owner’s consultant acknowledged that the as-designed pool vault would not achieve composite action due to the fact that the structural engineering plans by the SEOR did not include the necessary specifications/details to tie the walls and floor slabs together. As a result, the owner’s consultant performed a structural analysis utilizing finite element modeling software with a model that did not consider composite action of the concrete pool vault. Based upon the analysis of non-composite action, it was concluded by the owner’s consultant that the floor slab of the concrete pool vault experienced stresses that exceeded the allowable stress limits of the applicable building code.

The owner’s consultant also performed an alternative structural analysis utilizing finite element modeling software with a model that considered composite action

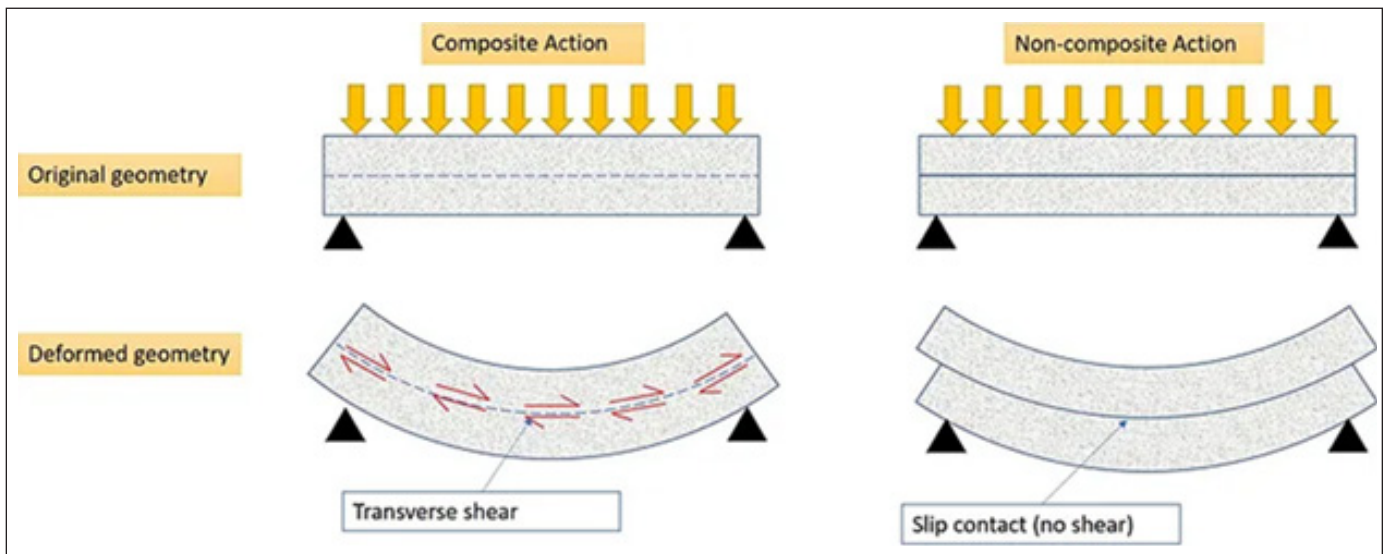


**Figure 9**

Composite vs. non-composite action.

of the concrete pool vault in case it was the intent of the SEOR for the walls and floor slabs to achieve composite action. Based upon the analysis of composite action, it was concluded by the owner’s consultant that the floor slab of the concrete pool vault still experienced stresses that exceeded the allowable stress limits of the applicable building code.

The authors also performed their own structural analyses of the concrete pool vault utilizing RAM with a model that did not consider composite action of the concrete pool vault as well as a model that considered composite action<sup>7</sup>. They also determined that the design of the concrete pool vault by the SEOR was not adequate to support the required design loads of the superstructure regardless of whether or not the vault was intended to achieve composite action.

Based upon the structural analysis performed by the authors for the scenario of non-composite action, it was found that the as-designed structure stress was 236 percent of the allowable stress in bending. For the scenario of po-

tential composite action, it was found that the as-designed internal shear stress in the floor slab was 244 percent of the allowable stress in punching shear at the central columns of the pool vault. The inability of the as-designed pool vault to support the required design loads of the superstructure (within the allowable stress limits) was determined by both the authors and the owner’s consultant to be a design deficiency.

It should be noted that a load-bearing wall that supported the wood-framed superstructure from the fourth-floor to the roof was supported on the third-floor podium slab approximately 11 feet away from the concrete pool vault. Based upon the aforementioned structural analyses, it was determined by both the authors and the owner’s consultant that the SEOR failed to accurately consider the portion of the design load applied from the aforementioned load-bearing wall that would be transferred through the third-floor podium slab into the concrete pool vault, which contributed to the structural inadequacy of the engineered design, as illustrated in **Figure 10**.

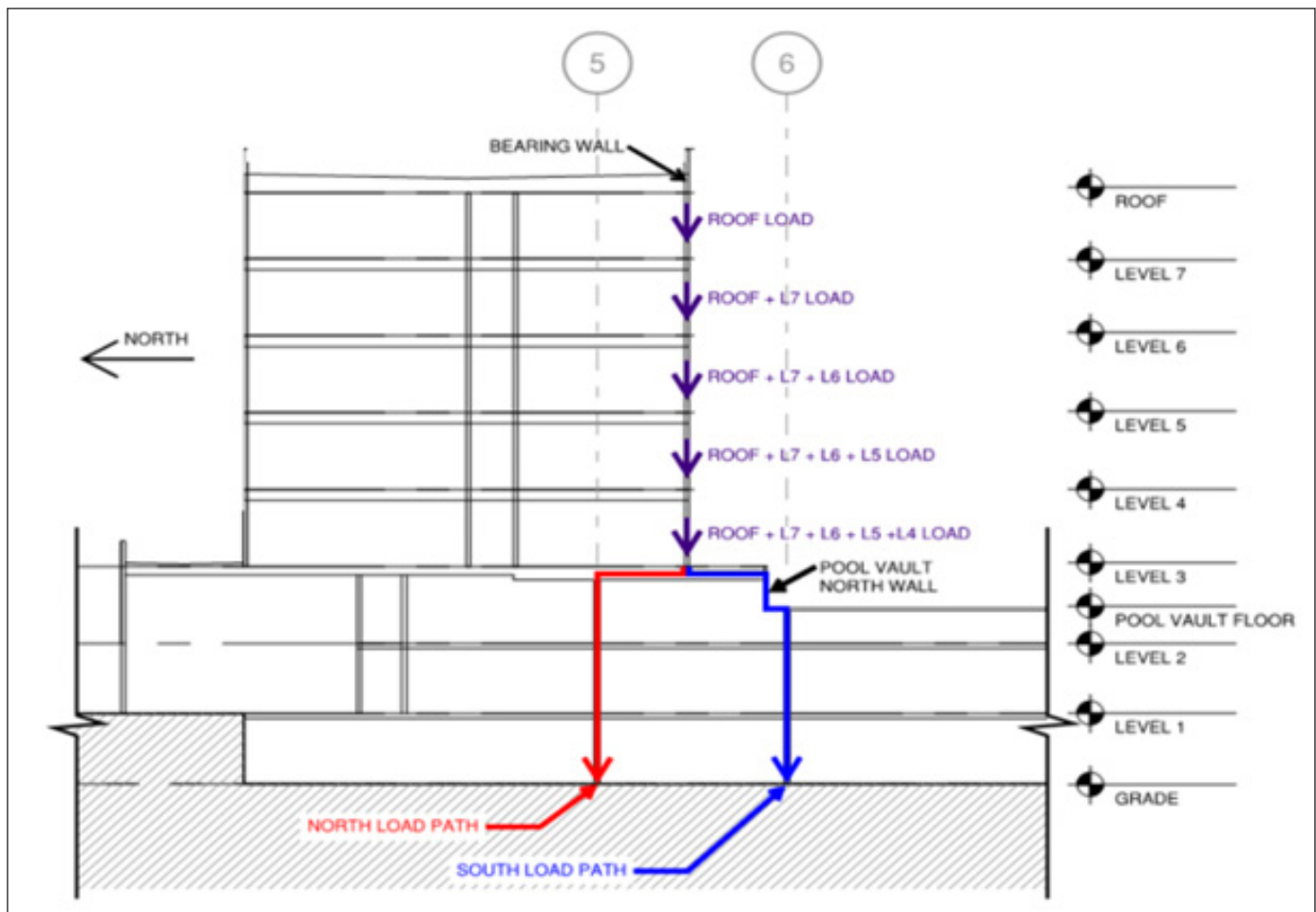


**Figure 10**  
Load-bearing wall supported on the third-floor podium slab.

Based upon a review of the structural engineering plans for the subject building, the authors found that the SEOR did not include any sections or details associated with the abutment/connection of the floor of the concrete pool vault to the walls of the concrete pool vault, including the construction of a shear key at the abutment/connection of the floor and walls, if necessary. The owner's consultant concluded that the SEOR was responsible for a design deficiency associated with the failure to incorporate an abutment/connection of the floor of the concrete pool vault to the walls of the concrete pool vault; however, the SEOR's consultant contested that an adequate load path was provided.

While the general contractor and/or its subcontractors should review the construction drawings related to the constructability of the design, the general contractor and/or its subcontractors are not responsible for (or capable of) performing an independent peer review of the structural engineering plans to verify that the design is structurally adequate or determine whether a shear key should have been incorporated into the design.

The owner's consultant also asserted that the SEOR failed to incorporate adequate bonded, non-prestressed reinforcement (conventional steel reinforcement bars) to meet the minimum requirements of Section 18.9.1 of ACI 318-11 by the American Concrete Institute (ACI) as stipulated by the applicable building code<sup>8</sup>. Due to a lack of required bonded steel reinforcement (i.e., deformed steel reinforcement bars embedded in the concrete), the floor slab of the concrete pool vault was more susceptible to cracking under service loads.

The structural analyses models by the authors corroborated the aforementioned findings of the owner's consultant with respect to a lack of bonded, non-prestressed reinforcement. The inadequate amount of bonded, non-prestressed reinforcement in the floor slab of the concrete pool vault was causally related to a design deficiency by the SEOR. The structural engineering plans for the subject building did not specify an adequate amount of bonded, non-prestressed reinforcement to comply with ACI and the applicable building code.

The SEOR's consultant performed a structural analysis of the as-designed pool vault; however, the consultant did not provide any discussion and/or results of the structural analysis performed. The consultant rather simply asserted that the analyses performed by the owner's consultant incorporated inaccurate assumptions.

### **Alleged Construction Deficiencies**

In addition to the aforementioned design deficiencies, the owner's consultant also asserted claims of various construction deficiencies against the general contractor and/or its subcontractors, including, but not limited to, the thickness of the pool vault floor slab, placement/securing of post-tensioned tendons, premature stressing of post-tensioned tendons, and roughness of concrete at cold joints. While one should endeavor to perform their services in accordance with the building code and/or construction documents, meeting code specifications and/or project specifications after-the-fact is mostly academic. A truly genuine forensic approach to asserted claims of construction deficiencies should not blindly follow codes of practice; rather, it should employ engineering analysis to consider performance aspects of the construction variances before concluding that such variances are construction defects<sup>9</sup>.

In the structural engineering plans for the subject building, the SEOR did not include any specifications associated with the thickness of the floor slab for the concrete pool vault. Based upon a review of the design calculations from the SEOR, the owner's consultant stated that the floor slab of the concrete pool vault was intended to be 12 inches thick. The referenced architectural plans for the subject building, however, indicated that the floor slab of the concrete pool vault was to be 14 inches thick. Post-tensioning shop drawings for the third-floor podium slab and concrete pool vault, which indicated that the floor slab of the concrete pool vault was to be 12 inches thick, were reviewed and approved by the SEOR as well as the architect of record (AOR). Following the approval of the aforementioned shop drawings, a concrete forming plan, which indicated that the floor slab of the concrete pool vault was to be 14 inches thick, was subsequently reviewed and approved by the SEOR and AOR. Based upon observations of the as-built floor slab of the concrete pool vault during demolition, the floor slab was constructed approximately 14 inches thick.

The owner's consultant claimed that the design team and the construction team both shared responsibility for the thickness of the pool vault floor slab not being constructed to the thickness intended by the SEOR. The SEOR's consultant claimed that the construction team held responsibility for the thickness of the pool vault floor slab not being constructed to the thickness intended by the SEOR. The owner's consultants claimed that the post-tensioned tendons were placed/profiled in the floor slab of the concrete pool vault in general conformance with the

aforementioned post-tensioned shop drawings in consideration of a floor slab that was expected to be 12 inches thick, and the construction of a floor slab 14 inches thick added 2 extra inches of concrete without modifying the tendon profiles. The owner's consultant did not provide any specific discussion regarding how the additional concrete thickness may have adversely affected the structure. The structural analyses models by the authors indicated that the additional thickness of the floor slab was not causally related to the structural inadequacy of the concrete pool vault, and the additional thickness of the floor slab actually decreased the magnitude by which the concrete floor slab was overstressed with respect to shear at column supports.

The owner's consultant also claimed that the elevations of the post-tensioned tendons at the ends of the slab varied from approximately  $3\frac{3}{8}$  inches for banded/grouped tendons (i.e., tendons spaced closely together) to approximately  $7\frac{5}{8}$  inches for distributed tendons (i.e., tendons spaced further apart) with an average of  $6\frac{3}{8}$  inches across the tendons assessed. The owner's consultant referenced Section 7.5.2.1 of ACI 318-11 with respect to tendon placement tolerances<sup>8</sup>. ACI 318-11 states that the allowable performance tolerance for an individual post-tension tendon is  $\pm \frac{1}{2}$  of an inch. Although some individual post-tensioned tendons exhibited elevations that exceeded the applicable individual placement tolerance, the average tendon anchor placement reported by the owner's consultant ( $6\frac{3}{8}$  inches) did not exceed the tolerance.

The SEOR's consultant claimed that the construction team held responsibility for any resultant damage attributed to the variance in elevation of the post-tensioned tendons; however, the consultant did not provide any analysis or discussion regarding the alleged construction deficiency.

The owner's consultant did not perform any structural analysis of the concrete pool vault in consideration of the as-built tendon placement and did not draw any conclusions regarding any potential effects of the as-built tendon placement with respect to the structural integrity of the concrete pool vault. The owner's consultant also suggested that the post-tensioned tendons in the floor slab of the concrete pool vault may have been stressed prior to the concrete attaining the minimum strength specified by the SEOR at the time of stressing. Compressive strength testing of concrete cylinders during construction indicated that the concrete placed at the floor slab of the concrete pool vault exhibited strengths of 3,420 pounds per square

inch (psi) at three days, 4,400 psi at seven days, and 5,670 psi at 28 days. The structural engineering plans for the subject building specified that the post-tensioned tendons should not be stressed until the in-place concrete attained a minimum compressive strength of 3,750 psi. The owner's consultant surmised that the required concrete compressive strength for stressing of post-tensioned tendons was likely attained in the concrete test cylinders at an age between three and seven days. Based upon construction-era documentation, the post-tensioned tendons were stressed five days after the concrete had been placed.

The owner's consultant suggested that the actual compressive strength of the in-place concrete could have been lower than the compressive strength of the laboratory-cured concrete cylinders due to the fact that the cylinders were cured at temperatures ranging from 70°F to 74°F while the in-place concrete at the job site likely experienced a temperature range between 75°F to 100°F.

The authors and the SEOR's consultant opined that the owner's consultant failed to prove that the concrete in the floor slab of the concrete pool vault had not attained the minimum required strength prior to stressing of the post-tensioned tendons. In addition, the authors opined that the owner's consultant failed to prove that the cracks observed at the edge of the pool vault floor slab were causally related to premature stressing of the post-tensioned tendons. If the cracks at the edge of the pool vault floor slab were causally related to premature stressing of the post-tensioned tendons, the cracks would have manifested at the time of stressing (or shortly thereafter); however, no documentation was provided that suggested cracks were observed and reported at the time of original construction.

The owner's consultant and the SEOR's consultant also claimed that the construction team failed to roughen the surface of the floor slab of the pool vault prior to placement of the walls. The surface of the cold joint between the floor slab of the pool vault and the walls of the pool vault was reportedly not roughened to an amplitude (measurement of vertical surface deviation between peaks and valleys) of  $\frac{1}{4}$  of an inch as specified by the SEOR.

The authors opined that the original as-built concrete roughness at a location of demolished concrete may be difficult to evaluate during post-construction demolition. The owner's consultant did not perform any structural analysis of the concrete pool vault in consideration of the purported as-built roughness of the pool vault floor slab at the cold joint between the floor slab and the walls, and

the consultant did not draw any conclusions regarding any potential effects of the concrete surface roughness with respect to the structural integrity of the concrete pool vault.

The authors maintained the position that none of the construction deficiencies asserted by the owner's consultant were causally related to the inability of the concrete pool vault to support the design loads of the superstructure. Even if the concrete pool vault had been constructed in absolute perfect conformance with the structural engineering plans, the concrete pool vault would still be structurally deficient due to an inadequate design by the SEOR. Remediation/replacement of the concrete pool vault would still be warranted at the subject building.

### Summary of Findings

The general contractor and/or its subcontractors should review the construction drawings related to the constructability of the design. The general contractor and/or its subcontractors, however, are not responsible for (or may not be capable of) performing an independent peer-review of the structural engineering plans to verify that the design is structurally adequate, which is what would have been required to avoid the documented structural issues with the concrete pool vault.

The design of the concrete pool vault by the SEOR was not adequate to support the required design loads of the superstructure, regardless of whether the vault was intended to achieve composite action or non-composite action and regardless of whether additional loads were considered from the adjacent load-bearing wall on the third-floor podium slab. The structural inadequacy of the concrete pool vault was causally related to a design deficiency by the SEOR, and it was not causally related to any potential construction deficiencies by the general contractor and/or its subcontractors.

None of the alleged construction deficiencies associated with the as-built thickness of the pool vault floor slab, placement/securing of post-tensioned tendons, premature stressing of post-tensioned tendons, and/or roughness of concrete at cold joints was causally related to the inability of the concrete pool vault to support the applied loads. Even if the concrete pool vault had been constructed in absolute perfect conformance with the structural engineering plans, the concrete pool vault would still be structurally deficient due to an inadequate design by the SEOR, and remediation/replacement of the concrete pool vault would still be warranted.

### Conclusion

This case highlights a matter where distress observed in the plaster lining and gunite/shotcrete of an elevated pool structure due to ASR ultimately led to the demolition of the pool structure and subsequent discovery of a more-serious structural issue associated with one or more design deficiencies.

Although the owner's consultant asserted allegations of both design and construction deficiencies, the alleged construction deficiencies were found to be unproven and/or inconsequential to the performance of the structure. Due to inaccurate design and analysis with finite element modeling software, the omission of specifications/details for tying walls and floor slabs together, errors associated with load paths, and inadequate specifications for minimum amounts of bonded reinforcement, it was determined that the as-built construction of the concrete pool vault was found to be inadequate. As a result, the vault had to be demolished and reconstructed.

### References

1. ACI Committee 201, 2008, "Guide for Conducting a Visual Inspection of Concrete in Service," American Concrete Institute, Farmington Hills, MI, 2008.
2. N. S. Admad and R. Hamid, "Relationship between Moisture Content and Dielectric Values of Concrete using Ground Penetrating Radar Method," *Journal of Advanced Research Design*, vol. 57, no. 1, pp. 21-33, 2019.
3. American Shotcrete Association, Compressive (Strength) Values of Pool Shotcrete [Online]. Available: [https://shotcrete.org/wp-content/uploads/2020/01/ASAPositionPaper\\_PoolRec\\_1.pdf](https://shotcrete.org/wp-content/uploads/2020/01/ASAPositionPaper_PoolRec_1.pdf).
4. ASTM Standard C856-04, 2004, "Standard Practice for Petrographic Examination of Hardened Concrete," ASTM International, West Conshohocken, PA, 2004, DOI: 10.1520/C0856-04.
5. E. Giannini, K. Folliard, J. Zhu, O. Bayrak, K. Kreitman, Z. Webb, and B. Hanson, "Non-Destructive Evaluation of In-Service Concrete Structures Affected by Alkali-Silica Reaction (ASR) or Delayed Ettringite Formation (DEF) – Final Report, Part 1", Center for Transportation Research, The University of Texas at Austin, Austin, TX, Texas A&M Transportation Institute, College Station, TX, FHWA/TX-13/0-6491-1, 2013.

6. Michael, D.A. Thomas, Kevin J. Folliard, Benoit Fournier, Patrice Rivard, and Thanos Drimallas, "Methods for Evaluating and Treating ASR-Affected Structures: Results of Field Application and Demonstration Projects – Volume I: Summary of Findings and Recommendations," The Transtec Group, Austin, TX, FHWA-HIF-14-0002, 2013.
7. Bentley Systems, Inc., Exton, PA, USA, 2024. RAM Concept. Available: <https://bentley.com/software/ram-concept/>
8. ACI Committee 318, 2011, "Building Code Requirements for Structural Concrete (ACI 318-11) and Commentary," American Concrete Institute, Farmington Hills, MI, 2011.
9. B. Eubanks, D. Patoskie, and G. Ryan, "Beyond the Building Code: A Forensic Approach to Construction Defect Evaluation Utilizing the Construction Variance Evaluation Methodology," JotNAFE, vol. 41, no. 2, Jan. 2025.



# Failure of a Climbing Treestand Due to Corrosion and Selective Leaching of Cable's Galvanic Layer: Failure Analysis and Experimental Study

By Olin Parker (NAFE 1334A), Jahan Rasty, PhD, PE (NAFE 768S), and Matthew Mills, PE (NAFE 1199A)

## Abstract

*Both supporting cables of a climbing treestand failed when a user stepped onto the stand's foot platform. Analysis of the failed cables revealed extensive corrosion and selective zinc leaching of the galvanized steel cables due to an electrical connection between the treestand cables and the steel frame. Experimental measurements of corrosion rates were performed through accelerated immersion tests utilizing mass-loss and DC current measurements as well as cyclic voltammetry. Results indicated a ~79% to 300% increase in the rate of corrosion as measured by millimeters of cross-sectional area reduction per year. Flaws in the design that led to the creation of a galvanic cell between the treestand cable and its frame are discussed, and alternative designs are proposed. Finally, the manufacturer's failure to properly account for anticipated use environment of the treestand in its design while being aware of similar prior incidents as well as their over-reliance on warnings are presented.*

## Keywords

Treestand, design defect, steel cable failure, galvanic corrosion, cyclic voltammetry, forensic engineering

## Introduction

Hunters often utilize a variety of equipment to augment their experience. One such piece of equipment is a treestand — a platform affixed to a tree that allows the hunter to take an elevated position (typically between 15 and 30 feet above the ground). Treestands are commonly utilized to allow hunters to ambush their prey at short ranges, making the use of bows and other short-range or less-precise weaponry more viable. According to conducted marketing research, treestands are utilized by around 87% of hunters in North America, making it one of the most-used pieces of hunting equipment<sup>1,2</sup>.

A treestand typically consists of a two-by-two-foot platform seat with straps and cords that affix the device to the trunk of the tree. Treestands come in a variety of distinctive styles and configurations. Fixed or hang-on treestands utilize straps, chains, and/or serrated metal teeth to secure the stand to the trunk of a tree. To reach a fixed stand that has been previously set up, hunters use climbing sticks that they insert into the trunk of the tree. Ladder stands, on

the other hand, provide the user with a ladder they can use to reach the stand platform. These stands offer greater stability because the load is carried by the ladder and the tree. Another commonly used variant is the climbing treestand. These two-piece stands (consisting of a foot-platform and a seat-platform) allow users to ascend the tree by wrapping the stand's cables around the tree trunk and moving one piece at a time until they reach their desired height.

According to the U.S. Consumer Product Safety Commission (CPSC), between 2005 and 2007, a total of 41 treestand-related deaths were reported, and 19,000 treestand-related injuries were estimated to have occurred<sup>3</sup>. In addition to this high incidence of injury, researchers have found that falls from treestands have become the leading cause of hunting-related injury<sup>4</sup>. For example, over a 10-year period in the state of Ohio, it was reported that around 50% of hunting-related injuries were due to falls (with 93% of these being falls from treestands) while only 29% resulted from gunshot wounds<sup>5</sup>. In 2014, the Indiana Department of Natural Resources reported that in 182

reported hunting accidents over a five-year period, 55% involved falls from a treestand<sup>6</sup>. A report by the CPSC found that nearly 40% of reported treestand incidents were due to a problem with the treestand<sup>7</sup>. Of those who fell from a treestand, 80% were noted to have required surgery, and 10% experienced permanent neurological disability or death<sup>8</sup>. Based on the above information, it is clear that falls from treestands present a significant hazard to the average hunter.

Treestands are known to experience failure from a variety of mechanisms. For example, the plastic deformation or fracturing of the load-bearing sections of a treestand can result in loss of load-bearing capability, causing the user to fall to the ground. Repeated usage can gradually induce fatigue in the load-bearing components, which can reduce the load-bearing capacity of the treestand to the point where normal operation can result in failure. Treestands that rely upon supporting cables or chains can have these components snap, resulting in the stand and its user falling. A treestand and its load-bearing components can also experience excessive corrosion, which renders the stand

unfit for use. The mechanism (whether chains, straps, or serrated metal teeth) engaging the stand to the trunk of a tree may also experience failure, leading to the stand disengaging from the tree.

### Incident Background

The plaintiff of this case was a 5'10" male weighing approximately 225 pounds. Following his initial purchase of the treestand, the plaintiff kept it in its box, and stored it in his garage for two years. Following this two-year period, he unboxed the treestand and affixed it to a tree on a hunting ranch in close proximity to the South Carolina coast — where it was left on the tree for three hunting seasons. Afterward, the treestand was noted to have been taken off the tree and stored in his garage for one year, after which he affixed the treestand on the tree once more. Two weeks before the subject incident, the plaintiff climbed up to the treestand to verify it was fit for use. According to his testimony, he then sat down in the treestand and determined it to be in a reasonably safe condition. During the evening of the incident, the plaintiff used the climbing sticks affixed to the tree to climb up to the treestand. As soon as he put both feet on the foot platform and attempted to attach his safety belt, the supporting cables snapped, sending the plaintiff falling toward the ground and resulting in him becoming paralyzed from the neck down.

### Subject Treestand

The subject treestand was a fixed treestand marketed by a U.S.-based manufacturer. Discovery documents, however, revealed that the treestand was actually designed and manufactured in mainland China, and the U.S. manufacturer was a shell company that falsely advertised the stand as being made in the United States. The treestand was comprised of a foot platform and a seat platform that were both connected to a vertical support (**Figures 1 and 2**).

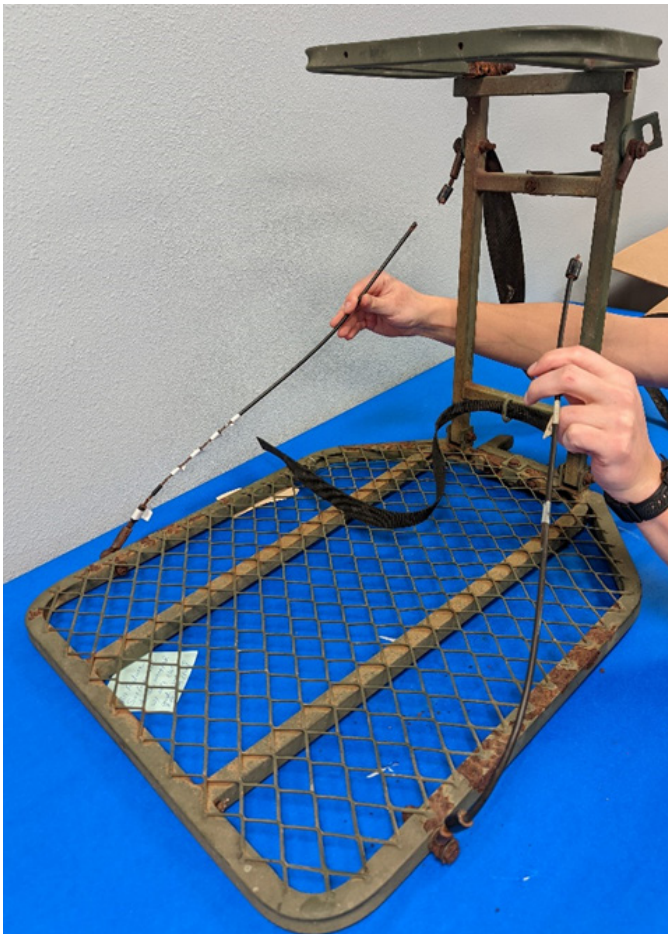


**Figure 1**

Image of the subject treestand taken by the authors.

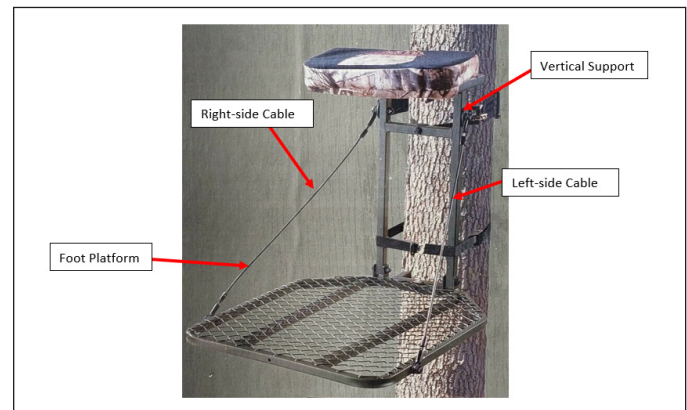


**Figure 2**

Image of a treestand from the owner's manual, labeled to show the components of the subject treestand.

The vertical support and seat platform are able to fold flat against the foot platform for easy transport. Two galvanized steel cables support the weight of a person standing on the foot section when unfolded.

According to the manufacturer’s documentation, the treestand frame was made of Q195 steel with a stated yield strength of 340 MPa, tensile strength of 425 MPa, and “percent elongation” of 39%. A certificate of quality was provided with the raw steel used in manufacturing, verifying that the steel met the above mechanical properties. However, the manufacturer’s documents did not state the type, grade, make, or quality of the galvanized steel utilized in the construction of the cables. In addition, a quality certificate for the galvanized steel cable was not provided.

**Observations Regarding the Nature and Sequence Of Cable Failures**

The two galvanized steel cables that support the foot platform were found to have separated at their connection points to the vertical support (Figure 1). Evidence of corrosion was observed on the cables, the cable eyelets, and their attachment bolts.

The left-side cable also failed adjacent to the eyelet in the segment between the copper crimp and the eyelet (Figure 3). The right-side cable failed near where it connects to the frame’s vertical support. The right-side cable broke between the copper crimp and the plastic-coated section of the cable (Figure 4). Brittle fracture failure of the right-side cable occurred immediately adjacent to the copper crimp near the vertical support (Figure 4).

Near the foot platform, the right-side cable eyelet is

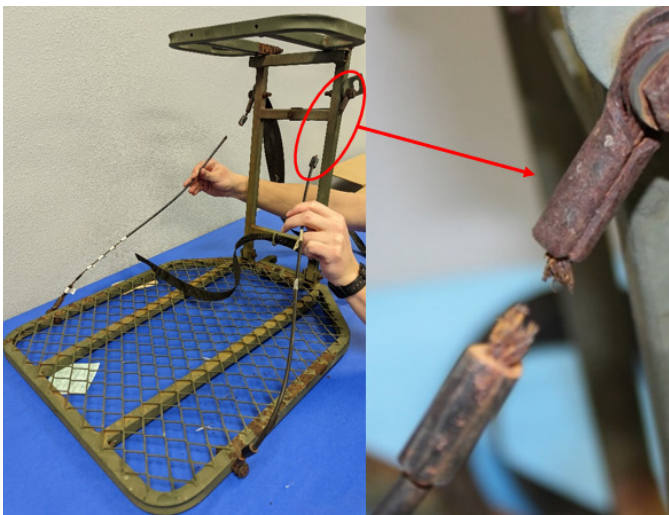


**Figure 3**  
Failure location on the left-side cable.



**Figure 4**  
Subject treestand showing failure location of the right- and left-side cables.

attached backward, which likely introduced additional bending stresses on the cable at the area next to the eyelet. This segment of the cable between the eyelet and the copper crimp showed moderate signs of fraying attributable to ductile overload, as evidenced by the elongated fractured tips of the individual wire strands in the frayed area (Figure 5). As evidenced by the ductile nature of the individual strand failure, the fraying observed in the segment of the cable between the crimp and eyelet near the foot platform was limited to the loading experienced during the failure event due to overload and not a condition that pre-existed the failure.



**Figure 5**  
Right-side cable foot platform attachment and the frayed segment between the eyelet and crimp with focus on elongated strands, characteristic of ductile failure.

Based on the analysis of the right- and left-side cables, it was determined that the failure of the cables did not occur simultaneously. The failure of the left-side cable likely occurred first due to corrosion degradation and loss of strength in the cable segment between the eyelet and copper crimp, as shown in **Figure 3**. The corrosion degradation and the ensuing loss of strength in the failed segment of the left-side cable are evidenced by the fact that the cable segment adjacent to and below the crimp — having one-half of the cross-sectional area as the failed area and subjected to the same forces — did not fail.

Following the failure of the left-side cable, the right-side cable was subjected to dynamic loading that resulted in brittle failure of the right-side cable at the segment adjacent to and just below the copper crimp due to the small cross-sectional area of the cable combined with stress concentration effect of the copper crimp at this location (**Figure 4**). Additionally, this dynamic loading of the right-side cable, following the failure of the left-side cable, is evidenced by the fraying of some wire stands near the foot platform, as shown in **Figure 5**. Further evidence of dynamic loading of the right-side cable, following the failure of the left-side cable, can be seen in the brittle fracture of the cable coating next to the failed cable segment as well as outward bending of the cable segment between the copper crimp and the eyelet (**Figure 6**).

**Mechanisms of Corrosion**

Corrosion is the degradation of a material due to chemical reactions on its surface. A common example is the exposure of iron to an electrolyte (such as water), resulting in chemical reactions that reduce the iron to iron-oxide (common rust)<sup>9</sup>. While coatings such as paint or powder coating can reduce the corrosive effect of a medium on steel components, more effective methods include galvanization and alloying with more noble materials (stainless steel)<sup>10</sup>.

It is well known that corrosion significantly reduces a steel component’s cross-sectional area and reduces



**Figure 6**

Signs overload on the left-cable eyelet attached to the foot platform and signs of brittle failure of the polymer coating.

mechanical properties, such as fracture toughness and yield strength, which can result in failure of components at or below normal and expected operating loads<sup>11-14</sup>.

Galvanic corrosion refers to a type of corrosion caused by the coupling of two dissimilar metals. When two metals with different galvanic potentials are connected in a manner that allows for the flow of electrons from one material to the other, a galvanic cell is created. In this cell, the material with the more negative potential plays the role of the “anode,” while the material with the less negative potential plays the role of the “cathode” in the galvanic cell.

The anode liberates electrons from itself, which are then transferred over to the cathode in order to provide these electrons for the chemical reactions that are spontaneously occurring on the cathode’s surface. In effect, this arrangement causes the anode of the galvanic cell to corrode preferentially while the cathode is protected<sup>15,16</sup>. The galvanic series (**Figure 7**) illustrates the average galvanic potential of a variety of engineering materials, providing

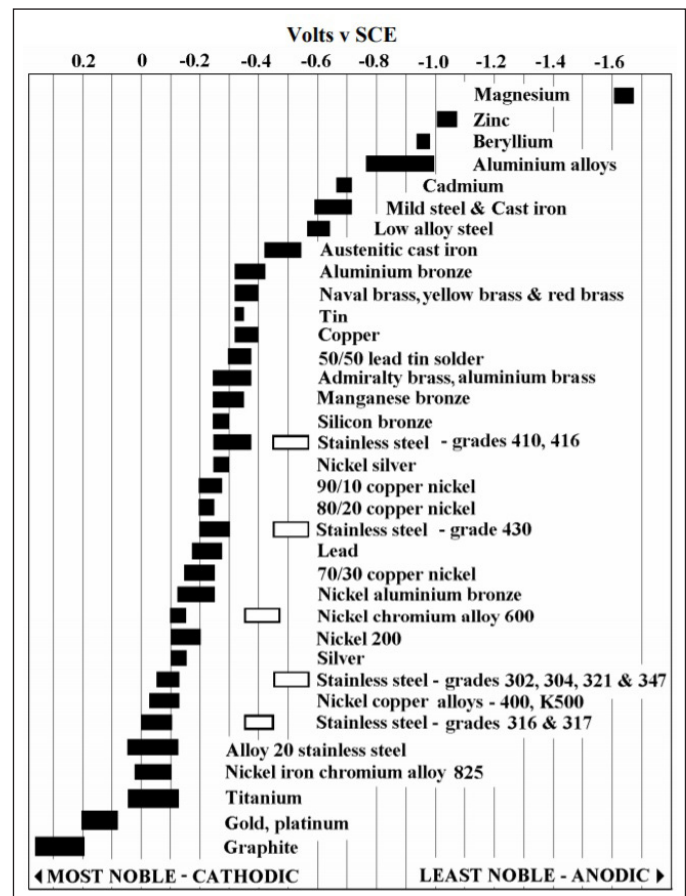


**Figure 7**

Galvanic series, showing the electrochemical potential of various materials.<sup>17</sup>

insight into which materials in a couple would act as an anode and which would act as a cathode.

Galvanization is the process of coating iron or steel with a layer of zinc in order to provide increased protection against corrosion<sup>18</sup>. Due to its relatively more negative galvanic potential, the zinc will preferentially corrode and protect the nearby or underlying iron or steel from degradation. However, over time, this zinc layer will be depleted, leaving the underlying steel susceptible to corrosion. An illustration of the galvanic connection between zinc and steel is shown in **Figure 8**.

Should a galvanized component be connected to more cathodic material, selective leaching of the zinc coating will occur. The zinc coating will liberate electrons and suffer from degradation to provide the driving voltage for the corrosion reactions that occur at the site of the cathodic material. In addition, the more corrosion-active sites on materials like steel greatly increase the electron drawn from the anodic material. Not only is it now having to protect this new material, but it is also having to do so at a greatly accelerated rate — far beyond what was intended in its design.

Another potentially more damaging form of corrosion is crevice corrosion. In general, crevice corrosion refers to corrosion of a material due to stagnant electrolyte (such as water) in a restricted environment or “crevice.” The corrosion reactions, which occur over time, gradually alter the chemistry of the entrapped electrolyte. This can take the form of the depletion of oxygen, acidification of the electrolyte due to corrosion byproducts, destruction of protective layers, or the buildup of aggressive ions.

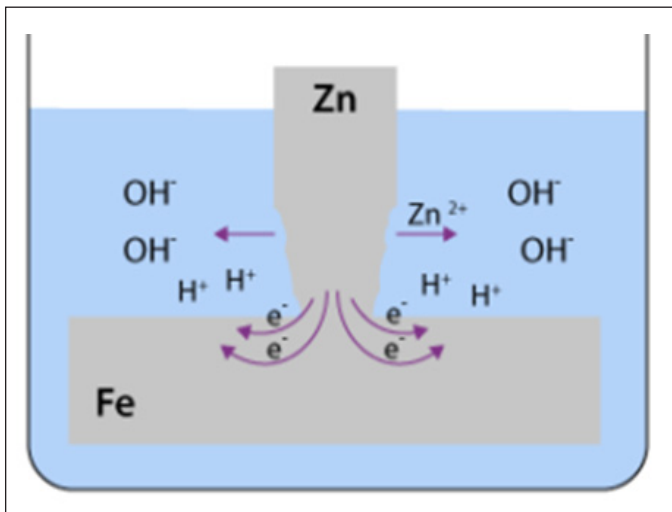


**Figure 8**

Galvanic corrosion of zinc and steel.<sup>19</sup>

The most common form of crevice corrosion is a differential oxygen corrosion cell — where the oxygen in the crevice is depleted over time, causing the crevice to become an anode in a galvanic cell with parts of the material not subjected to this crevice environment<sup>20</sup>. The other most commonly recognized form of crevice corrosion is the acidification of the crevice environment. This typically works alongside differential oxygen corrosion and results in the reduction in the pH of the local environment, causing corrosion to occur more rapidly due to the abundance of corrosive ions.

### Cable Analysis

The subject cable was made from  $\frac{1}{8}$ th-inch 7-7 galvanized steel cable. Due to its lower electrical potential and zinc's passive oxide layer's lower inherent susceptibility to corrosion, this zinc coating protects the underlying steel from corrosion.

Minimal sectioning of the subject cable's black polymer coating revealed iron oxide (rust) underneath the plastic-coated section (**Figure 9**). The galvanized zinc coating was noted to be depleted as such corrosion could only have occurred after a substantial portion of the zinc coating was depleted.

In order to determine the amount of zinc depletion at various locations along the subject cable, the surface elemental composition was analyzed at six different sections through energy-dispersive x-ray spectroscopy (EDS). Individual wire samples were carefully extracted from these locations and subject to the EDS analysis. The results from the EDS are shown in **Figure 9**.

As seen in **Figures 10** and **11**, the average percent composition of zinc decreased as samples were taken closer to the foot platform. This phenomenon is consistent with the zinc being selectively leached by the cable eyelet, copper crimp, uncoated wire, and foot platform.

The cables on the subject treestand were bolted onto the foot platform through the cable eyelets (**Figure 12**). Although three plastic washers were used to separate the bolt, eyelet, and foot platform, an electrical connection was still present between the bolt threads and edge of the



**Figure 9**

Iron oxide (rust) present underneath the subject cable's plastic coating.

frame’s square tubing. This configuration allowed the galvanized cable to be electrically connected to the eyelet, screw, and to the frame of the treestand itself. This connection allowed for the creation of a galvanic cell, which then caused selective depletion of the zinc from the galvanized steel wire near its connection to the vertical support.

	# of EDS Readings	Average % Zinc	Maximum % Zinc
WS1	13	0.26%	1.10%
WS2	15	11.93	29.20%
WS3	9	12.28%	32.20%
WS4	7	15.29%	44.10%
WS5	12	27.38%	64.10%
WS6	9	33.88%	

**Figure 10**

Variation of zinc content on the subject cable as a function of distance from the frame (WS1 closest to frame; WS6 farthest from the frame).



**Figure 11**

Limited sectioning of the subject cable’s black polymer coating to expose wire stands and to measure zinc content in the cable.



**Figure 12**

Connection between the foot platform and left-cable eyelet on the subject treestand.

The bolts connecting the cable eyelets to the vertical support of the treestand have 55 mm of thread — around 10 mm longer than the bolts used on the foot platform, which provides more surface area for corrosion to occur on and accelerate the depletion of the cable’s zinc coating. It can also be seen that a bracket intended for use with the tree strap is affixed to these bolts. While washers are present at this connection as well, there is no washer separating the bolt nut and vertical support (**Figure 13**). This results in an enhanced electrical connection between the treestand and galvanized cable, further accelerating zinc depletion. It is likely that the increased corrosion of these nearby components caused more rapid dealloying of the galvanized steel cables, which resulted in the cables failing near their attachments to the vertical support where the cable’s degradation and loss of nominal strength was greatest.

According to the owner’s manual, one is intended to use washers as shown in **Figure 14**. However, there are no warnings in the owner’s manual (or on the treestand itself) that warn a user of the danger associated with not placing the washers on correctly. Even if a user installed



**Figure 13**

Connection between the vertical support and left-cable eyelet on the subject treestand, displaying the direct coupling of the nut and frame.

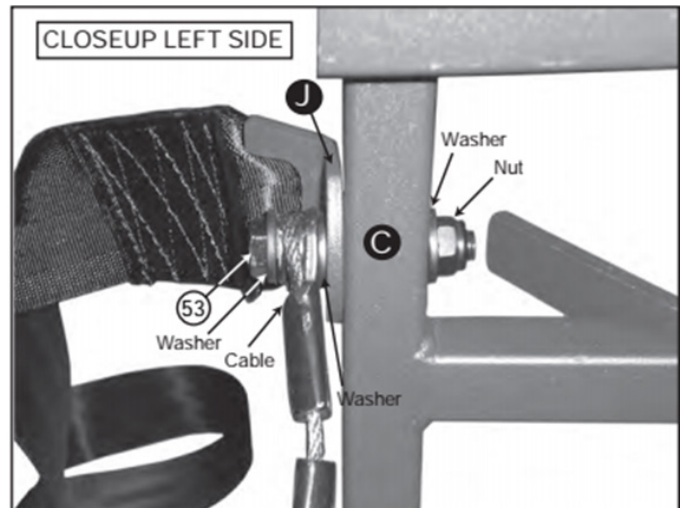


**Figure 14**

Diagram from the owner’s manual showing how to assemble the vertical support connection.

the washers exactly as shown in the owner's manual, the lack of an additional washer behind the bracket allows yet another large piece of metal to be electrically connected to the galvanized cable and provide an even larger surface for contact with the vertical support, enhancing the strength of the electrical connection and thus the rate of corrosion<sup>21</sup>.

It is well known that relatively small anode-to-cathode area ratios will corrode significantly faster at the anode than relatively large anode-to-cathode area ratios<sup>21</sup>. For the subject cable, the relative surface area of the exposed galvanized steel was significantly smaller when compared to the large surface area of the exposed surface on the bolt, eyelet, and treestand frame. As a result, the protective zinc coating of the galvanized cable depleted at a significantly higher rate in order to protect all the components it was connected to.

Both the right- and left-side cables were fitted with copper crimps that secured the cable around each eyelet. As shown in **Figure 15**, copper has a less negative electrical potential than both steel and zinc, meaning that both of these metals (when in contact with copper) will preferentially corrode to protect the copper piece.

The American Galvanizers Association (AGA) states that rapid corrosion of zinc may occur if there is contact between galvanized materials and copper with the two metals being considered incompatible in a marine atmosphere environment — much like the one present in the subject incident due to its close proximity to the shore<sup>23</sup>. The AGA states that precautions should be taken to prevent electrical contact between the two metals.

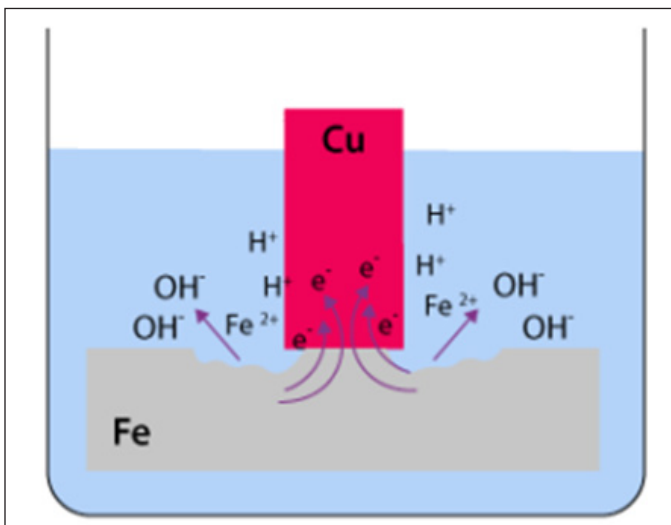


**Figure 15**

Galvanic reaction resulting from the coupling of copper and iron.<sup>22</sup>

By using copper as their crimping material, the manufacturer introduced yet another galvanic coupling of the cable material to a dissimilar metal, which caused the zinc layer on the subject cables to corrode faster than it would have due to its connection to the steel alone. After the zinc layer was sufficiently depleted, this would then accelerate the corrosion of nearby steel wire stands and significantly increase the likelihood of cable failure.

Stagnant water, which accumulated in the cable wire ropes (due to the ends of the cables being exposed), was the electrolyte through which corrosion was facilitated. It is likely that crevice corrosion within the coated sections of the wire ropes played a role in their degradation. Even so, a greater degree of zinc depletion noted closer to the eyelet — with the greatest depletion occurring on an exposed section of the wire as well as the wire rope failure occurring at these exposed sections as well. These facts indicate that, more likely than not, crevice corrosion was not the driving factor in the observed corrosion and that a galvanic cell was responsible for the initial depletion of the zinc layer, allowing for severe corrosion to occur on the exposed wire ropes and ultimately resulting in the failure of the supporting cables.

### Accelerated Corrosion Testing

In order to quantify the degree to which the coupling of the galvanized steel cable with the treestand increased corrosion, accelerated corrosion testing was performed on an exemplar treestand from the manufacturer (**Figure 16**),



**Figure 16**

Exemplar treestand utilized in accelerated corrosion testing.<sup>22</sup>

and in accordance with ASTM G31 “Standard Guide for Laboratory Immersion Corrosion Testing of Metals” and ASTM G71 “Standard Guide for Conducting and Evaluating Galvanic Corrosion Tests in Electrolytes.”

Multiple 1.25-inch-long samples of 1/8th-inch 7-7 galvanized steel cable were cut to size and weighed (Figure 17). In order to maintain a similar ratio of exposed wire-to-treestand surface area as that used in the full-scale treestand, the foot platform of the exemplar treestand was sectioned into 5"x5" square samples, with the bolt hole at the middle of the frame side (Figure 18). Where there was no bolt hole along the frame’s edge, additional 5"x5" square samples were cut from the remaining part of the frame, and a 5/16th-inch hole was drilled into the frame to emulate the bolt hole present on the first two samples. The defense refused to (or was not able to) provide information regarding the OEM hardware for the drilling of these holes. As such, these holes were drilled utilizing an industrial drill press in the possession of the Texas Tech Department of Mechanical Engineering. Each 5"x5" square treestand section used in the authors’ corrosion tests consisted of a portion of the



**Figure 17**  
Cable samples used in corrosion testing.

foot platform, a 5" portion of the frame, with one of the 45 mm bolts and three provided washers (Figure 19). The weight of each sample comprised of the above components was recorded.

Two separate baths of 1.025 specific gravity saltwater (typical of seawater salinity) were prepared for the immersion of the coupled cable and treestand samples. The cable and treestand immersed in each bath were then galvanically connected via Rodeostat potentiostats, which were programmed to monitor the current flowing between the samples. In addition, two cable samples and two treestand samples were each suspended in separate baths of 1.025 saltwater in order to measure their corrosion rate in the absence of a galvanic connection between the wire and treestand.

After 10 days (240 hours) of continuous immersion in saltwater, both the cable and treestand samples were removed from the test baths. The cable samples were then dried, cleaned via an ultrasonic bath, and weighed in order to quantify the amount of their corrosion based on their mass-loss. Based on mass-loss measurements for each sample, the corrosion rate of the samples and the effect of the galvanic coupling on increasing the corrosion rate were determined. As shown in Figure 19, the galvanic coupling between the wire and treestand frame was shown to increase the rate of corrosion by around 300%.

In order to verify the result of the galvanic immersion testing, accelerated corrosion testing utilizing direct physical connection between the wire and treestand frame was performed (Figure 20). Four treestand samples and four cable samples were prepared. Two treestand samples had a cable sample affixed to the bolt threads via zip ties in order to simulate a connection between the bolt and cable eyelet. The remaining two treestand samples and two cable samples were left separate to determine the effect of coupled vs. uncoupled wire and frame samples.

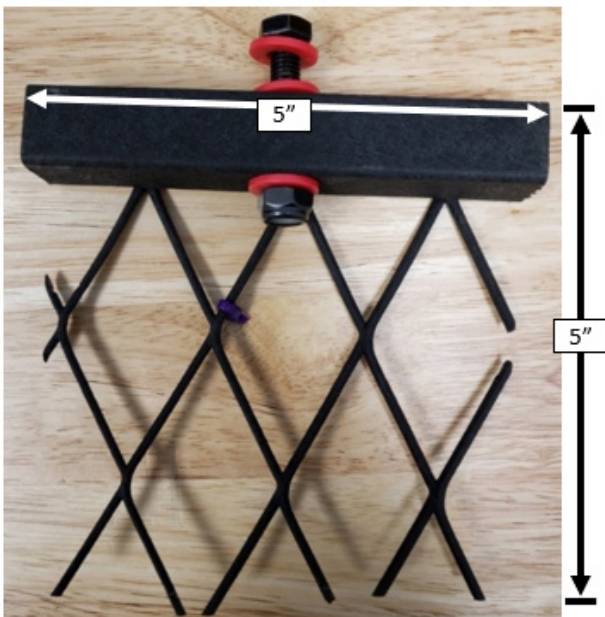


**Figure 18**  
5"x5" square samples utilized in corrosion tests.

	Average Corrosion Rate		
	Total Mass Loss grams / 240 hours	Equivalent radius reduction mm per year	Coupled vs. Uncoupled % Increase
Coupled Treestand and Galvanized cable	0.0509	3.0085	300%
Uncoupled Galvanized cable	0.0127	0.75065	

**Figure 19**  
Mass-loss based corrosion rates for coupled vs. uncoupled cable/treestand samples utilizing accelerated immersion testing with connections made via potentiostats. Radius reduction per year was calculated via equations provided in ASTM G1.



**Figure 20**

Sample of treestand and wire physically connected via zip ties.

The samples were then immersed in separate baths and left immersed for 10 days, after which they were removed, dried off, cleaned, and weighed for mass loss. The average corrosion rates of the cable for the coupled wire and frame as well as the uncoupled sample are shown in **Figure 21**.

Based on these results, the direct-connection test result showed that the galvanic connection increased the corrosion of the cable by ~79%. This lower percent increase in corrosion rate of 79% for the direct-connection samples as compared to the 300% increase in corrosion rate obtained from potentiostat measurements (**Figure 19**) is due to the imperfect and limited connection between the wire and bolt (**Figure 20**). It would be expected that the connection between the bolt and treestand would be better than this, so the overall corrosion rate of the subject treestand would likely lie somewhere between the results shown in **Figure 19** and **21**.

**Cyclic Voltammetry Testing**

In order to further verify the results of the accelerated corrosion testing, cyclic voltammetry was also utilized as yet another method for evaluating the increase in corrosion rate of the cable as a result of galvanic coupling with the treestand frame.

Cyclic voltammetry is an electrochemical analysis for measurement of corrosion rate between two dissimilar

	Average Corrosion Rate		
	Total Mass loss grams / 240 hours	Equivalent radius reduction in mm per year	Coupled vs. Uncoupled % Increase
Coupled Treestand and Galvanized cable	0.01395	0.8245	79%
Galvanized cable alone	0.007795	0.4607	

**Figure 21**

Direct connection corrosion rates.

metals. A potentiostat was used to alter the natural difference in potential (measured in volts) between the coupled cable and treestand (as well as uncoupled) while measuring the resulting current response to voltage alterations, which was then used to arrive at the corrosion rate of the coupled and uncoupled cable and treestand frame specimens.

To describe the cyclic voltammetry technique in general, a potentiostat is connected to three electrodes. These electrodes (working, counter, and reference) are used in order to provide data to the potentiostat. The working electrode is attached to the material whose properties one wishes to determine while the counter electrode is attached to a platinum rod or sheet to provide an electrically neutral material for the working electrode (cable or treestand segment in this case) to be coupled to, and the reference electrode is attached to an Ag/AgCl reference cell that will correct for any potential variation. The potentiostat then cycles the potential (voltage) from low to high while measuring the produced current response. Then the measured current vs. applied potential are plotted (**Figure 22**) to determine various electrical properties of the working electrode material. By transforming this plot into a “Tafel”

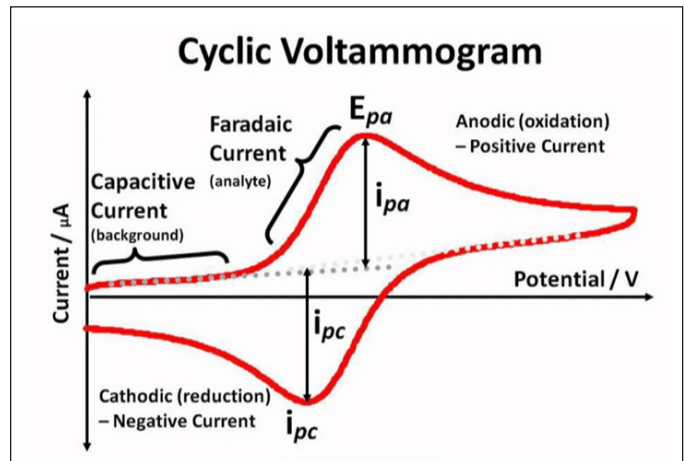


**Figure 22**

Graph of a cyclic voltammetry scan.<sup>24</sup>

plot (**Figure 23**), one can then extract the Tafel constants, corrosion current, and galvanic potential for each tested material. After these values have been determined for both materials, one can use the Mixed Potential Theory to find the coupled corrosion current and potential. Overlaying the two Tafel plots (**Figure 23**) allows one to find their intersection and extract the corrosion current and potential for the coupled configuration.

Results show that for two similarly sized pieces of galvanized steel cable and treestand steel, a galvanic couple increases the corrosion rate of the cable by around 175% (**Figure 26**). The cyclic voltammetry analysis displayed a slightly lower corrosion rate than the initial mass-loss analysis given in **Figure 19** (313%) but a higher corrosion rate than direct connection test results in **Figure 21** (79%). This lower rate (when compared to mass-loss results of

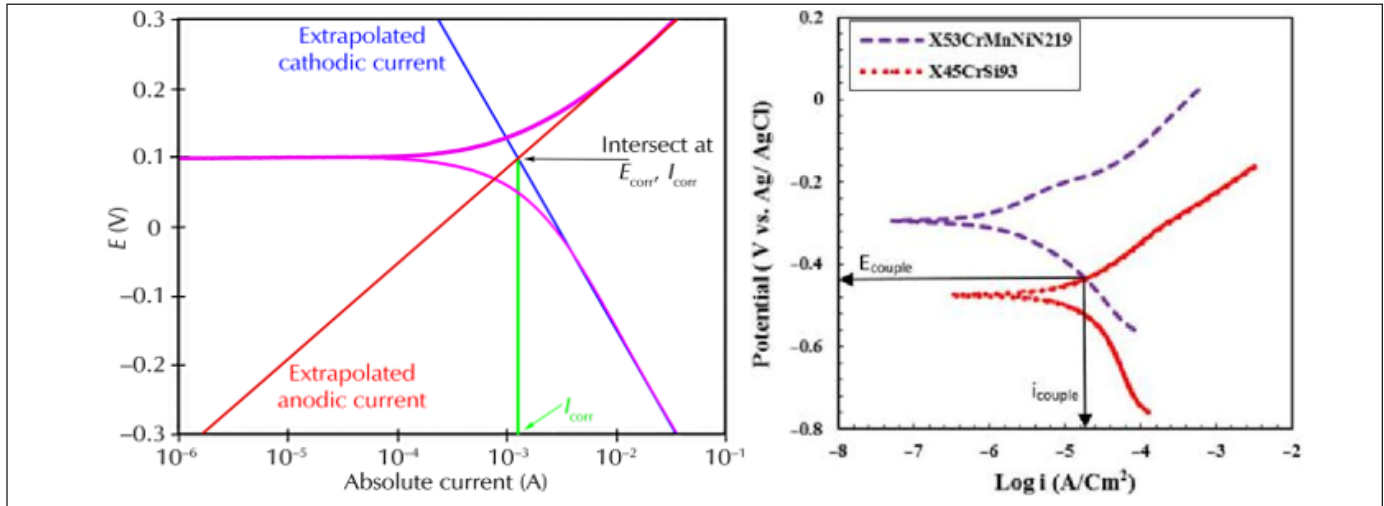


**Figure 23**

Tafel plot and data that can be extracted from it (left) and combination of Tafel plots to determine the effect of a galvanic connection (right)<sup>25,26</sup>.

Following the above-stated procedure for cyclic voltammetry, a platinum counter electrode and an Ag/AgCl reference electrode were placed in a bath of reverse osmosis water containing 0.008 moles of iron(III) chloride (FeCl<sub>3</sub>). Since the Ag/AgCl electrode and platinum electrode used in this study were small, a strand of cable material and a smaller segment of treestand frame (**Figure 24**) had to be used in relation to the size of electrode. The cable and treestand samples were individually connected to the working electrode and subjected to a voltage sweep while recording the corresponding current response.

The potential and corresponding current were plotted and converted to a Tafel plot from which the galvanic potential, corrosion current, and Tafel constants were extracted (**Figure 25**). The corrosion currents for the galvanized steel cable by itself and the cable galvanically connected to the treestand were then converted to corrosion rates via Faraday’s Law, as given in ASTM G102.

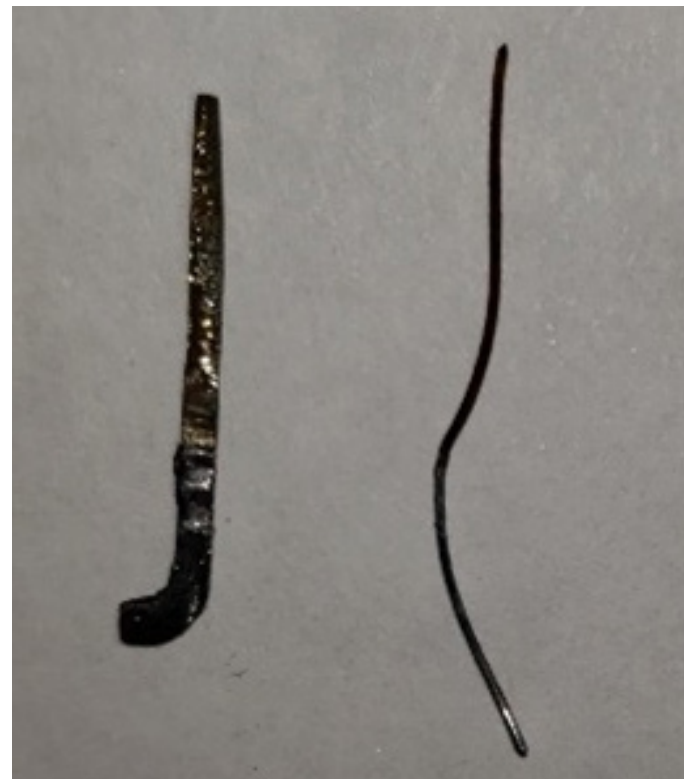


**Figure 24**

Treestand frame material (left) and cable strand (right) used in CV testing.

$$\text{Corrosion Rate} = K_1 \frac{I_{\text{corr}}}{\rho} EW$$

Where:  $K_1 = 3.27 \times 10^{-3}$  in mm g/ $\mu\text{A cm year}$   
 $I_{\text{corr}}$  = corrosion current density in  $\mu\text{A/cm}^2$   
 $\rho$  = density in g/cm<sup>3</sup>  
 $EW = \frac{\text{Atomic weight}}{\text{number of electrons required to oxidize an atom of the element}}$

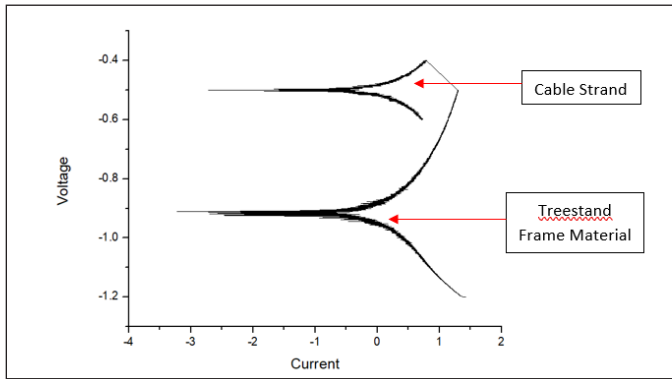


**Figure 25**

Tafel plots extracts for treestand frame material and cable strand.

	Cyclic Volt Corrosion Rate		
	Corrosion Current ( $\mu\text{A}/\text{cm}^2$ )	Equivalent radius reduction in mm per year	Coupled vs. Uncoupled % Increase
Coupled Treestand and Galvanized cable	105.4	1.5789	175%
Uncoupled Galvanized cable	38.34	0.5744	

**Figure 26**

Corrosion rate of coupled and uncoupled cable and treestand frame, utilizing cyclic voltammetry.

Figures 19 and 21) is due to the fact that our CV analysis was conducted with cable strand samples that had the same surface area as the treestand material as opposed to being proportionally smaller — as was the case in the direct connection tests and mass-loss analysis utilizing potentiostats.

In summary, the percent increase in corrosion rates of coupled cable/treestand frame samples was determined utilizing three different approaches, namely: 1) the accelerated immersion testing utilizing a potentiostat; 2) direct connection mass-loss based analysis; and 3) cyclic voltammetry. As shown in Figure 27, these percent increases were determined to be 300%, 79%, and 175%, respectively.

As previously stated, the subject treestand was in use for approximately four years prior to the incident at issue. Given the fact that direct coupling of the cable to the treestand frame resulted in a significant increase in corrosion rate of the support cable as shown earlier, Figure 28 shows the additional time (in years) that would have been necessary for the cable to reach the degree of corrosion that caused its eventual failure, had it not been directly coupled with the treestand’s frame.

**Similar Previous Incidents**

Discovery documentation revealed a number of previous incidents similar to the one that occurred in the subject incident (i.e., involving failure of the company’s treestands due to cable corrosion). In the first of these similar incidents, failure was observed in the segment between the right-cable eyelet and copper crimp near the vertical support. However, in the case being investigated here, the left-cable and right-cable both failed in the segment between the crimp and cable eyelet (Figure 29).

As in the previously reviewed incident, the second similar incident the authors reviewed showed that both

Test Method	% Increase in Corrosion Rate of Coupled Cable/Treestand Samples
Accelerated immersion Testing with Potentiostat Connection	300%
Accelerated immersion Testing with Direct Connection	79%
Cyclic Voltammetry	175%

**Figure 27**

Percent increase in corrosion rate of coupled cable/treestand frame samples as compared to uncoupled samples.

Test Method	Additional Time Before Cable Would Have Reached Failure
Accelerated immersion Testing with Potentiostat Connection	12 Years
Accelerated immersion Testing with Direct Connection	3.16 Years
Cyclic Voltammetry	7 Years

**Figure 28**

Additional time (years) before cable would have reached failure as determined by the various test methods conducted.



**Figure 29**

Failures observed on the treestand of the first similar incident with both failures occurring between the eyelet and crimp.

cables failed at the segments between the eyelet and crimp near the vertical support (**Figure 30**). The fracture surface of the right-side cable showed clear signs of ductile failure. Fraying of the right-side cable was observed in the segment between the cable eyelet and the crimp due to dynamic loading experience when the other cable failed suddenly, shifting the force to this side — similar to what happened in the subject incident.

In the third similar incident, both the right and left cables failed just below the eyelet affixed to the vertical support. The bolts on this section were attached backward with the nut directly adjacent to the eyelets (**Figure 31**). As in other cases, the important factor to note is the fact that the thicker cross-section of the cables failed before the thinner cross-section below the crimp indicates that the segment between the crimp and eyelet experienced severe degradation of its strength due to corrosion as a result of galvanic coupling between the cable, copper crimp, and treestand frame. Fraying of the cables similar to the previous incident was observed (**Figures 32 and 33**). This fraying and the elongated strands suggest the occurrence of ductile overload.

The fourth similar incident involved a newer model of the manufacturer’s treestand. As shown in **Figure 34**, newer models of the manufacturer’s treestands come with a thermoplastic coating over the cables. This coating, however, is loosely attached and allows water to easily seep and become trapped on the inside, corroding the cable. At the same time, the coating prevents users from observing the degradation state of the cables.

The fifth similar incident involved a hang-on treestand

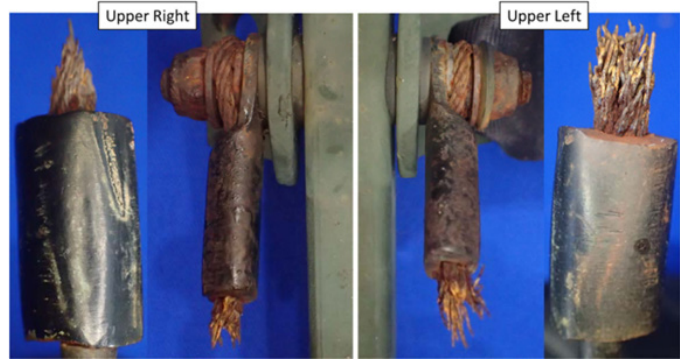


**Figure 31**

Locations of failure observed on treestand in the third similar incident.



**Figure 30**

Cable failure in the second similar incident.

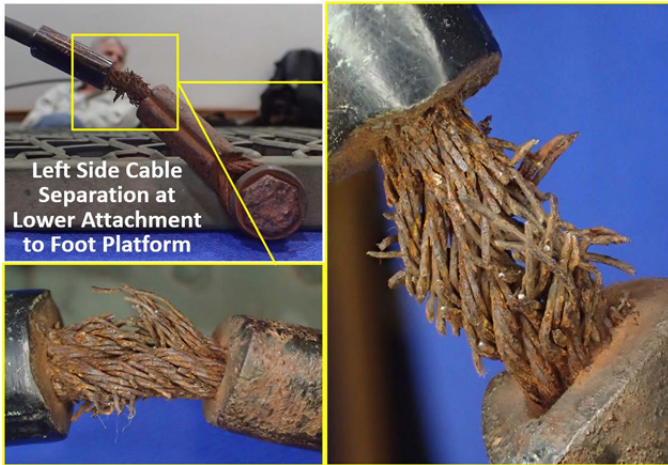


**Figure 32**  
Fraying of wire strands in the segment between the eyelet and crimp that occurred following the initial failure.



**Figure 33**  
Close-up view of cable failure in the third similar incident.



**Figure 34**  
Failed cables the fourth similar incident.

produced by the manufacturer. The documents for this incident included an expert report on behalf of the plaintiff. In this report, the expert explains that even though the treestand was intermittently used, it suddenly failed after five years of use. As shown in **Figure 35**, the support cables fractured between the cable eyelet and copper crimp at the attachment point in the vertical support. Similar to the authors' analysis, the expert determined that the failure was due to accelerated corrosion degradation of the cables due to a galvanic coupling between the copper crimp and galvanized steel cable material.

A report from the CPSC describes an incident involving a similarly constructed treestand<sup>27</sup>. In this incident, the treestand, which had been installed for two hunting seasons and stored in the user's garage during the off-season, failed when the user was attempting to take down the stand at the end of this second hunting season. The failure occurred when one of the corroded cables holding up the foot platform broke (**Figure 36**), which caused the user slip off of the stand, although his fall arrest harness broke his fall. Examination of the treestand and similar stand owned by the user revealed that their cables were also corroded and showing signs of degradation failure.

Despite the large number of previous similar incidents, both to their own products and the products of companies they shared designs with, the manufacturer made



**Figure 35**  
Failed cables from the treestand in the fifth similar incident displaying extensive corrosion.



**Figure 36**

The failed cable on the climber treestand fractured between the copper crimp and plastic coating, showing the same design as the subject cable in the subject case.

no attempt to release a safety notice or recall the subject treestand. The number of previous incidents should have alerted the manufacturer to the propensity of its treestand cables for corrosion and the danger that they presented. As such, the subject failure was reasonably foreseeable by the manufacturer — yet it made no attempt to fix its design or warn users of the hazard it presented.

### Testing Conducted by the Manufacturer

According to testing documentation provided, the manufacturer did not perform environmental testing on the subject treestand in order to determine its suitability for outdoor use.

The current president of the manufacturer asserted that it would have been impossible for them to do environmental testing on the subject treestand due to different environments it could be exposed to. Therefore, the manufacturer decided to not test its design to any of these possible environments instead of performing testing according to the worst foreseeable environment, as is standard practice in engineering design.

A reasonably prudent manufacturer would have considered corrosion as a foreseeable degradation mechanism for a product designed for outdoor use. Had the manufacturer performed accelerated corrosion testing to simulate outdoor environment usage, it would have observed that the subject treestand (in its as-designed condition) was unreasonably susceptible to corrosion and degradation of the cable system, which is the most significant load-bearing component of the treestand.

### CPSC Hierarchy of Controls

The hierarchy of controls represents the necessary steps for elimination or reduction in the probability of exposure to a known hazard<sup>28</sup>. **Figure 37** is a graphic representation of the hierarchy of controls. These well-established and universally utilized controls begin with the most effective measures for hazard reduction and continue

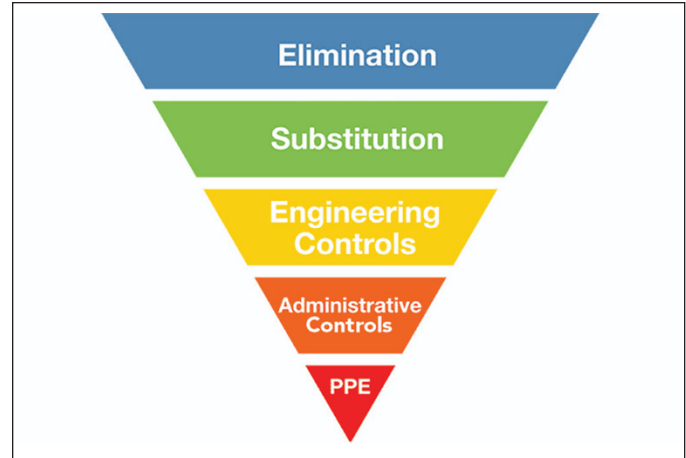


**Figure 37**

Engineering Hierarchy of Controls.<sup>29</sup>

to lesser effective measures. These steps, in order of effectiveness, are elimination, substitution, engineering controls, administrative controls, and PPE.

The engineering hierarchy for reducing/eliminating hazards requires that a known hazard should be eliminated by designing the hazard out of the system when possible. If a hazard cannot be eliminated through design, the next step is to guard against the hazard.

### Analysis of Warnings and Non-Compliance with Safety Engineering Principles

As mentioned in the section on the Hierarchy of Controls, one must eliminate a hazard by designing it out of the system when possible. If elimination of a hazard through design is not feasible, one is to utilize the next most effective means of controlling a hazard. Merely warning a user of a hazard when it is economically and technologically feasible to address the said hazard through more effective means of hazard control is in gross violation of this basic safety engineering principle.

Several factors contribute to the low placement of warnings on the hierarchy of controls. As indicated later in this paragraph, the main reason for this low placement is the fact that all warnings partly rely on the user's understanding and executing the warning's instructions in order to be effective — an approach that is highly unreliable, especially when more effective means that do not rely on human interaction exist.

The effectiveness of warnings depends on the user and a variety of psychological factors that can influence how the user reads, understands, and interprets warnings given to them. For example, users might feel they are “educated”

and ignore a series of warnings or not read them thoroughly enough out of a feeling that they already know what it's going to say — or that they are already knowledgeable enough about the topic<sup>30,31</sup>. Exposing the user to too many warnings within a small area (or within a short period of time available for the user to digest them) can cause the reader to either become desensitized to the stated hazards or simply ignore the warnings altogether. This is a well-known phenomenon in safety engineering referred to as “overwarning.”<sup>32</sup> It should also be reasonably expected that a user could gloss over or forget certain warnings<sup>31</sup>. For this reason, standards state that warnings for critical hazards should be placed on or near the hazard itself or be made in a manner that is too obvious to ignore. By doing so, users are reminded of the hazard each time they are in a situation that has the potential to expose them to it.

The above principles, which, if not considered, would render a warning deficient in design, are internalized in the ANSI Z535 family of standards, which are universally accepted among the safety engineering community. Requirements for the design, wording, and placement of warnings are given in ANSI Z535, all of which combine to form warning labels that effectively communicate the hazard to a user and ensure that, on a more-likely-than-not basis, the user would follow the recommendations of the warning for hazard avoidance.

In the subject incident, the owner's manual had a number of deficiencies that further reduced the effectiveness of its stated warnings. The owner's manual contained a total of 66 warnings, all of which lacked signal words and appropriate coloration, which were in direct violation of ANSI Z535 requirements. This large number of warnings also induces overwarning, and, when combined with the lack of proper warning designs, makes it highly likely that a reader would zone out and stop paying attention or just not bother to continue reading. Another deficiency of the subject treestand's warnings is the inadequacy of most of the warnings in describing why the warnings are there in the first place or what to look for in order to execute the instructions stated in the warning<sup>31-33</sup>.

The manufacturer claimed compliance with the requirements of TMA 02, yet fails to conform with the universal requirements of ANSI Z535, which supersedes the TMA standards. The instructions and warnings provided by the manufacturer, in fact, are in direct violation of many of the safety engineering principles underlying warnings discussed earlier. Specifically, TMA 02 fails to give proper instructions regarding proper signal words, coloration,

and warning information as outlined in ANSI Z535. Contrary to the teachings of ANSI Z535, Section 6.5.1.1 of TMA 02 states: “The warning label must contain the signal word ‘WARNING’ and be preceded with or follow the words ‘failure to follow all warnings listed could result in serious injury or death’.” These requirements result in “overwarning” and “warning fatigue,” which are specifically discouraged when designing an effective warning. In all likelihood, the warnings/instructions accompanying the subject treestand were not written with knowledge of the above principles of effective warning in mind. The fact that the manufacturer's warnings failed to account for these well-known phenomena highlights the deficiencies in TMA standards, which openly ignore the universally recognized ANSI Z535 guidelines.

As stated in Joseph Ryan's *Design of Warning Labels and Instructions*: “Warning labels that cannot be seen, or those that do not adequately describe the hazard, serve the same purpose as no warning label at all.” By giving too many warnings and instructions to the user in the owner's manual, the manufacturer's warnings are deemed deficient and in violation of well-accepted principles of effective warning design. Additionally, the manufacturer's failure to rank and differentiate between different levels of risk associated with different hazards encountered in the use of the treestand resulted in the most critical warnings not having proper emphasis to attract the user's attention, further reducing the effectiveness of the stated warnings.

On page 4 of the subject treestand's 2011 owner's manual, under the section entitled “Proper Care and Maintenance,” it states: “Inspect for defects (damage, rot, corrosion, cracks, freezing, excessive heat, etc.) before every use is required. Do not use if the damage is detected or suspected.” While this section of the owner's manual does talk about the need for inspection of the treestand for signs of corrosion, the discoloration observed on the exposed sections of the subject treestand's cables near the eyelets would not appear to be significant enough to an average user to conclude that the subject cable's mechanical strength was significantly degraded and unsuitable for use.

The plaintiff testified that he did not consider the rust present on the subject treestand to be an issue, as most equipment he worked with experienced similar rusting to some degree due to his proximity to the coastal environment. Furthermore, the above warning is stated only once among a plethora of other warnings about the treestand and placed on the final page containing warnings in the manual. Such an important warning should have been placed on

the treestand itself or, at a minimum, earlier in the manual and heavily emphasized in order to ensure readers were not desensitized by the number of warnings in the manual.

If the manufacturer wanted its users to inspect the treestand for corrosion, it should have placed a warning instructing them to do so on the body of the treestand — where it is more likely to be seen and followed on a regular basis. However, the warning label, which was affixed to the subject treestand, did not once mention corrosion as a factor that should be considered during inspections.

In the event that there was a similar treestand with corrosion damage that could have been apparent to the average user, the presence of a proper warning would make the user more likely to inspect the cables and come to the conclusion that they were in a dangerous condition. The plaintiff testified that if such a warning existed on the subject treestand, he would have followed it to the best of his ability.

The 2011 owner's manual for the subject treestand also states "DO NOT leave your treestand outside since weather or animals may cause damage. Tree growth can also cause stress and damage straps and buckles. It must be stored inside when not in use." This warning is once again stated once among a plethora of other warnings. As such, one could reasonably expect a user to gloss over or forget it.

A significant number of hunters are known to leave their treestands up on the tree between use. Since a user needs to hammer in climbing sticks and strap the stand on, some users (especially those advanced in age) might choose to forgo this hassle and simply leave the stand up in order to save time and avoid destroying a good hunting tree. In addition, the very design of a fixed treestand makes it difficult for users to attach and remove it on a regular basis, resulting in some to simply leave it up on the tree. Furthermore, the reference to its name as "fixed" treestand provides a connotation of the device being permanent and may contribute to a decision to leave the stand up on the tree — as one would assume a permanent device would be reasonably capable of withstanding the environment it is to be used in. The prevalence of users leaving up their treestand (and their reasoning to do so) is a foreseeable risk that a prudent designer should consider when constructing this type of product.

Various employees from the manufacturer have provided testimony stating that they know hunters will leave

their treestands up for extended periods of time. The former president stated in his deposition that they know hunters will not take the treestand down after each use — and that the stand will be fine if left up for a few weeks (if not months). The current president of the manufacturer expanded upon this and asserted that no matter what environment the treestand is left up in, the cable will be perfectly fine for at least two years. In addition, the original founder of the manufacturer stated that users can leave their treestands up for 11 months out of the year and have the stand still be in safe condition. Though all of these representatives define differing amounts of acceptable exposure, their combined testimony shows a clear understanding that hunters cannot be expected to take down their treestand after each use.

Magazine interviews with the executive director of the Treestand Manufacturers Association (TMA) and testimony from the employees of the manufacturer show that the industry not only knows many hunters leave up their treestands, but, to a degree, they also expect it<sup>34</sup>. If the manufacturer truly wished for users to not leave their treestands outside, they should have put this warning by itself on the treestand in bold, noticeable print so users would see it every time they use the treestand.

The founder of the manufacturer as well as their current president stated in their respective depositions that warnings have limited effectiveness and that they (as manufacturers) have an obligation to design out hazards when possible. They additionally stated that they should take into account known misuses of their product as well as the hazards this would create and design out as much as they can. Despite agreeing with this basic principle of engineering design, the manufacturer repeatedly placed the blame for the previous incidents involving cable failure on the user for not following their warnings. The manufacturer had a duty to go beyond merely warning the users about the hazards they knew about but failed to design out the hazards present in their design.

According to the CSPEC, between 2005 and 2007, a total of 41 treestand-related deaths were reported, and a total of 19,000 treestand related injuries were estimated to have occurred<sup>35</sup>. In addition to this high incidence of injury, researchers have found that falls from treestands have become the leading cause of hunting-related injury. For example, over a 10-year period in the state of Ohio, it was reported that around 50% of hunting related injuries were due to falls, with 93% of these falls being falls from treestands, while only 29% resulted from gunshot

wounds<sup>36</sup>. In 2014, the Indiana Department of Natural resources reported that in 182 reported hunting accidents over a five-year period, 55% involved falls from treestand<sup>37</sup>. A report by the CPSC found that nearly 40% of reported treestand incidents were due to a problem with the treestand<sup>38</sup>. Although most these studies do not indicate how many of these incidents were the result of user errors or product failures, combined with injury and fall reports from litigation and CPSC recalls, the manufacturer knew, or should have known, that there were unreasonably dangerous hazards present in their products that were not being sufficiently designed, guarded, or warned against.

The Executive Director of the Treestand Manufacturers Association stated in an interview that treestand cables are “notorious for failing<sup>34</sup>.” This once again shows a clear understanding within the industry that cable failures are an issue that needs to be addressed, yet nothing has been done to alleviate the potential for failure by utilizing common sense alternative designs.

The founder of the manufacturer stated in their deposition that it is ultimately their duty to design a safe product and that this design should, to the best of its ability, take into account and design out known hazards, as is recommended by the hierarchy of controls. The manufacturer failed to adhere to this duty and instead of designing out the hazard posed by their own cables, they negligently shifted the responsibility to the end user.

**Use of Safety Harness**

Treestand manufacturers recommend the use of safety harnesses, yet the use of such a device is not without its own risk. An HSC Contract Research report<sup>39</sup>, entitled “Harness Suspension: Review and Evaluation of Existing Information,” presents a study conducted on the Wright-Patterson Air Force Base in Ohio, in which young, healthy individuals were suspended in four different designs of full-body harnesses. During the study, the tests were terminated when either the test subject voluntarily chose to end the study (due to symptoms including nausea, tingling, and numbness of the extremities) or on-site medical professionals chose to end the test. The average suspension time was 14.38 minutes before the test was terminated. Further, an OSHA Safety and Health Information Bulletin (SHIB) 03-24-2004<sup>40</sup> describes the hazards associated with suspension trauma. It states that a worker using a fall arrest system, if not rescued from the harness, can experience venous pooling, which can result in death in as little as 30 minutes.

The engineering hierarchy for reducing/eliminating hazards requires that a known hazard should be eliminated by designing the hazard out of the system when possible. If a hazard cannot be eliminated through design, the next step is to guard against the hazard. Providing a safety harness/fall arrest system, which is accompanied by its own set of risks and hazards, does not give the designer/manufacturer free rein to produce and introduce into the stream of commerce defective and unreasonably dangerous tree-stands.

**Alternative Designs**

Another cable material that is commonly used in corrosive environments is stainless steel — the preferred material for cables in extremely corrosive environments<sup>41,42</sup>. Stainless steel is also known to have increased strength compared to galvanized steel, further increasing the benefits of its use<sup>43</sup>.

In order to determine the reduction in corrosion if the cables had been made of stainless-steel, galvanic corrosion testing and cyclic voltammetry was performed using the same experimental test setup as described earlier. The results of corrosion testing using stainless steel cables are shown in **Figure 38**.

In tests performed using stainless steel cable material, due to having a galvanic potential near zero, the current response from cyclic voltammetry was too low to discern any valuable data. Likewise, the variation between initial and final mass of the stainless-steel cables after 14 days of immersion in 1.025 specific gravity salt water was so minimal as to be negligible.

In order to determine how economically feasible the use of stainless steel would be, a basic economic analysis was performed. According to various suppliers that were contacted at the time of the authors’ initial report, the

	<b>Corrosion Rate (Radius reduction in mm/year)</b>
Coupled Treestand and Stainless-Steel cable	0
Stainless Steel cable alone	0
Uncoupled Stainless Steel cable	The current response was too low to get meaningful data

**Figure 38**  
Corrosion rates for stainless steel.

average cost of galvanized steel cables is around \$0.20 per foot while 304 stainless steel cables cost (on average) \$0.40 per foot. Considering that each cable uses around 28 inches of 7-7 1/8-inch galvanized steel; changing the cable to 304 stainless steel would increase the price of the treestand from \$54.99 to \$55.92 or 1.7%.

As such, it is economically and technologically feasible that the manufacturer could have chosen to use stainless steel for its cables yet chose not to do so as a reasonably prudent manufacturer would. The increased corrosion resistance offered by the use of stainless-steel cable would have vastly outweighed the minimal economic cost associated with their usage. A prudent designer/manufacturer would have easily been able to determine, through a basic cost-benefit analysis, that the usage of stainless-steel cables was beneficial to the success of their product and safety of their users. By failing to perform this common-sense design change, the manufacturer at issue designed a product that could not reasonably be expected to withstand the environment it was intended to be subjected to. As such, it was unreasonably dangerous for its intended use.

As previously noted, the usage of a copper crimp on the subject cable increased corrosion by a considerable amount. It was determined that aluminum was an alternative crimping material the manufacturer could have used, as it is relatively easy to form and is already extensively used in crimping applications. In order to determine how the usage of an aluminum crimp would have affected the corrosion rate of the galvanized steel cables, additional accelerated immersion corrosion testing was conducted.

Exemplar cables were cut ~1.5 inches into the plastic coating, providing a total of four samples (Figure 39). The copper crimp on two of these samples was removed



**Figure 39**

The copper (right two) and aluminum (left two) crimp samples.

and replaced with a commonly available aluminum crimp of a similar size. These samples were then weighed and immersed in 1.025 specific gravity salt water (typical seawater) for 14 days. As shown in Figure 40, visual observation alone shows that the cables with the copper crimp corroded significantly more.

Various competitor treestands displayed an alternative cable attachment method, which allows the cables to be coated in a plastic sheath that prevents contact with air or water, cutting off one of the required conditions for corrosion to occur. While it is possible that this coating could degrade over time, constructing it out of UV-resistant materials would greatly reduce the likelihood of this occurring. The plastic sheath could also be made out of a semi-transparent material, which would allow users to see the cable corroding should water find a way in (Figure 41).

In order to verify that cables coated in a plastic sheath would not experience significant corrosion, additional accelerated corrosion testing was conducted utilizing cable samples cut from the midsection of the exemplar treestand cable. One of the ends of the cable was sealed in a flexible polymer sealant to prevent the ingress of water on this end (Figure 42). These samples were then partially



**Figure 40**

Corrosion present on the copper (right two) and aluminum (left two) crimp samples after 28 days of immersion.



**Figure 41**

Competitor treestand displaying fully coated cables and an alternative attachment mechanism.



**Figure 42**  
Sample cut from middle of exemplar cable; one end coated in polymer sealant.

submerged in salt water with one of the samples galvanically connected to a treestand sample through the use of potentiostat wires.

Results showed minimal corrosion in both cases with any mass loss or current being so low as to be negligible and within margin for noise and error. Based on the results of these tests, the polymer coating was found to be effective in blocking out the salt water bath and keeping the cable from corroding.

Another method that could be utilized to prevent a galvanic connection between the treestand cable and frame would be to insulate the bolt holes (Figure 43).

All of the design alterations discussed above are technically and economically feasible, and their implementation would have greatly increased the lifespan of the subject cable, preventing the incident from happening at the time it did. Although no projected corrosion time could be determined due to lack of any observed corrosion, it is likely that incident would likely have been postponed by at least bifold the amount of time the plaintiff had been using the treestand — by which time it would be reasonable to assume the plaintiff would have thrown away the treestand due to the degradation elsewhere on its frame.

Another method that could be utilized to prevent a galvanic connection between the treestand cable and frame would be to insulate the bolt holes (Figure 43). All of the design alterations discussed above are technically and economically feasible, and their implementation would have greatly increased the lifespan of the subject cable, preventing the incident from happening at the time it did. Although no projected corrosion time could be determined due to lack of any observed corrosion, it is likely that incident would likely have been postponed by at least bifold the amount of time the plaintiff had been using the treestand — by which time it would be reasonable to assume the plaintiff would have thrown away the treestand due to the degradation elsewhere on its frame.

**Summary and Conclusions**

Visual analysis of the subject treestand revealed severe corrosion of the galvanized steel cables near their connection points with the frame. The left-side cable failed between the cable eyelet and copper crimp, while

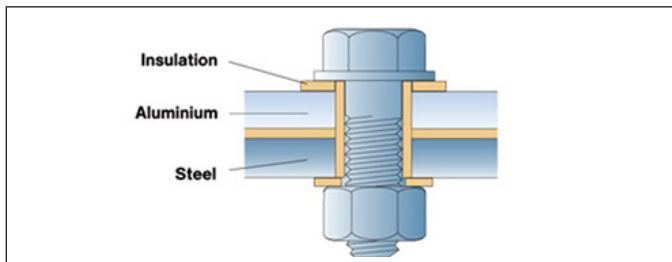


**Figure 43**

A potential design that could be used to prevent contact between the bolts and treestand.

the right-side cable failed just below the copper crimp. Based on the fracture surface characteristics of the cable strands and location of the failure points at each cable, it was concluded that the left-side cable failed first, leading to sudden overload failure of the right-side cable.

EDS analysis of the galvanized steel cables from the subject treestand revealed lower concentrations of zinc closer to the cable/frame connections, indicating that they experienced substantial depletion of its protective zinc coating, which, in turn, led to severe corrosion-induced degradation at these locations and their ensuing failure under normal and anticipated use.

It is well known that contact between dissimilar metals can result in the formation of a galvanic cell, which, in turn, can cause accelerated corrosion of one of the metals. It was concluded that corrosion of the subject cable connection points was caused by the phenomenon described above, due to improper contact between the cable eyelet, copper crimp, and treestand frame.

The degree to which the improper connection of the cables to the treestand resulted in its degradation under normal and anticipated use was measured through accelerated corrosion testing and electrochemical analysis. Test results indicated that the as-designed and as-assembled cable/frame connection point resulted in ~79% to 300% increase in the rate of corrosion measured in millimeters of cross-sectional area reduction per year, depending on the test method utilized.

It was further concluded that the significant increase in the rate of corrosion caused by improper design of the subject treestand resulted in premature degradation of its cables at the connection points with the frame, which lead to its premature failure under normal and anticipated use. Had the cables on the subject treestand been properly attached to the frame in a manner that would not have resulted in the formation of a galvanic cell, it would have lasted 79% to 300% longer (or four to 16.5 years) before reaching the same degree of degradation that caused its failure on the day of incident.

Susceptibility of the subject cables to corrosion degradation as a result of galvanic cell phenomenon discussed earlier was (or should have been) known to the manufacturer, given the occurrence of similar failures and associated investigations identifying improper design of the cable/frame connections as the root cause of the failure. Given the manufacturer’s knowledge of the occurrence of similar

incidents in the past, a reasonably prudent manufacturer would have either recalled the subject treestand or issued a product safety notice alerting owners of the susceptibility of the cables to premature failure.

While the owner's manual states that users should keep the treestand indoors when not "in use," no instructions are given regarding the period of time that the treestand can stay outdoors without significant degradation of its cables — nor are any warnings given regarding the susceptibility of the treestand cables to premature degradation should the treestand be left outdoors.

The manufacturer's reliance on warnings and instructions to inform a user of the hazards associated with the use of its product, while prudent in some situations, is not an effective means of protecting users from the hazard when it is possible to design the hazard out of a product or guard against user's exposure to the hazard. As such, the manufacturer did not act as a reasonably prudent manufacturer to address well-known safety issues associated with its product, which directly caused the failure at issue in this case.

Extensive research and testing of various cable connection methods revealed that the failure at issue in this case could have easily been prevented through the implementation of one or more of the following technologically and economically feasible alternatives:

1. Proper insulation of the cable from coming into direct contact with the frame.
2. Use of an aluminum crimp in place of copper crimp to decrease the susceptibility to galvanic corrosion.
3. Use of stainless-steel cables in place of the galvanized steel cables due to their increased resistance to corrosion.
4. Provide a barrier to the elements or coating the exposed portion of the cable to protect from environmental exposure.

The design of the subject treestand was unreasonably dangerous and defective, given the existence of multiple technologically and economically feasible alternative designs that would have prevented the failure of the subject cables under its reasonably foreseeable environmental exposure and use.

## Acknowledgments

*The authors would like to thank the legal experts they worked with on this case as well as their dedicated team of forensic engineers and interns.*

## References

1. DDH Staff "One in Three Hunters Will Fall" Deer and Deer Hunting, [Online]. Available: [https://www.deeranddeerhunting.com/deer-hunt/deer-hunting-tips/p3\\_one\\_in\\_three\\_hunters\\_will\\_fall](https://www.deeranddeerhunting.com/deer-hunt/deer-hunting-tips/p3_one_in_three_hunters_will_fall) Accessed: Aug. 23, 2022.
2. J. Smith et al., "Injuries Due to Falls from Hunters' Tree Stands in Pennsylvania," *American Journal of Preventative Medicine*, vol. 37, no. 5, pp. 422-436, Nov. 2009.
3. Consumer Product Safety Commission, "CPSC Safety Alert: Hunting Treestands and Harnesses," [Online]. Available: [https://www.cpsc.gov/s3fs-public/pdfs/blk\\_pdf\\_5200.pdf](https://www.cpsc.gov/s3fs-public/pdfs/blk_pdf_5200.pdf).
4. M. Metz et al., "Tree stand falls: a persistent cause of sports injury," *Southern Medical Journal*, vol. 97, no. 8, pp. 715-719, Aug. 2004.
5. A. Crockett et al., "Tree stands, not guns, are the midwestern hunter's most dangerous weapon," *American Surgeon*, vol. 76, no. 9, pp. 1006-1010, Sep. 2010. PMID: 20836352.
6. H. Greninger, "Falls From Tree Stands Top Hunting Accidents," *Indianapolis Tribune-Star*, Nov. 11, 2014.
7. P. Pollizer, "Subject: Petition CP 02-3; Hunting Tree Stand Petition," U.S. Consumer Product Safety Commission.
8. C. A. Pierre et al., "Tree stand falls: A persistent cause of neurological injury in hunting," *World Journal of Clinical Cases*, vol. 2, no. 8, pp. 345-350, Aug. 2014.
9. D. A. Jones, *Principles and Prevention of Corrosion*, New York, NY, USA: Maxwell Macmillan International Pub. Group, 1992.
10. Teknos, "Handbook for Corrosion Protection of Steel Surfaces by Painting," [Online]. Available: <https://www.teknos.com/globalassets/teknos.com/industrial-coatings/metal-wet-paints-general/handbook-for-corrosion-protection.pdf>.

11. Zhang et al., "Effect of corrosion on the fracture properties of steel plates," *Construction and Building Materials*, vol. 225, pp. 1202-1213, 2019.
12. Hou et al., "Experimental Investigation on Corrosion Effect on Mechanical Properties of Buried Metal Pipes," *International Journal of Corrosion*, Sep. 2016.
13. N. Pavlovic, "Effect of Corrosion on a Material's Tensile Strength and Ductility," *Corrosionpedia*, [Online]. Available: <https://www.corrosionpedia.com/effect-of-corrosion-on-a-materials-tensile-strength-and-ductility/2/5976>.
14. Chen et al., "Experimental Investigation into Corrosion Effect on Mechanical Properties of High Strength Steel Bars under Dynamic Loadings," *International Journal of Corrosion*, Jan. 2018.
15. "Galvanic Corrosion," AMPP, [Online]. Available: <https://www.ampp.org/resources/impact/corrosion-basics/group-1/galvanic-corrosion>. Accessed: Mar. 15, 2024.
16. K. Nanan, "The Basics of Cathodic Protection," *Corrosionpedia*, Dec. 9, 2023. [Online]. Available: <https://www.corrosionpedia.com/2/1368/prevention/cathodic-protection/cathodic-protection-101>.
17. Staff, *Corrosionpedia*, "An Introduction to the Galvanic Series: Galvanic Compatibility and Corrosion," [Online]. Available: <https://www.corrosionpedia.com/an-introduction-to-the-galvanic-series-galvanic-compatibility-and-corrosion/2/1403>. Accessed: Dec. 9, 2023.
18. U.S. General Services Administration, "Galvanized Iron And Steel: Characteristics, Uses And Problems," [Online]. Available: [https://www.gsa.gov/real-estate/historic-preservation/historic-preservation-policy-tools/preservation-tools-resources/technical-documents?Form\\_Load=88553?bypassAkamaiCache=1507917842](https://www.gsa.gov/real-estate/historic-preservation/historic-preservation-policy-tools/preservation-tools-resources/technical-documents?Form_Load=88553?bypassAkamaiCache=1507917842).
19. D. Kopeliovich, "Galvanic Corrosion," [Online]. Available: [http://www.substech.com/dokuwiki/doku.php?id=galvanic\\_corrosion](http://www.substech.com/dokuwiki/doku.php?id=galvanic_corrosion).
20. Crevice Corrosion," AMPP, [Online]. Available: <https://www.ampp.org/technical-research/impact/corrosion-basics/group-1/crevice-corrosion>.
21. D. Prayitno and M. Irsyad, "Effect of ratio of surface area on the corrosion rate," *Sinergi*, vol. 22, no. 1, pp. 7-12, 2018.
22. D. Kopeliovich, "Galvanic Corrosion," [Online]. Available: [http://www.substech.com/dokuwiki/doku.php?id=galvanic\\_corrosion](http://www.substech.com/dokuwiki/doku.php?id=galvanic_corrosion).
23. American Galvanizers Association, *Performance of Hot-Dip Galvanized Steel Products in the Atmosphere, Soil, Water, Concrete, and More. Centennial, CO, USA, 2010*. [Online]. Available: <https://galvanizeit.org/education-and-resources/publications/performance-of-hot-dip-galvanized-steel-products>.
24. M. Khan, A. Asif, S. Khawaldeh, and A. Tekin, "Dopamine Detection using Mercaptopropionic Acid and Cysteamine for Electrodes Surface Modification," *Journal of Electrical Bioimpedance*, vol. 9, pp. 3-9, 2018, doi: 10.2478/joeb-2018-0002.
25. Gamry, "Quantitative Corrosion Theory," [Online]. Available: [https://www.gamry.com/Framework%20Help/HTML5%20-%20Tripane%20-%20Audience%20A/Content/DC/Introduction\\_to\\_DC\\_Corrosion/Quantitative%20Corrosion%20Theory.htm](https://www.gamry.com/Framework%20Help/HTML5%20-%20Tripane%20-%20Audience%20A/Content/DC/Introduction_to_DC_Corrosion/Quantitative%20Corrosion%20Theory.htm).
26. Z. Shahriyari and K. Gheisari, "Galvanic corrosion susceptibility between X53CrMnNiN219 and X45CrSi93 stainless steels in chloride solution using electrochemical measurements," *Anti-Corrosion Methods and Materials*, vol. 65, 2018, doi: 10.1108/ACMM-04-2018-1926.
27. Epidemiologic Investigation Report, U.S. Consumer Product Safety Commission, Report 130823CCC1080, Aug. 26, 2013.
28. U.S. National Institute for Occupational Safety and Health, "Hierarchy of Controls," [Online]. Available: <https://www.cdc.gov/niosh/topics/hierarchy/>. Accessed: Aug. 23, 2022.

29. K. Druley, "Hierarchy of Controls," *Safety and Health Magazine*, [Online]. Available: <https://www.safetyandhealthmagazine.com/articles/16790-the-hierarchy-of-controls>.
30. B. Fischhoff, "Mental Models of Warning Decisions: Identifying and Addressing Information Needs," in *Handbook of Warnings*, CRC Press, 2006.
31. Dr. Stephen Rosen "The Duty to Warn Handbook"
32. M. Wogalter, "Attention switch and maintenance," in *Handbook of Warnings*, CRC Press, 2006.
33. M. Wogalter, "Communication-Human Information Processing (C-Hip) Model," in *Handbook of Warnings*, CRC Press, 2006.
34. K. Hey, "Will Your Treestand Fail this season?" *Bowhunting.com*, [Online]. Available: <https://www.bowhunting.com/blog/2019/08/21/will-your-treestand-fail-this-season/>.
35. Consumer Product Safety Commission, "CPSC Safety Alert: Hunting Treestands and Harnesses," [Online]. Available: [https://www.cpsc.gov/s3fs-public/pdfs/blk\\_pdf\\_5200.pdf](https://www.cpsc.gov/s3fs-public/pdfs/blk_pdf_5200.pdf).
36. A. Crockett et al., "Tree stands, not guns, are the midwestern hunter's most dangerous weapon," *American Surgeon*, vol. 76, no. 9, pp. 1006-1010, Sep. 2010. PMID: 20836352.
37. G H. Greninger, "Falls From Tree Stands Top Hunting Accidents," *Indianapolis Tribune-Star*, Nov. 11, 2014.
38. P. Pollizer, "Subject: Petition CP 02-3; Hunting Tree Stand Petition," U.S. Consumer Product Safety Commission.
39. P. Seddon, *Harness Suspension: Review and Evaluation of Existing Information*, HSE Contract Research Report 451/2002.
40. O Occupational Safety and Health Administration, "Suspension Trauma/Orthostatic Intolerance," OSHA SHIB 03-24-2004.
41. "Stainless Steel vs. Galvanized Steel," [Online]. Available: <https://www.rigidlifelines.com/blog/stainless-steel-vs-galvanized-steel/>.
42. "Galvanized Cable versus Stainless Steel Cable: When Do the Differences Matter?" [Online]. Available: <http://www.elitesalesinc.com/galvanized-cable-versus-stainless-steel-cable/>.
43. "Galvanized Steel vs Stainless Steel: Which Is the Better Choice?" [Online]. Available: <https://crossroadsgalvanizing.com/2020/03/03/galvanized-steel-vs-stainless-steel-which-is-the-better-choice/>.

# Using Ground Penetrating Radar Techniques in Forensic Structural Engineering

By Chakradhar Gondi, PE (NAFE #1329A), J. Vincent Barnes III, PE, and Michael J. Wightman

## Abstract

*One of the most powerful non-destructive testing methods in forensic structural engineering is ground penetrating radar (GPR). It is utilized to detect subsurface features such as rebar, voids, and corrosion in concrete. It is also helpful in investigating differential settlements in structures by identifying voids and anomalies in sub-surface soils that can cause structural instability. GPR works by emitting electromagnetic waves that reflect off materials with varying electrical properties, producing 2-dimensional images or profiles of the sub-surface. This paper explores the application of GPR techniques in gathering important structural data and identifying subsurface anomalies and defects. Additionally, it also presents case studies from real-world forensic engineering investigations that demonstrate the use of GPR to diagnose structural defects and prepare repair solutions while minimizing project costs. The challenges and limitations of GPR are also discussed. In summary, GPR is an invaluable tool engineers can use to assess the structural integrity and design without damaging the structure.*

## Keywords

Ground penetrating radar, GPR, non-destructive testing, NDT, structural damage, reinforced concrete, soils, forensic structural engineering

## Introduction

In forensic structural engineering, accurately diagnosing structural issues without damaging the structure is an important initial step of investigation. Non-destructive testing (NDT) methods allow engineers to assess a structure's internal condition, construction, and placement of reinforcement. This information can be obtained non-intrusively, thus avoiding any partial demolitions that can further damage the structure and increase costs associated with the examination. Among these NDT methods to evaluate non-visible components, ground penetrating radar (GPR) has gained prominence for its ability to detect subsurface features and anomalies, providing crucial data on structural performance.

GPR is particularly useful in concrete investigations. It is able to detect internal features such as rebar placement configuration, internal and/or underlying voids, reductions in underlying soil support, and rebar corrosion<sup>1</sup>. These findings can determine structural integrity when used to predict the inherent strength and overall conditions of existing material and support conditions. This paper explores the applications of GPR in forensic engineering, highlighting real-world cases where it has been instrumental in

detecting structural findings and guiding repair strategies. GPR's technical principles, practical applications, and inherent limitations are discussed to provide a comprehensive understanding of this powerful NDT tool.

The use of GPR in forensic structural engineering is guided by several well-established standards that ensure consistency and reliability in data collection and interpretation. ASTM D6432-19 is the primary guide for surface GPR methods<sup>1</sup>. It describes how to calibrate equipment, collect signals, and interpret subsurface data. ASTM D6087-22 provides a specific method for evaluating asphalt-covered concrete bridge decks using GPR<sup>2</sup>. This is especially useful for detecting delamination or deterioration beneath the asphalt overlay.

The results from GPR methods are often validated by other testing methods. For example, ASTM C1383-23 provides a standard method for measuring the thickness of concrete members using impact echo testing<sup>3</sup>. This is another NDT method often used to complement GPR findings and confirm concrete member dimensions. For corrosion assessment, ASTM C876-22 defines the standard method for measuring corrosion potentials of uncoated

reinforcing steel in concrete<sup>4</sup>. This method is often used alongside GPR to help predict the extent of corrosion in the reinforcing.

### **Ground Penetrating Radar (GPR): Technical Background**

GPR operates by transmitting electromagnetic waves into a material that reflect back when encountering objects or interfaces with contrasting dielectric properties<sup>5</sup>. These dielectric properties are primarily controlled by electrical conductance, material density, and moisture content. GPR consists of a set of integrated electronic components that transmits high-frequency electromagnetic waves and records the energy reflected back to the material surface. The typical frequency range used for forensic studies ranges from 800 megahertz (MHz) to 2.6 gigahertz (GHz). The GPR system consists of an antenna, which serves as both a transmitter/receiver and a profiling recorder that both processes the incoming signal and provides a graphic digital display of the data. The GPR data can be reviewed and analyzed in real time or recorded for later review using specialized analysis software.

A GPR survey provides a graphic cross-sectional view of subsurface conditions. This cross-sectional view is created from the reflections of repetitive short-duration electromagnetic (EM) waves that are generated as the antenna is moved across the surface. The reflections occur at the subsurface boundary contacts between materials with differing electrical properties. The GPR method is commonly used to identify such targets as thickness of concrete, configuration and placement of rebar, internal or external voids, underground utilities, underground storage tanks or drums, buried debris, or geological features.

A GPR survey is conducted along survey lines (transects), which are measured paths along which the GPR antenna is moved. Horizontal and vertical scale are integrated into the GPR graphic output along with an electronic marker to indicate the current antenna position. This electronic marker and scales allow for a correlation between the GPR data and the position of the GPR antenna on the surface along with an estimated depth of any target of interest.

The greater the electrical contrast between the surrounding materials (earth or concrete) and target of interest, the greater the amplitude of the reflected return signal. Unless the buried object is metal, only part of the signal energy will be reflected back to the antenna. The remaining portion of the signal continues to propagate downward

to be reflected by deeper features. When the GPR signal encounters metal, the high electrical conductivity and permittivity of the material cause all of the signal energy to be reflected back to the antenna, resulting in a strong, high-amplitude response that is easily identifiable in the GPR data.

It is noted that because of the 100% reflection that it is not possible to identify any objects that are directly below the metallic object. However, if there is little or no electrical contrast between the target and surrounding earth materials, it will be very difficult (if not impossible) to identify the object using GPR. For example, steel rebar surrounded by concrete is very easily detected, but a PVC conduit that is filled with water that is below the water table may be very difficult to detect. This is because both the PVC water pipe and the surrounding saturated soils would have similar dielectric properties, resulting in low electrical contrast and a very weak or non-existent signal reflection. In contrast, steel rebar in concrete creates strong reflections due to the distinct contrast in dielectric properties between concrete and rebar.

The depth of penetration of the GPR signal is also reduced as the antenna frequency is increased. However, as antenna frequency is increased, the resolution of the GPR data is improved. Therefore, when designing a GPR survey, a tradeoff is made between the required depth of penetration and desired resolution of the data. As a rule, the highest frequency antenna that will still provide the desired maximum depth of penetration should be used.

For many void studies focused on detecting voids in soils beneath structures, an antenna frequency of 800 to 900 MHz is often used. Most rebar and concrete characterization studies are completed using antennas with a frequency of above 1.5 GHz. Depending on the objectives of an investigation, multiple frequency antennas may need to be used for the same project area. For example, a void study might also require that the thickness of the concrete slab and design of the reinforcement be determined.

It should be noted that the penetration depth of the GPR signal can be greatly impacted by the age of the concrete. While newly poured concrete is going through the initial curing process, the signal penetration depth will be significantly reduced due to the elevated conductivity of the concrete that is caused by the high moisture content. It is the author's experience that a minimum of two weeks be allowed before attempting a GPR study for a concrete structure.

## Application of GPR in Concrete Rebar Mapping and Corrosion Evaluation

In structural investigations, verifying rebar placement configuration and in-place condition is essential to ensure compliance with design specifications and assess structural safety. GPR can accurately map rebar depth and configuration, identify missing reinforcements, and evaluate corrosion<sup>6</sup>.

GPR can be integrated with other complementary NDT tools to extend its capabilities and also help confirm the GPR results<sup>7</sup>. Some of these complementary NDT tools include impact echo (IE), electromagnetic (EM) meters, and half-cell corrosion potential testing.

The IE method is used for thickness evaluations and to assess the condition of concrete slabs, walls, and beams<sup>8</sup>. The method requires access to only one surface of the target area. The concrete thickness accuracy of the IE method is +/- 2% when it is possible to calibrate the instrument to a known concrete thickness at the site. The IE equipment consists of a portable hand-held unit with an electro-mechanical solenoid that generates acoustic compressional waves that reflect back from the bottom or back of the tested member or from a discontinuity or debonding surface within the concrete. The response of the IE system is then measured by the acoustic receiver mounted next to the solenoid impact point and analyzed. The instrument produces a real-time waveform display while testing. For each data point collected, multiple waveform “stacks” are recorded and used to produce the final estimated thickness. The data can also be recorded for further analysis.

EM devices consist of a set of integrated electronic components that can detect the presence of metallic objects within concrete. The system operates on the principle of pulse induction where a primary EM field is created by the equipment. Any metallic objects within the equipment’s sensitivity range will have created within them a secondary EM field that is sensed by the equipment. Modern EM devices can also provide an estimate of cover depth and rebar size for simple rebar configurations and where the bars are sufficiently spaced far enough apart.

It should be noted that while GPR is effective for locating reinforcement in concrete and estimating cover depth, it is not typically reliable for accurately determining rebar diameter — particularly for smaller bar sizes<sup>9</sup>. Although GPR can detect rebar and provide an approximate indication of bar size based on using advanced processing techniques, more precise estimation often requires

complementary tools, such as EM devices. In most studies, the estimated rebar diameter is reported as plus/minus one bar size. The rebar survey results obtained from GPR and EM systems are best validated through destructive testing methods such as coring, which provide direct physical confirmation of the reinforcement size.

The half-cell potential method is used to monitor the corrosion of steel rebar in concrete. Half-cell testing is performed by connecting one electrode (the base electrode) to an exposed piece of rebar within the concrete and placing a second electrode (roving electrode) at testing locations across the concrete surface. The potential response between the two electrodes is measured in millivolts (mV). This test may involve selective chipping of concrete at test locations to expose the rebar. Using the rebar layout from GPR data, half-cell tests can focus on specific regions where moisture or concrete anomalies are detected, allowing for a more targeted and efficient corrosion assessment<sup>10</sup>. Based on the ASTM C876-09 standards, half-cell measurements of less than -350 mV are considered to indicate with a greater than 90% probability of rebar corrosion. Values between -200 to -349 mV are considered to indicate uncertain conditions, and values greater than -200 mV and above are considered to have less than 10% probability of rebar corrosion<sup>4</sup>.

**Figure 1** and **Figure 2** show GPR data samples from a geophysical investigation performed by the authors for a warehouse metal frame building in Clearwater, Florida. This geophysical investigation was performed at multiple locations throughout the concrete first floor slab, exterior wall foundations, and interior column foundations of the building. The existing building foundations were required to be analyzed for increase in loading due to new proposed additions on the roof. Since original as-built drawings of the building were not available, a GPR survey was performed to document foundation size and location of steel

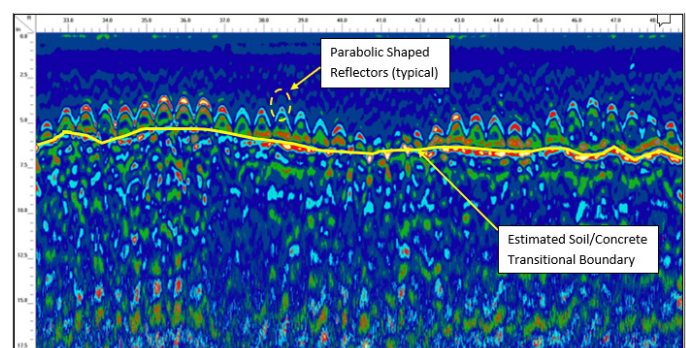


**Figure 1**  
GPR data sample at concrete slab.

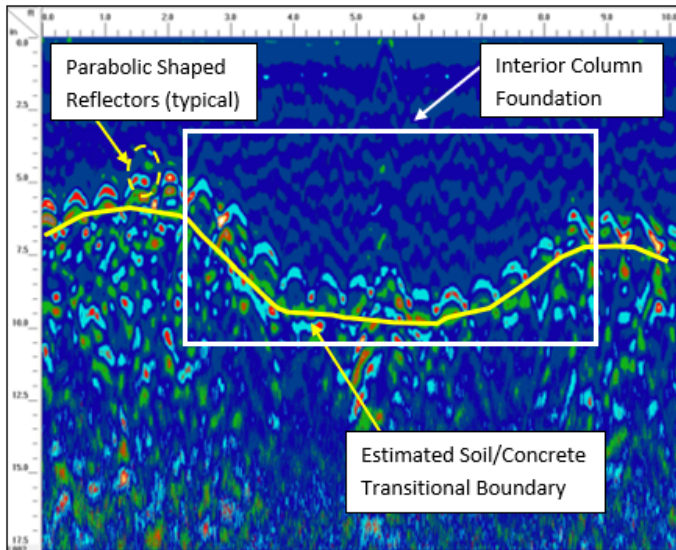


**Figure 2**

GPR data sample at interior column foundation.

reinforcement. To validate the results, the GPR survey was supplemented with additional NDT methods, including EM and IE techniques. The IE testing was conducted in accordance with ASTM C1383 to determine the thickness of concrete elements. The EM survey was performed using the Proceq 650 AI, which is capable of identifying rebar to a maximum depth of 5 to 7 inches. The features observed on GPR data that are most commonly associated with rebar are:

- The occurrence of high-amplitude parabolic-shaped GPR reflectors.
- If the reinforcing is continuous, the associated GPR reflectors should match in both estimated depth below surface and lateral position on parallel GPR transect lines.

The horizontal scale in the sample two-dimensional GPR scans shown in **Figure 1** and **Figure 2** represents longitudinal distance in feet, while the vertical scale denotes the depth within the concrete member in inches. The peaks of the hyperbola in **Figure 1** and **Figure 2** clearly define the position of the rebars, while the distance between the peaks represents the spacing between each rebar<sup>6</sup>.

Based on the scan data, a single layer of reinforcement was identified near the bottom of the slab. Reinforcement was present in both orthogonal directions; one direction is visible in the figures, and the perpendicular direction was confirmed from a separate set of GPR transects performed orthogonal to those shown and correlated with typical

construction practices. The GPR data also identified the transition boundary between the concrete and supporting soil, allowing for the thickness of the concrete slab to be estimated.

The GPR investigation determined that the concrete slab for the main building ranges in thickness from 5.5 to 6.5 inches (**Figure 1**) and is reinforced with a rebar mat on 6-inch spacing. Using EM, the rebar size is estimated to be either #4 or #5, with a cover depth ranging from approximately 4.5 to 5.5 inches (**Figure 1**). The interior column foundation does not appear to be a separate pad, but rather an excavated thickening of the floor slab (**Figure 2**). The foundation width at the bottom is approximately 3-foot by 3-foot, and the maximum thickness at center of foundation is approximately 10 to 12 inches. No additional reinforcement — besides what is present in overall slab — is observed within the foundations.

### Application of GPR in Identifying Possible Voids

Voids in soils beneath a structure can lead to differential settlement and instability of foundations and floor slab systems. GPR assists in detecting such voids, particularly in areas where soil erosion, poor compaction, or subsurface water flow have occurred. Identifying these voids helps engineers devise solutions to stabilize foundations, protecting against future settlement and structural damage. The features observed on GPR data that are most commonly associated with void formation are:

- A downwarping of GPR reflector sets that is associated with suspected lithological contacts toward a common center. Such features typically have a bowl or funnel-shaped configuration and can be associated with a deflection of overlying sediment horizons caused by the migration of sediments into underlying voids. If the GPR reflector sets are sharply downwarping and intersect, they can create a “bow-tie”-shaped GPR reflection feature, which often designates the apparent center of the GPR anomaly.
- A localized significant increase in the depth of the penetration and/or amplitude of the GPR signal response. The increase in GPR signal penetration depth or amplitude is often associated with void formation.
- An increase in the amplitude of horizontal reflector sets below the concrete slab indicating an air space void.

The case study in the next section is a real-life project example that demonstrates how GPR was used effectively to identify anomalies in subsurface soils to prepare solutions for a loading dock slab repair.

**Case Study — Loading Dock Slab Settlement Investigation**

A loading dock slab for an office facility located in Tampa, Florida began exhibiting signs of settlement, including noticeable cracks and uneven surfaces that disrupted operations (Figures 3, 4, and 5). The building served by the loading dock is a seven-story office building built approximately in 2007. The loading dock area consists of an elevated concrete slab that rises about 4 ft from the ground surface and a concrete retaining stem wall. This area is being used for loading/unloading the shipping supplies of

various businesses in the building. The slab and retaining wall itself are independent structures and not connected to the main building. The slab is tied into the retaining wall with rebar dowels.

A forensic investigation using GPR survey was performed across the loading dock area to identify and locate any possible voids or heterogeneities (e.g., buried debris) in the soil underneath the concrete slab that could be associated with the differential settlement and concrete cracking. The GPR survey was conducted along a grid series of GPR transects that were spaced 2 ft apart, as shown in Figure 6. The GPR data was collected using two GPR systems.

A high-resolution imaging of soil conditions directly below the slab was obtained using GSSI Mini Structure Scan with a 2.6 GHz antenna with a time range setting of 10 nanoseconds. This provided a very high-resolution imaging of soil conditions directly below the slab to a depth of approximately 1.5 ft below land surface (bls). The

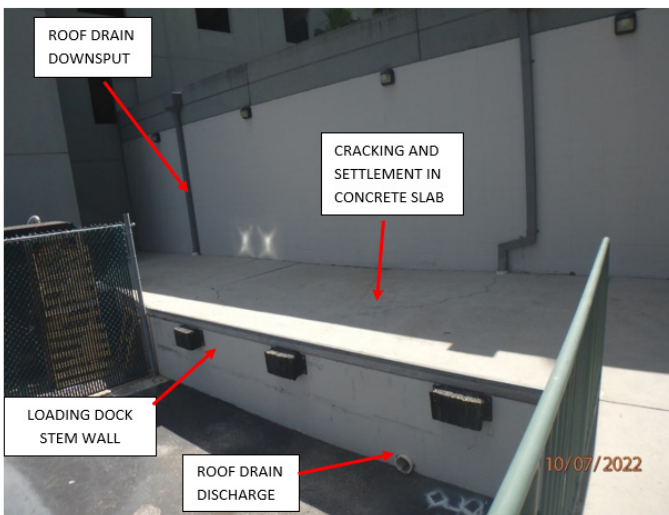


**Figure 3**  
Loading dock area.



**Figure 4**  
Up to 1/2-inch-wide crack across the slab.



**Figure 5**  
Up to 2 inches of slab drop in the eastern edge.

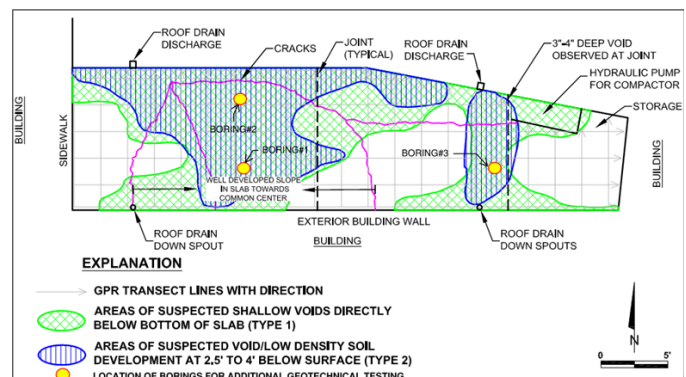


**Figure 6**  
Site map showing results of GPR investigation.

assessment of deeper soil conditions was completed using a GSSI SIR 3000 with a 900 MHz antenna and a time range setting of 30 nanoseconds. This equipment configuration provided an estimated depth of investigation of 2 to 3 ft bls.

The results of the geophysical investigation are presented in **Figures 6, 7, and 8**. Based on the GPR results, the authors identified two types of anomalous subsurface conditions. Type 1 anomalies are suspected shallow voids directly below the bottom of the slab. For the majority of the anomaly areas, these voids appear to be less than 0.25 inches in height. However, in some areas, they could be up to 3 to 4 inches in height — as was observed at the northern end of the slab joint in the eastern portion of the site. Type 2 anomalies are characterized by a localized increase in the amplitude of the GPR signal response at a depth range of 2.5 to 4 ft bls. Examples of the GPR data collected across each of the Type 1 and Type 2 anomaly areas are provided in **Figure 7** and **Figure 8**. The coloration of the interpreted voids in **Figures 7 and 8** was produced by the equipment software, which offers options for selecting

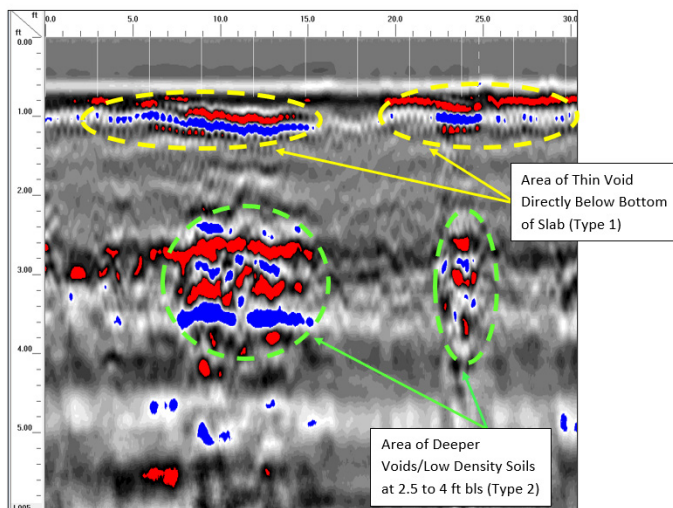


**Figure 7**

GPR data collected with 900 Mhz antenna.

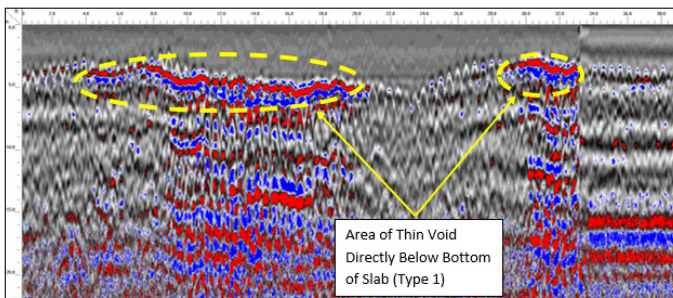


**Figure 8**

GPR data collected with 2.6 GHz antenna.

both the color palette and how the amplitudes of the returns are displayed. Further evaluation of these GPR study results indicated the following:

- Type 1 and Type 2 anomalies are present in the majority of the area where the concrete slab is sloping to a common center in the western portion of the slab.
- Type 1 and Type 2 anomalies are present along the entire route of the eastern roof drain but are only present in a portion of the western roof drain.
- Type 2 (deep) anomalies are present within the entire lateral extent of the Type 1 (shallow) anomalies.
- The original building structural drawings indicated that the slab construction is 5 inches thick with 6x6-W2.9xW2.9 welded wire reinforcement (WWR). The GPR results, as shown in **Figure 8**, determined that the concrete slab thickness ranged from approximately 2.5 to 5 inches, based on the depth of the last consistent horizontal reflector before signal attenuation. The regular spacing and consistent pattern of low-amplitude hyperbolic reflections observed near the bottom of the slab suggested a rebar or mesh pattern with a 6-inch grid spacing. However, as previously discussed, GPR has limitations in distinguishing fine mesh elements from closely spaced small-diameter rebar, particularly when the wire is of a smaller gauge.

It was considered that the GPR anomalies were associated with voids or low-density soils/buried debris. Hence, a follow-up shallow geotechnical soil testing was performed in this area to evaluate the soil profile and confirm the GPR findings of any suspected voids. A total of three hand auger borings were drilled into existing concrete slab and soil fill to a depth of about 5 ft below top of slab or auger refusal. A dynamic cone penetrometer (DCP) test was performed at each hand auger location to evaluate soil density in the upper approximate 4 to 5 ft of the soil profile<sup>11</sup>. The soil samples were also visually classified soil samples in the laboratory using the Unified Soil Classification System<sup>12</sup>.

The results of soil profiles from hand auger borings is shown in **Figure 9**. The summary of lime rock bearing ratio (LBR) results obtained from DCP tests at each hand auger location is presented in **Figure 10**. The LBR is

Depth (feet)		Material Description
From	To	
<b>HA-01</b>		
0	0.5	2 inches of void below 4 inches thick slab core
0.5	1.5	Gray fine sand (SP) with rock fragments and clay clods
1.5	2.5	Gray fine sand (SP) with rock fragments, plastic sheet, burnt wood, and clay clods
2.5	3.5	Gray fine sand (SP) with roots and metal debris
3.5	5.0	Gray fine sand (SP) with rock fragments and clay clods
<b>HA-02</b>		
0	0.75	4.75 inches of void below 4.25 inches thick slab core
0.75	2.5	Gray fine sand (SP) with clay clods
2.5	4.5	Gray fine sand with fragments of old cast iron pipe
<b>HA-03</b>		
0	0.5	3 inches of void below 3 inches thick slab core
0.5	4.5	Gray fine sand (SP) with clay clods and limerock fragments
4.5	5.0	Gray fine sand (SP) with fragments of shells and limerock

**Figure 9**  
Summary of hand auger boring results.

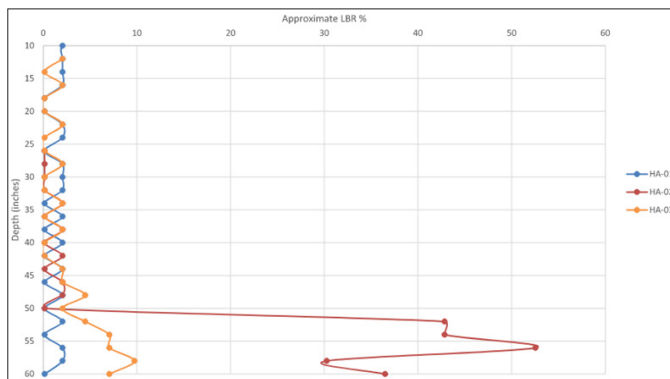


**Figure 10**

Relative subgrades density vs depth at hand auger boring results.

a measure of soil strength commonly used in Florida for evaluating roadway subgrades. It is a variation of the California Bearing Ratio (CBR), which is used outside of Florida with the conversion  $LBR = 1.25 \times CBR^{13}$ . The DCP test was conducted in accordance with ASTM D6951, where the number of blows over a specific depth interval was converted to an equivalent CBR or LBR percentage.

Essentially, LBR quantifies the relative strength of a material as a percentage of lime rock strength, with higher values representing greater compaction and lower values indicating looser material. Different materials have characteristic maximum LBR values when properly compacted. For instance, crushed concrete typically has an LBR of around 150%. Lime rock (limestone) has a standard LBR of 100%, meaning an LBR of 100% represents material strength equivalent to that of lime rock. Clean fine sand, when well-compacted, typically has an LBR of 20% to 22%<sup>14</sup>.

Further evaluation of the geotechnical testing results from **Figures 9** and **10** indicated:

- Hand auger borings and DCP soundings indicated that the supporting soil is very loose and filled with buried debris, which confirmed the Type 2 (deep) anomalies depicted in the GPR survey results shown in **Figures 6** through **8**.
- In **Figure 10**, all recorded LBR values were below 5%, indicating that the soil beneath the loading dock slab is extremely loose. If the soil had been properly compacted or had not experienced degradation due to material loss, the LBR should have been at least 15 to 20%<sup>14</sup>. Additionally, the DCP data for hand auger #3 showed a few outliers corresponding to higher LBR percentages at greater depths, which likely indicate obstructions or very hard materials within the soil profile.
- These results indicated that the soil underneath the loading dock slab contained debris (burnt wood, debris and other unsuitable material) prior to filling the area for the construction of the dock. Debris inherently contained void spaces, and, over time, soil gradually migrated into these openings. This soil migration loosened the soil and caused settlement, which resulted in the settlement of the slab itself.
- Since the loading dock was constructed as a soil-supported slab, the supporting soil settlement led to distress in the concrete slab through differential settlement and concrete cracking.

Based on the results of the GPR survey and geotechnical soil testing, recommendations were provided for the complete removal of all existing loading dock slab and the underlying fill soil to a depth of at least 4 ft below the top of the slab. Subsequently, the forensic team designed a new replacement slab and new compacted fill under the slab in loading dock area. The new slab was tied into the existing 4-ft-tall concrete stemwall with rebar dowels. Additionally, existing roof drain downspout pipes, which pass under the loading dock slab and discharge at the bottom of the concrete stem wall, were examined during the excavation and removal of the existing slab and soil fill. The existing roof drain pipes were found to be intact, free from debris, and without leaks. As a result, the existing drain pipes were salvaged and reused with the new slab and soil fill.

## Challenges and Limitations of GPR in Structural Investigations

While GPR is a valuable tool in forensic investigations, it does have limitations that engineers must consider. The analysis and collection of GPR data is both a technical and interpretative skill. Misinterpretation of the findings can lead to unnecessary repairs or overlooked issues. The technical aspects of GPR investigations are learned from both training and experience. Having the opportunity to compare GPR data collected in numerous settings to the results from geotechnical and structural studies performed at the same locations allows the forensic engineer to develop interpretative skills for soil and concrete characterization studies.

The penetration depth of GPR is limited by the frequency of the electromagnetic waves and the material's properties. For instance, highly conductive materials (like wet clay or metal-reinforced concrete) can significantly reduce depth penetration. Selecting the appropriate frequency is critical but often involves trade-offs between resolution and depth.

The ability of GPR to collect interpretable information at a project site is limited by the attenuation (absorption) of the GPR signal by underlying soils. Once the GPR signal has been attenuated at a particular depth, information regarding deeper geological conditions will not be obtained. GPR data can only resolve subsurface features that have a sufficient electrical contrast between the feature in question and surrounding earth materials. If an insufficient contrast is present, the subsurface feature will not be identified.

Environmental factors, such as moisture, metal inclusions, and closely spaced rebar, can interfere with GPR signals, creating noise that complicates data interpretation. Thus, the forensic engineer should consider complementary NDT or destructive methods necessary to confirm findings or improve accuracy.

## Conclusion

GPR has proven to be an indispensable tool in forensic structural engineering, offering non-destructive insights into subsurface conditions that are critical for structural assessment. Through case studies, this paper has demonstrated GPR's application in rebar mapping, void detection, and corrosion assessment, highlighting its cost-effectiveness and diagnostic precision. While GPR has limitations, such as depth restrictions and sensitivity to environmental conditions, its advantages make it a valuable resource for engineers seeking to preserve structural

integrity without invasive testing. Pairing the GPR technology with other complementary NDT tools like impact echo, electromagnetics, and half-cell potential tests — or with limited destructive testing or borings — will further enhance its applications and accuracy in forensic investigations.

## References

1. ASTM D6432-19: Standard Guide for Using the Surface Ground Penetrating Radar Method for Subsurface Investigation, ASTM International, West Conshohocken, PA, USA, 2019.
2. ASTM D6087-22, "Standard Test Method for Evaluating Asphalt-Covered Concrete Bridge Decks Using Ground Penetrating Radar," ASTM International, West Conshohocken, PA, USA., 2022.
3. ASTM C1383-23, "Standard Test Method for Measuring the P-Wave Speed and the Thickness of Concrete Plates Using the Impact-Echo Method," ASTM International, West Conshohocken, PA, USA, 2023.
4. ASTM C876-22b, "Standard Test Method for Corrosion Potentials of Uncoated Reinforcing Steel in Concrete," ASTM International, West Conshohocken, PA, USA, 2022.
5. A. P. Annan, *Ground Penetrating Radar: Principles, Procedures, and Applications*, 1st ed, Ontario: Sensors & Software Inc., 2003.
6. K. Tešić, A. Baričević and M. Serdar, "Comparison of cover meter and ground penetrating radar performance in structural health assessment: case studies," *Građevinar (Zagreb)*, vol. 73 (11), pp. 1131-1144, 2021-12.
7. A. Elseicy, A. Alonso-Díaz, M. Solla, M. Rasol and S. Santos-Assunção, "Combined Use of GPR and Other NDTs for Road Pavement," *Remote sensing (Basel, Switzerland)*, vol. 14 (17), p. 4336, 2022.
8. M. Sansalone, J. LIN and W. B. STREETT, "Determining Concrete Highway Pavement Thickness Using Wave Speed Measurements and the Impact-Echo Method," *Structural Materials Technology*, pp. 348-353, 1996.

9. W. Cheng, H.-H. Sun, K. H. Tan, and Z. Fan, "Estimating the diameter of reinforcing bars using an ultra-wideband MIMO GPR array," *Construction and Building Materials*, vol. 365, p. 129924, 2023-02.
10. FPRIME C SOLUTIONS, "How to use GPR in Structural Assessment?," 7 OCTOBER 2020. [Online]. Available: <https://fprimec.com/how-to-use-gpr-in-structural-assessment/>.
11. ASTM D6951/D6951M-18, "Standard Test Method for Use of the Dynamic Cone Penetrometer in Shallow Pavement Applications," ASTM International, West Conshohocken, PA, 2018.
12. ASTM D2487-17, Standard Practice for Classification of Soils for Engineering Purposes (Unified Soil Classification System), West Conshohocken, PA: ASTM International,, 2017.
13. W. VIRGIL PING, LING GE, AND ZHILIANG YU, "Evaluation of Pavement Bearing Characteristics Using Florida Limerock Bearing Ratio Test," *TRANSPORTATION RESEARCH RECORD*, vol. 1547, no. 1, pp. 53-60, 1996.
14. Iowa Department of Transportation, Iowa State University, "Iowa Statewide Urban Design and Specifications (SUDAS), Section 6E-1 – Subgrade Design and Construction," 2013. [Online]. Available: <https://www.intrans.iastate.edu/wp-content/uploads/sites/15/2020/03/6E-1.pdf>. [Accessed 29 5 2025].



# Assessing Weather Event Damage in Forensic Engineering: Data Sources and Challenges

By Chad T. Williams, PE, DFE (NAFE #937M), Doug J. Heady, and Ryan L. Allen

## Abstract

Forensic engineering evaluations often involve assessing damage from weather events such as thunderstorms, tornadoes, and hurricanes. A crucial aspect of these evaluations is verifying whether the reported weather event occurred on or around the specified date and determining relevant meteorological parameters from the available historical data. Two primary sources of historical meteorological data are the National Oceanic and Atmospheric Administration (NOAA) National Weather Service's Storm Prediction Center Local Storm Reports (SPC-LSR) and the National Centers for Environmental Information Storm Events Database (NCEI-SED). These databases rely on reports from various sources and may sometimes provide imprecise or inconsistent data. Therefore, forensic engineers should not rely solely on these sources but instead use them in conjunction with data or observations from multiple other sources.

## Keywords

Hail, tornado, forensic engineering, forensic meteorology, weather, weather event, damage assessment, meteorological data, NOAA, wind, NCEI, NCEI-SED, SPC-LSR, NWS

## Introduction

Forensic engineering evaluations often involve assessing conditions attributed to thunderstorms, tornadoes, hurricanes, winter storms, or other weather phenomena. While field work can provide information such as spatter marks (**Figure 1**), forensic engineering evaluations require further information to determine the date or period of occurrence for identified meteorological events and to establish meteorological conditions such as size, fall directionality, and duration for hail events, directionality and duration for wind events, and potentially other parameters related to other identified meteorological events.

This analysis commonly begins with the review of online meteorological databases. It is necessary for the forensic engineer to understand the sources of the referenced data and the purpose of the respective databases. While information from online databases can provide information to assist with a forensic engineering evaluation, online databases may not provide sufficient information to establish, refute, or otherwise understand historical meteorological events. Hence, it is often necessary to include forensic meteorologists as part of the

evaluation of historical meteorological events.

## Common Meteorological Databases

Historic meteorological data can be obtained from numerous weather data sources. Two of the most commonly used data sources in forensic engineering include:

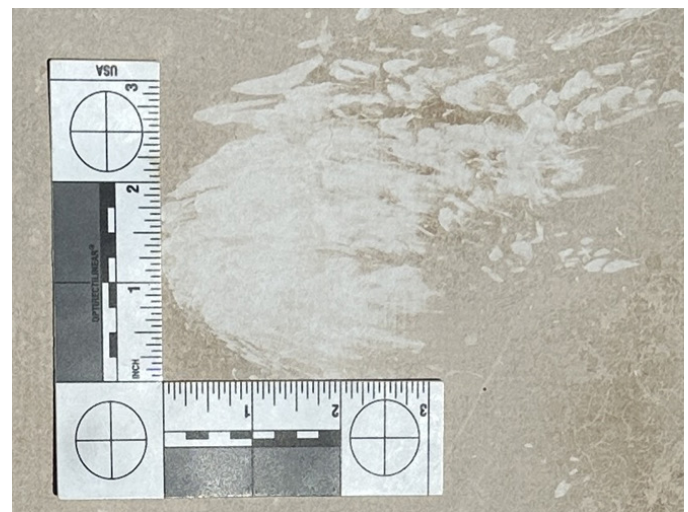


**Figure 1**

View of a hail spatter mark, Dallas, Texas (spring 2023).

the databases maintained by National Oceanographic Atmospheric Administration's (NOAA) National Weather Service (NWS); the Storm Prediction Center Local Storm Reports (SPC-LSR)<sup>1</sup>; and the National Centers for Environmental Information Storm Events Database (NCEI-SED)<sup>2</sup>.

The Storm Prediction Center Frequently Asked Questions (FAQ) page states<sup>3</sup>:

*“The listings on the SPC Storm Reports page are automatically collected from thunderstorm-related local storm reports (LSRs) sent out by the local NWS offices. If there was no LSR for an event, or it arrived more than 10 days after the event, the report won't show up here. Our storm reports list is preliminary and likely does not contain all severe weather reports for any particular event. Storm surveys may be needed to confirm tornadoes, EF scale, find out if damage really was from a tornado or other thunderstorm winds, etc.”*

According to the NCEI-SED Storm Data Frequently Asked Questions (FAQ) page<sup>4</sup>:

*“NCEI receives Storm Data from the National Weather Service. The National Weather Service receives their information from a variety of sources, which include but are not limited to: county, state and federal emergency management officials, local law enforcement officials, skywarn spotters, NWS damage surveys, newspaper clipping services, the insurance industry and the general public, among others.”*

Forensic engineers should note that the data in both databases are dependent upon receiving storm reports from human observations. Therefore, they may not receive data for all storm events. The lack of a report in either of these databases may reflect that a report was not received, but may not indicate that an event did not occur.

### **Purpose and Limitations of NWS Reports**

When working with any data set, it is important to understand the original purpose or context for why the data was gathered. While many data sources can be used by forensic engineers, they may not have been originally created to specifically support this purpose. Inherently, this will impose limitations in how the data can be applied to support ancillary uses, such as those involving forensic

engineering analyses. This holds true for the SPC-LSR and NCEI-SED databases. They were created for the National Weather Service's purposes (and to support research), and do not directly support the needs of forensic engineering or forensic meteorology evaluations.

*“The Storm Events Database contains the records used to create the official NOAA Storm Data publication, documenting:*

- 1. The occurrence of storms and other significant weather phenomena having sufficient intensity to cause loss of life, injuries, significant property damage, and/or disruption to commerce;*
- 2. Rare, unusual, weather phenomena that generate media attention, such as snow flurries in South Florida or the San Diego coastal area; and*
- 3. Other significant meteorological events, such as record maximum or minimum temperatures or precipitation that occur in connection with another event.”<sup>5</sup>*

Given such a broad application in what and how the data is collected and used, NOAA offers several disclaimers and limitations.

From the “Storm Data FAQ Page,” NOAA provides the following disclaimer<sup>6</sup>:

*“Some information appearing in Storm Data may be provided by or gathered from sources outside the National Weather Service (NWS), such as the media, law enforcement and/or other government agencies, private companies, individuals, etc. An effort is made to use the best available information but because of time and resource constraints, information from these sources may be unverified by the NWS. **Therefore, when using information from Storm Data, customers should be cautious as the NWS does not guarantee the accuracy or validity of the information.** Further, when it is apparent information appearing in Storm Data originated from a source outside the NWS (frequently credit is provided), Storm Data customers requiring additional information should contact that source directly.”*

Forensic engineers should pay particular attention to the bolded sentence shown in the previous quote. The SPC-LSR and NCEI-SED databases are created for the National Weather Services and do not necessarily correspond to the needs of forensic engineering or forensic meteorology evaluations. As such, it is advisable for SPC-LSR and NCEI-SED databases to be used as part of a broader forensic assessment toolset — not as a stand-alone data source in an evaluation.

### **Known Concerns with Reported Storm Dates**

Considering the limitations of the NWS mentioned earlier, the following sections highlight the various challenges associated with using and relying on the data in the SPC-LSR and NCEI-SED databases.

#### *A. Day/Time Referencing*

Weather data can be reported using different time zone references. For instance, some data sets use the local date and time for the location where the event occurred, while others use Coordinated Universal Time (UTC) for their reporting.

The SPC-LSR database is one such database that records data in UTC. Additionally, the SPC-LSR database does not follow the standard midnight to midnight day. Instead, the SPC states:

*“The Storm Reports page is organized based on reports received from 1200 UTC to 1159 UTC the next day. For example, storm report page for 20150430 covers reports from 20150430 at 1200 UTC to 20150501 at 1159 UTC.”*

Because of the time and date differences contained within this database, particular care must be taken when evaluating its contents relative to local time and the time formatting of other data sources.

When reviewing forensic meteorology data, it’s crucial to check the time references used to ensure events are viewed in the correct context. It may be necessary to adjust the recorded data to align with a specific time zone.

#### *B. Accuracies in Storm Event Reporting*

As weather-related claims commonly rely on human reporting, the reported date of occurrence may not reflect the actual date of the storm event. For example, this can happen with events that occur in the evening and then are not reported until the following day — or when a storm event occurs after the close of normal business hours on

Friday and is not reported until the following Monday. In some cases, large-scale damaging events (especially those associated with large electrical power outages such as hurricanes, ice storms, and broad-range thunderstorms/damaging winds) have been reported days to weeks after the specific event.

Given these common types of delays in reporting, a forensic engineer must be cautious with this data and verify that reporting times and actual event times are clearly understood. This can be done by verifying the date of any storm-related event with the property owner, owner’s representative, or others who have any direct knowledge of the occurrence.

Caution should be exercised when considering an identified date or period of occurrence, as a nearby memorable storm event date may be inaccurately referenced by involved parties. Therefore, it is recommended that the engineer engage with the property owner, witnesses, or other involved parties to develop an understanding of the reported meteorological conditions. This will help provide further context and improve the accuracy of the timing and the potential conditions associated with the weather event.

For some events, such as wind and hail associated with a thunderstorm, the specific date(s) of the occurrence may be ambiguous. In these situations, individuals may report the date and time using generalities such as “late April,” “the big storm earlier this year,” or other similar sentiments. When investigating circumstances where the storm dates are ambiguous, the forensic engineer should review weather data beyond the reported date of occurrence.

Extending the data review period at least 30 days before and after the reported date of occurrence will reduce the possibility of missing a potential wind or hail event that could have contributed to the conditions observed as part of the assessment. In some cases, it may be necessary to review meteorological data over longer periods of time (e.g., months or years), depending on the specific situation.

#### *C. Reliability of Storm Reporting*

The challenge when relying on the NWS for forensic purposes is that it lacks consistent, reliable event reporting. In particular, there may be a lack of storm reporting in non-residential areas, areas of low population density (rural areas), or during hours of darkness. In some cases, the authors have observed that storm conditions beyond the leading edge of a storm event have not been documented

or recorded in the NWS systems. Therefore, the forensic engineer should take caution as the storm events may not be fully recorded or validated depending on the situation and location.

Scott Blair et al in their paper, “High-Resolution Hail Observations: Implications for NWS Warning Operations,” observes<sup>7</sup>:

*“Unfortunately, there remains a high degree of uncertainty that the hail reports obtained during NWS warning verification efforts are representative of the true hailfall of a given storm. Nocturnal severe weather may lead to a reduction in reporting efficiency due to limited visibility for identifying large stones, and the majority of the public may be asleep (Ashley et al. 2008). Regardless of the time of day, the number of hail reports may fluctuate based on a storm’s path over rural versus urban areas (Dobur 2005; Cecil 2009). Even with storms over densely populated regions, large hailstones may go unidentified or unreported (Blair and Leighton 2012). Available NWS resources dedicated to seeking out ground-truth information may vary from event to event, and also between differing NWS offices’ emphasis on aggressive report collection verification (Doswell et al. 2005). Human reporting error in the form of exaggeration or underestimation of hail sizes, along with the potential for incorrect locations and times, can introduce further uncertainty in the quality and representativeness of these hail reports (Amburn and Wolf 1997; Baumgardt 2011).”*

This paper continues to argue that an undetermined amount of uncertainty must therefore be accepted in order to use the hail data in support of post-event warning verification, training, research and development when conducting risk assessments. It also cites that verification of NWS warnings in which they had forecasted a maximum hail size had been largely “unexplored.”

#### *D. Single-Point or Peak Point Reporting of Meteorological Data*

Data reported in the SPC-LSR and NCEI-SED provide single points of data relative to the largest reported hail or peak wind gusts. This is known as “single-point” or “peak-point” data. Due to its specific nature, this data lacks additional information that could be crucial for

identifying other environmental conditions that may have contributed to or caused the damage. Such ancillary information is necessary to provide overall context to the data.

For example, when conducting:

- Hail evaluations — the duration of the hail event as well as the velocity and directionality of winds associated with the thunderstorm are not included in the databases.
- Wind-related damage evaluations — single-point reports of wind events, such as those associated with a thunderstorm, do not indicate the directionality of the winds (or if the winds occurred over extended periods of time). Note: It is important to remember that fatigue failures due to prolonged lower velocity wind events can be as damaging as wind events that exceed initial design velocities over a shorter duration of time.

### **Reported Data Limitations: Case Studies**

The following four case studies demonstrate limitations related to the use of SPC-LSR and NCEI-SED data. The first example relates to variations in data between different NWS sources and the start/stop points indicated in the NCEI SED. The second and third case studies relate to variations among the indicated coordinates (assumed for a locale or rounded off) and stated locations within the report text.

#### *A. Software Used to Support the Analyses*

The software used in the following analyses includes ArcGIS Pro mapping software and for case study 4, GR2-Analyst (Gibson Ridge Level II Analyst) storm analysis software.

ArcGIS Pro is a mapping software that can be used to perform spatial and data analyses for scientific purposes. In the following examples, ArcGIS Pro was used to perform a spatial analysis of storm reports in relation to areas that experienced thunderstorms capable of producing storm damage. Storm reports and tornado damage survey tracks from the NWS databases were loaded into ArcGIS Pro and compared spatially to areas of reported storm damage.

GR2-Analyst is an advanced radar analytical application that is often used for post-storm analysis and reconstruction. GR2-Analyst allows analysis of traditional and dual-polarization radar data, cross-sectional 3D storm

analysis, and high-resolution derived radar products. In the following case studies, GR2-Analyst was used to reconstruct thunderstorms by analyzing radar data to obtain information on storm characteristics for the purpose of diagnosing hail or a tornado within a storm. The software was also used to create 3D-storm images in order to further diagnose the presence of hail, a tornado, or other forms of severe weather within a thunderstorm.

*B. Case Study 1: Moore, Oklahoma, Tornado (May 20, 2013)*

On the afternoon of May 20, 2013, a large and powerful tornado formed in McLain County, Oklahoma. The tornado continued northeast, entering Cleveland County, Oklahoma, and the City of Moore, finally ending at Lake Stanley Draper just south of Oklahoma City. **Figure 2** highlights the NCEI-SED straight line path for this event. It shows the beginning (“B”) and ending (“E”) points of the tornado with a straight line connecting the two ends. Note that NCEI-SED does provide a caution on the map citing that the “actual tornado path may differ from the straight line”<sup>8</sup>.

**Figure 3** is the tornado path obtained from the NWS’s “The Tornado Outbreak of May 20, 2013” website<sup>9</sup>. The dashed red line represents a linear path between the

reported start and stop points of the tornado as indicated by NCEI-SED in **Figure 2**. However, the tornado contour lines from NWS show that it is evident the tornado damage path lies predominantly north of the linear, red, NCEI-SED line. **Figure 4** includes the portion of the tornado path in McLain County, Oklahoma.

While obvious in this example, it is a reminder that forensic engineers should take caution when reviewing and relying on this type of information. Any representation of a natural event by a straight line or by standard geometric shapes (e.g., circles, squares, triangles, etc.) is likely used as a rough estimation to demonstrate a trend. The engineer is advised when using such data to only rely on it as an approximation of where an event may have happened.

Forensic engineers also need to be aware that NCEI-SED data is reported separately by county. NCEI-SED lists data under the headings of “Begin Location,” “End Location,” “Begin Lat/Long,” and “End Lat/Long” — and those points may be the edge of a county line, not necessarily the actual start and end points of the tornado’s path. Therefore, when a tornado crosses county lines, there will be reports for each county. Under the “Storm Data FAQ” Page subheading “How are Tornadoes Counted,” it states:

**Event Map:**

Note: The tornado track is approximate based on the beginning (B) and ending (E) locations. The actual tornado path may differ from a straight line.

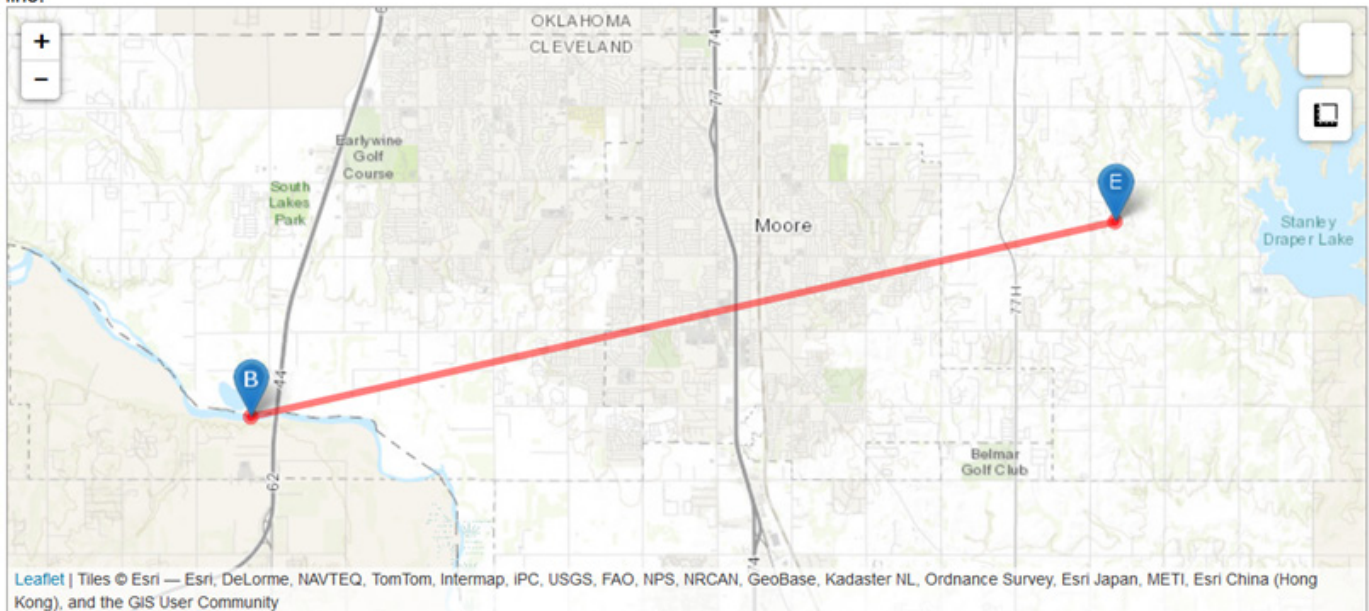


**Figure 2**

NCEI-SED path image for the Moore Tornado from its event details web page. The red line represents a linear interpretation of the tornado path between the NCEI-SED beginning and end points.



**Figure 3**

NCEI-SED path image (red dashed line) overlaid on the NWS storm path. (Image Source: NWS storm path from National Weather Service, 2013). “The Tornado Outbreak of May 20, 2013” [ESRI Map], <https://www.weather.gov/ou/evnts-20130520>).



**Figure 4**

Moore Tornado: Initial tornado touchdown comparison points using Google Earth Pro®. There is an approximate distance discrepancy of 1.8 miles between the two points.

*“Tornadoes may contain multiple segments. A tornado that crosses a county line or state line is considered a separate segment. Also, a tornado that lifts off the ground for less than 4 minutes or 2 miles is considered a separate tornado segment. If the tornado lifts off the ground for greater than 4 minutes or 2 miles, it is considered a separate tornado. Tornadoes reported in Storm Data and the Storm Events Database are in segments.”<sup>10</sup>*

Additionally, National Weather Service Instruction 10-1605, paragraph 47.12.1, guides storm data preparers to enter tornadoes that cross county/parish lines as segments with one segment per county/parish, and not to segment a tornado within a county/parish<sup>11</sup>.

The tornado data contained within the NCEI-SED can be used to provide a basic understanding of a tornado’s path and the areas potentially impacted by the event. The determination of the conditions at the site will require further review of additional available meteorological data sources and an examination of the on-site conditions noted at the specific assessment location.

*C. Case Study 2: Norman, Oklahoma, Hailstorm (April 28, 2021)*

On April 28, 2021, a hailstorm occurred in Norman, Oklahoma. This hail event was recorded as having produced hailstones of 3 inches or larger in diameter. During this storm event, an individual was reported as experiencing a head injury from hail at a restaurant located at “Robinson and I-35.” The coordinates provided in the SPC-LSR were given to two decimal places<sup>12</sup> (Figure 5). When the coordinates were reviewed using three decimal places on Google Earth Pro® for the restaurant location and the SPC-LSR provided location, there is a .32-mile distance disparity. Figure 5 cites the incident location by indicating

0155	100	4 S HELOTES	BEXAR	TX	2952 9869	(EWX)
0155	275	3 WNW NORMAN	CLEVELAND	OK	3523 9749	*** 1 INJ *** REPORTED HEAD INJURY AT THE BRAUMS AT ROBINSON AND I-35 FROM HAIL. (OUN)
0155	150	4 NW NORMAN	CLEVELAND	OK	3526 9750	(OUN)

Figure 5

April 28, 2021, SPC-LSR location (red circle) of reported head injury incident in Norman, Oklahoma.

the nearby cross streets; however, **Figure 6** demonstrates the difference between the actual location of the event and the truncated coordinates provided in the SPC-LSR report. This example offers another cautionary consideration when relying on SPC-LSR data for forensic purposes.

*D. Case Study 3: Tulsa, Oklahoma, Hailstorm (April 4, 2017)*

An April 4, 2017 hailstorm event provides another example of SPC-LSR issues related to the published coordinates for storm events. In this example, a hail event was reported in Tulsa, Oklahoma. **Figure 7** is a section of the SPC-LSR data obtained from the SPC-LSR for this event<sup>13</sup>. In this data set, there are two references to 1-inch hail at “61st and Memorial.” However, notice that the coordinates

for these two locations are different. The described location was between approximately 2.5 miles and 4.2 miles south-east of the indicated coordinates (**Figure 8**).

This same SPC-LSR report included multiple listings using the same coordinates, but, again, the specific address locations deviated from these coordinates (**Figure 9**). In this case, the described locations varied from approximately 4.6 miles to the south to 4.2 miles to the southeast and 1.6 miles to the northeast from the coordinate location (**Figure 10**).

Under the “Storm Data FAQ” Page subheading “How are the latitude and longitudes determined?” it states<sup>14</sup>:

*“Storm Data information is entered into the database in two ways:*

*As a distance in miles and a direction on 16-point compass scale from a known location, usually a town or city. Example: 4.5 miles ESE Atlanta. The NWS uses a database of over 106,000 cities and towns including their latitudes and longitudes. Using an algorithm, the location 4.5 miles ESE of Atlanta can be derived from the known latitude and longitude of Atlanta. These latitude and longitude pairs are generated by the NWS and populated into the database. The latitude and longitude are in*



Figure 6

Google Earth Pro® image highlighting the coordinate differences of approximately .32 miles between SPC-LSR referenced locations.

2202	175	BRISTOW	CREEK	OK	3583 9639	(TSA)
2205	175	BROKEN ARROW	TULSA	OK	3605 9579	71ST AND MEMORIAL (TSA)
2205	175	TULSA	TULSA	OK	3613 9592	65TH AND MEMORIAL (TSA)
2210	100	TULSA	TULSA	OK	3613 9592	41ST AND GARNETT (TSA)
2211	100	TULSA	TULSA	OK	3613 9592	61ST AND MEMORIAL (TSA)
2224	275	TIANAH	ROGERS	OK	3626 9556	RELAYED BY KOTV ... PICTURE ACCOMPANIED REPORT (TSA)
2232	100	<b>Different coordinates</b>			3562 9596	(TSA)
2235	100	RED ROCK	NOBLE	OK	3646 9718	(OUN)
2236	100	MUSKOGEE	MUSKOGEE	OK	3575 9537	(TSA)
2236	100	3 W TULSA	TULSA	OK	3613 9598	49 WEST AND EDISON (TSA)
2238	100	2 SE TULSA	TULSA	OK	3611 9590	61ST AND MEMORIAL (TSA)

Figure 7

SPC-LSR data for the April 4, 2017 hailstorm in Tulsa, Oklahoma.

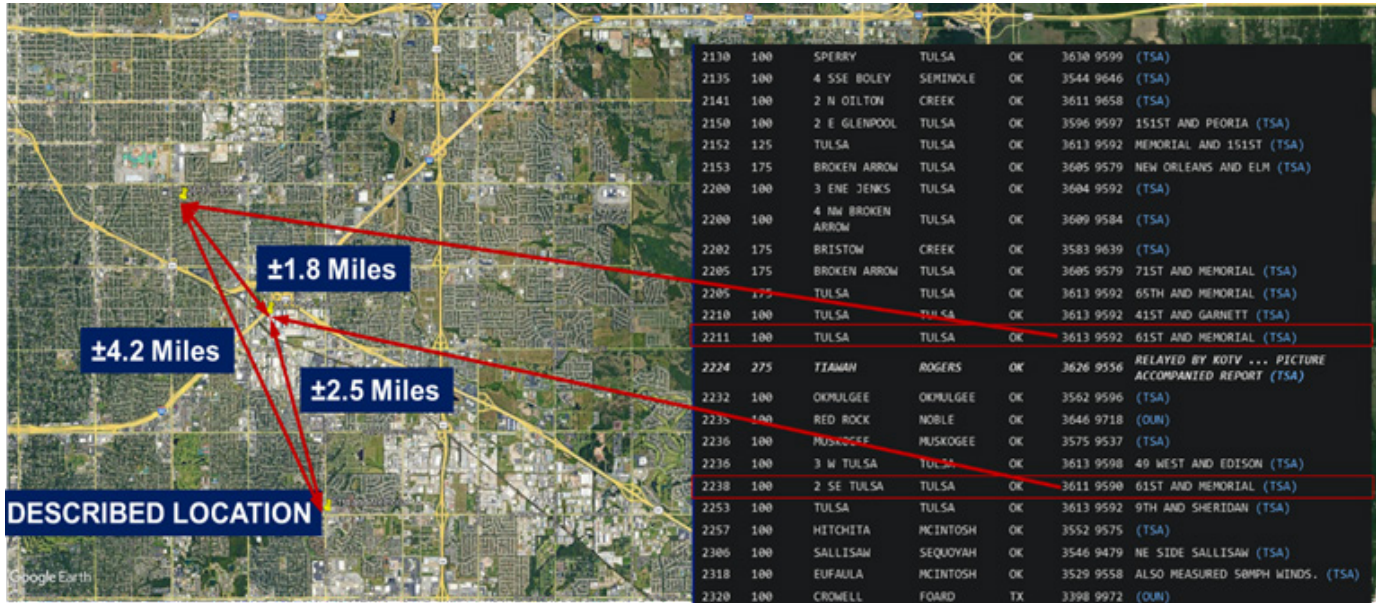


Figure 8

Hailstorm georeferenced data's location vs. the identified address location. (SPC-LSR data from Fig. 7 shown on the right side in black.)

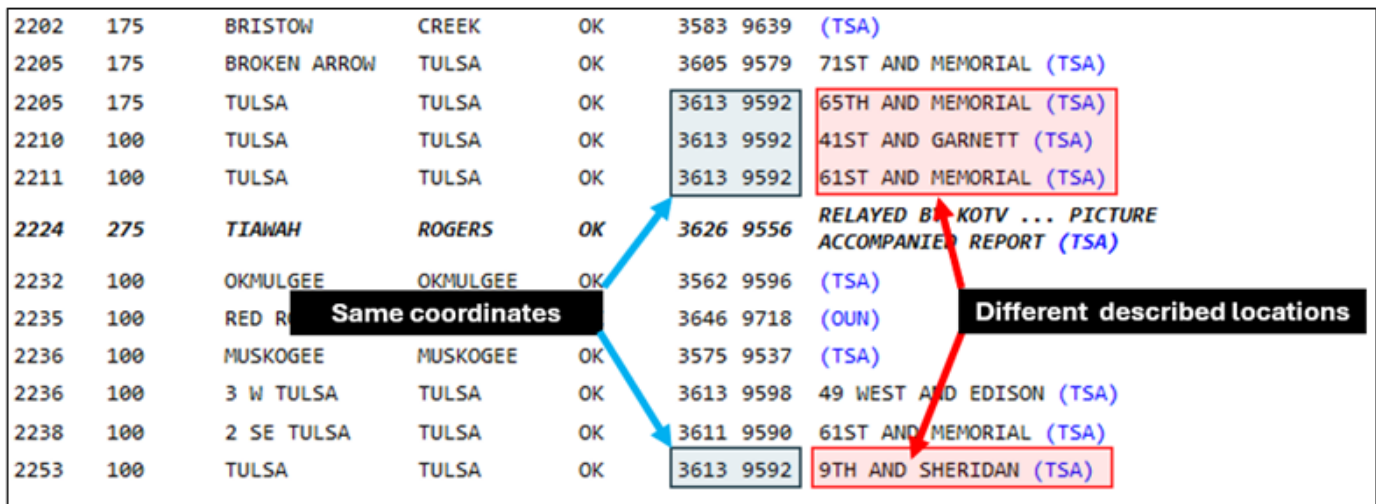


Figure 9

SPC-LSR data for Tulsa, Oklahoma April 4, 2017 event.



Figure 10

SPC-LSR Data for Tulsa, Oklahoma April 4, 2017 event highlighted on Google Earth Pro® generated map.

*Decimal Degrees format.*

*Or*

*By entering the latitude and longitude directly. The range, azimuth and nearest city/town are calculated from the latitude.*

Again, these discrepancies highlight the need to use caution with the data provided in the SPC-LSR. The coordinates indicated may reflect conditions relative to a known city reference point that may not represent the location of the weather report. When available, information identifying specific landmarks, cross street locations, or other identifying information should be used to confirm the indicated coordinates. These locations should also be reviewed or

verified against other available meteorological data

**Storm Reporting Reliability**

This final case study demonstrates the limitation of the reporting underlying the storm report data created by the NWS and how using radar data can be used to supplement and validated conditions during a forensic analysis of an event.

*A. Case Study: Southwestern Missouri, Hailstorm (May 4, 2020)*

On May 4th, 2020, a major storm front hit southern Missouri, causing extensive damage. Storm damage reports from the NCEI-SED included overturned semitrailers and power outages. These reports were uploaded into ArcGIS for analysis. The analysis identified a large spatial and temporal gap between the storm reports of approximately 24.28 miles and 40 minutes. Due to the sporadic reporting in this rural area, sparse storm reports are common.

In this example, a location between the two hail reports was identified for further assessment. As shown in **Figure 11**, the sample location was approximately 11.25 miles southeast of the first storm report (1.75-inch hail) and approximately 13.09 miles northwest of another report (1.25-inch to 1.5-inch hail). Gaps in weather reports such as these have been used to indicate that no hail event could have occurred as a result of the storm, which caused the two closest hail reports. Further assessment of this temporal and geographic gap was assessed through a forensic meteorological review utilizing the review of radar and other weather data entered into GR2-Analyst and ArcGIS.

The hail core within the supercell was impressive at the location where 1.75-inch hail was recorded in the NCEI-SED. High reflectivity greater than 50 dBZ and

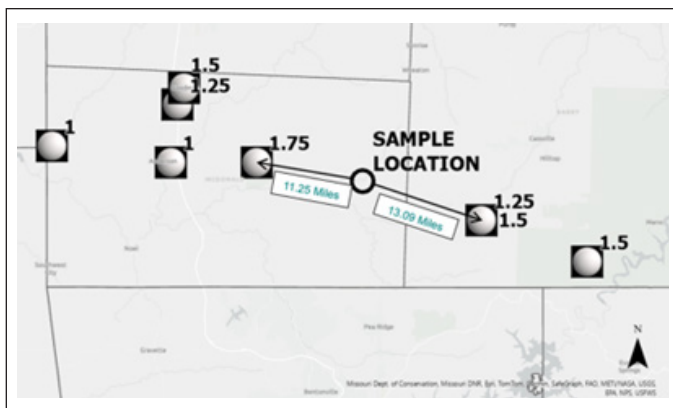


**Figure 11**

Hail reports on May 4, 2020 in southwestern Missouri.

lowered correlation coefficient (CC) values below 0.95 can be seen in conjunction with one another, indicating the presence of hail within the thunderstorm (**Figure 12**). CC values about or below 0.95 co-located with high reflectivity greater than or equal to 50 dBZ is an indication of radar detected objects of increasingly various size and shape — and a strong determinant of falling hail.

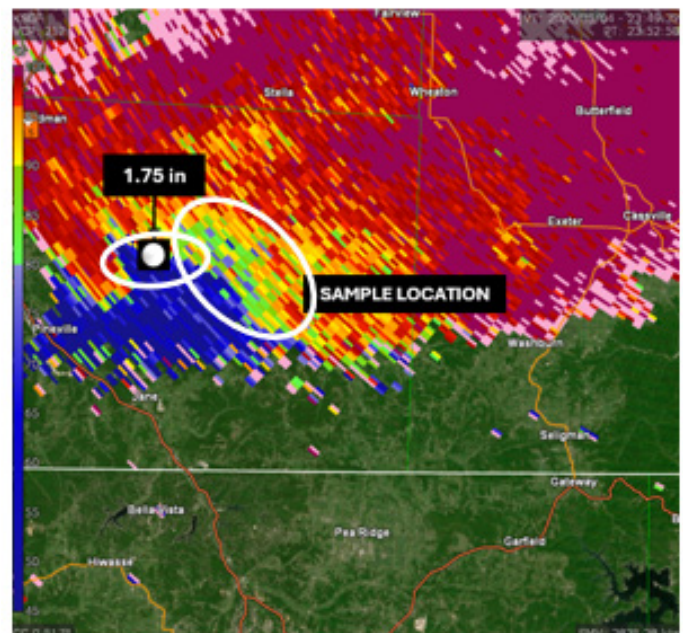
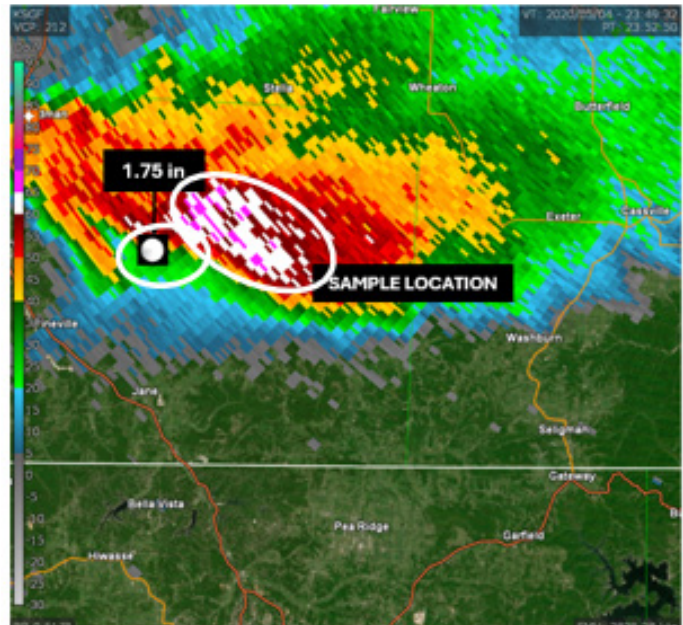


**Figure 12**

Reflectivity (top) and correlation coefficient (bottom) analysis of location where 1.75-inch diameter hail was reported. Regions with high reflectivity and lowered correlation coefficient typical of a hail signature are circled in white in this and following figures.

(6:52 p.m. CDT May 4, 2020)

As the storm approached the sample location, the supercell continued to cycle, minorly strengthening for a few scans and slightly weakening for a few scans. Regardless of the cyclical nature of the supercell, the high reflectivity and lowered CC that consisted of the thunderstorm's hail signature remained present within the storm as it moved through the spatial and temporal gap between storm reports. At this point, it was moving through a more rural portion of southwest Missouri, which is likely why there were no storm reports in this location. The hail within the

storm began to move over the sample location at 6:54 p.m. (Figure 13).

At 6:56 p.m. CDT, the hail core continued its way over the subject location (Figure 14). A 3D scan was used to show the distribution of hail within the storm. As can be seen in Figure 15, a large hail core extending up to approximately 30,000 feet was present within this supercell as it continued to impact the subject location. These values of high reflectivity at the noted heights within the storm signify that the updraft is suspending hail within the

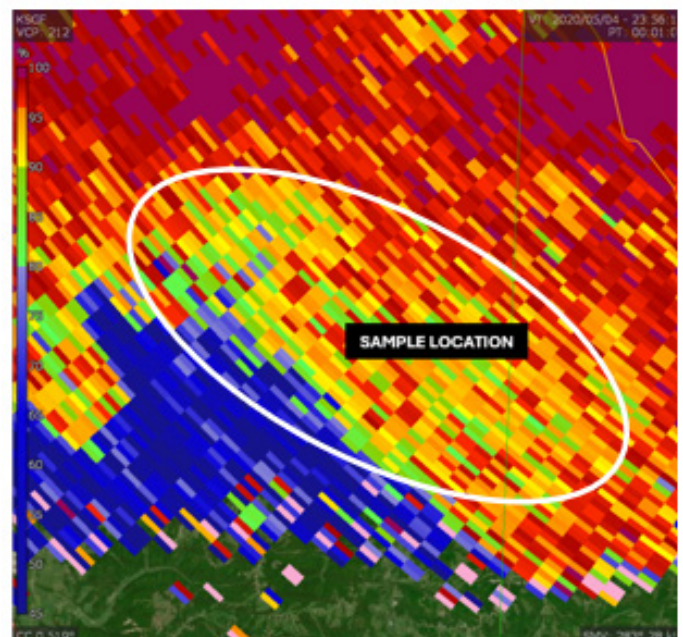
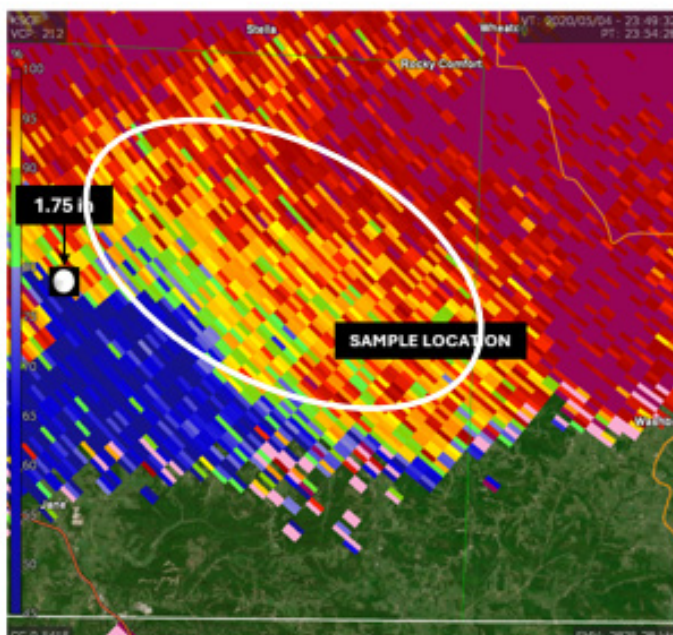
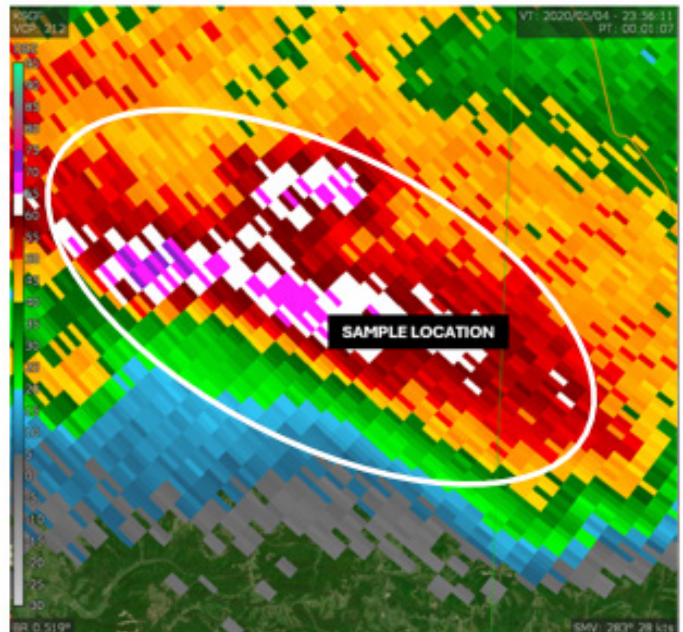
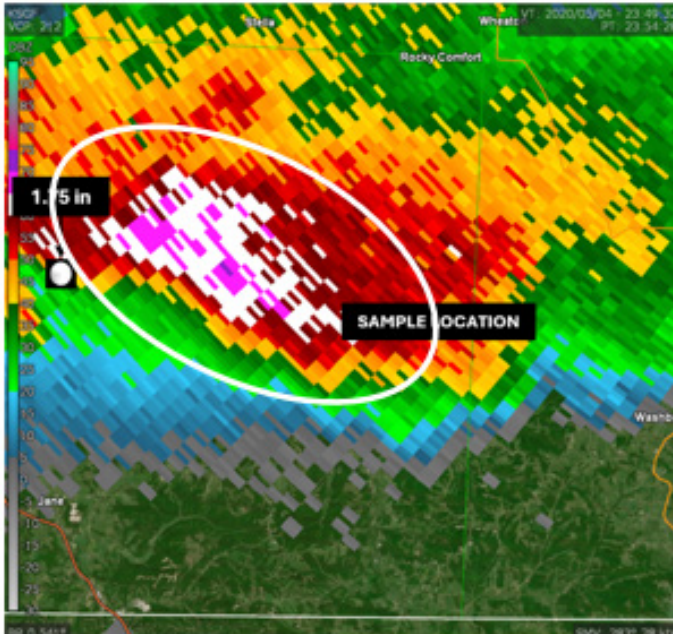
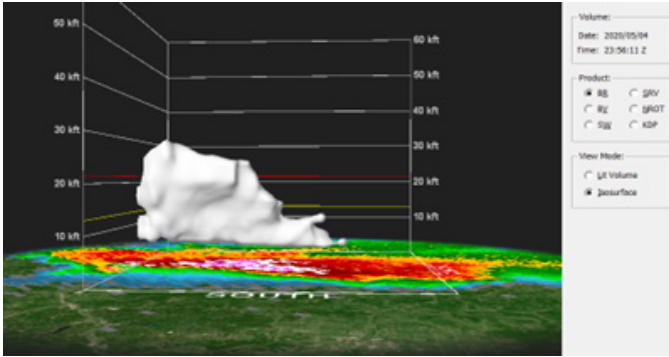


Figure 13

Reflectivity and correlation coefficient of the sample location at 6:54 p.m. CDT.

Figure 14

Reflectivity and correlation coefficient recordings at 6:56 p.m. CDT.



**Figure 15**

3D scan demonstrating hail core size and location (plotted using 60-dBZ reflectivity values at 6:56 p.m. CDT).

part of the thunderstorm most favorable for hail growth, between the  $-10^{\circ}\text{C}$  and  $-30^{\circ}\text{C}$  temperature layers. In the 3D scan of the thunderstorm, GR2-Analyst plots the  $0^{\circ}\text{C}$  temperature level in yellow and  $-20^{\circ}\text{C}$  temperature level in red for reference. Hail massive enough to no longer be suspended by the updraft then fell downward into the thunderstorm’s downdraft and to the surface — where hail would be observable.

Hail was still impacting the subject location at 7:14 p.m. CDT but was finally beginning to depart the sample location. At this point, hail had been present at the subject location for approximately 20 minutes. The presence of hail was still indicated by high reflectivity and correlation coefficients (**Figure 16**).

As the storm began to move over the area of the secondary storm report, radar readings continued to indicate the hail potential within the storm (**Figure 17**). However, for this location, the hail indicators were less impressive than they were when they moved over the sample location — this is noted by a decreased reflectivity maximum and slightly less defined region of co-located lowered CC values.

This case study highlights the limitations of simply relying solely on storm reports. Since the general public voluntarily contributes storm reports to the NWS — and hazardous weather is often not reported within rural communities due to the lower number of housing and residents — information documenting actual conditions can be omitted or overlooked. In this case study, the meteorological interpretation of radar data allowed the tracking of this intense supercell and highlighted how large hail was probable along the majority of this 24-mile gap identified between storm reports.

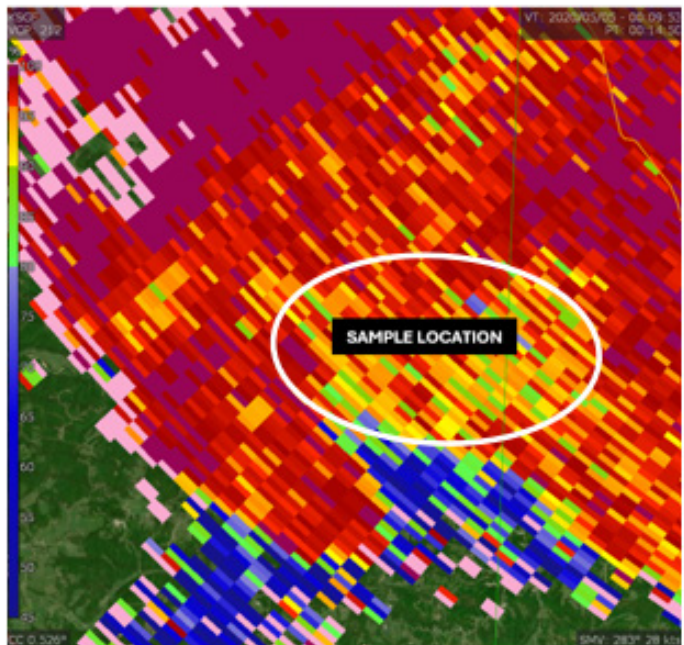
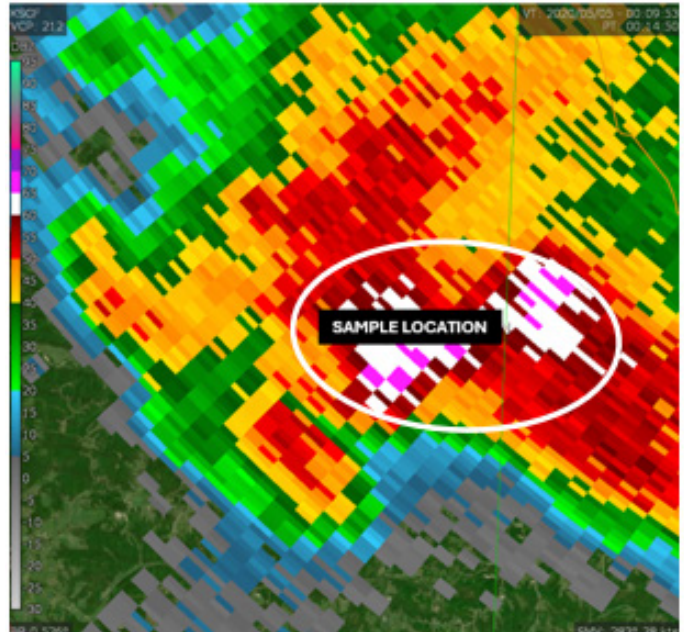


**Figure 16**

Reflectivity and correlation coefficient recordings indicate hail at the sample location at 7:14 p.m. CDT.

**Layering of Meteorological Data Sources**

A concept commonly used in risk management is the “Swiss Cheese Model.” In this approach, individual points of failure are represented as holes within individual cheese slices. The individual cheese slices represent processes or physical means of preventing a failure. By layering multiple cheese slices, the potential for a failure to occur (i.e., pass through all holes in a line) is reduced. From the perspective of reviewing meteorological data, the layers

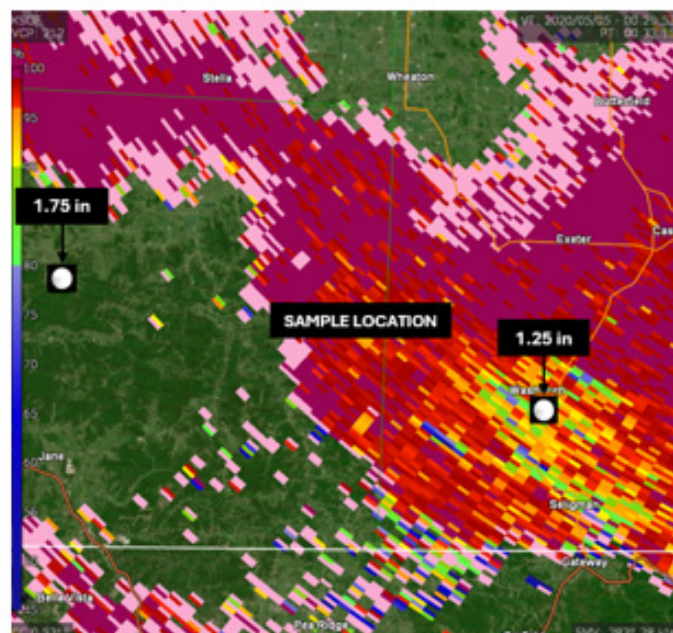
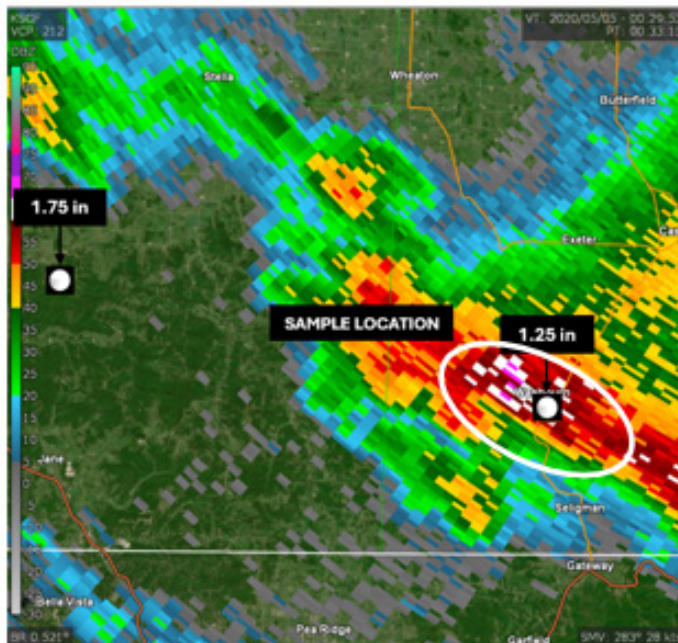


**Figure 17**

Reflectivity and correlation coefficient reading for secondary location (7:33 p.m. CDT).

of cheese in the model represent the review of multiple data sets. A failure (a pass through all layers) would be a damaging storm event that was not identified for further assessment.

This analysis involves contributions from both forensic engineers and the forensic meteorologists. The engineer examines the conditions at the site, while the meteorologist reviews a wide array of weather data. This data

can include broader weather discussions, NWS watches and warnings, radar information, and storm reports (such as those in the SPC-LSR, the NCEI-SED, and others). The goal is to provide enough layers of information to understand what was possible and probable in the atmosphere at the time of the reported weather event. By reviewing the full range of weather information available for a specific event or series of events, the forensic engineer can better understand the probable circumstances that led to the observed conditions.

## Conclusions

Based on examples in this paper and previous references, the forensic engineering and forensic meteorology communities are well aware of the accuracy and reliability issues with the SPC-LSR and NCEI-SED. Whether through database limitations, differences between databases, insufficient data reporting due to location or time of day, single-point or peak-point reporting — or even through human error — flaws in these data sources remain a major concern that can lead to a weather event's occurrence being denied due to insufficient or missing data. Therefore, relying solely on SPC-LSR or NCEI-SED data is not sufficient for establishing or denying the occurrence of weather conditions in a forensic engineering investigation.

Forensic engineers and forensic meteorologists, when working together, offer a synergistic expertise. The collaboration between forensic engineers and forensic meteorologists provides a comprehensive approach to investigating weather-related damage that can overcome the limitations that each field would face alone.

## References

1. Storm Prediction Center, "Storm Prediction Center Severe weather summaries." [Online]. Available: <https://www.spc.noaa.gov/climo/online/>. [Accessed: Aug. 28, 2024].
2. National Oceanic and Atmospheric Administration, "Storm Events Database | National Centers for Environmental Information." [Online]. Available: <https://www.ncdc.noaa.gov/stormevents/>. [Accessed: Sep. 8, 2024].
3. National Oceanic and Atmospheric Administration, "Storm Prediction Center Frequently Asked Questions (FAQ): Section 6.1." [Online]. Available: <https://www.spc.noaa.gov/faq/>. [Accessed: Sep. 8, 2024].

4. National Oceanic and Atmospheric Administration, "Storm Events Database - FAQ | National Centers for Environmental Information." [Online]. Available: <https://www.ncdc.noaa.gov/stormevents/faq.jsp>. [Accessed: Sep. 8, 2024].
5. National Oceanic and Atmospheric Administration, "Storm Events Database | National Centers for Environmental Information." [Online]. Available: <https://www.ncdc.noaa.gov/stormevents/>. [Accessed: Sep. 8, 2024].
6. National Oceanic and Atmospheric Administration, "Storm Events Database - FAQ | National Centers for Environmental Information." [Online]. Available: <https://www.ncdc.noaa.gov/stormevents/faq.jsp>. [Accessed: Sep. 8, 2024].
7. S. F. Blair et al., "High-resolution hail observations: Implications for NWS warning operations," *Weather and Forecasting*, vol. 32, no. 3, pp. 1101–1119, May 2017, doi: 10.1175/WAF-D-16-0203.1.
8. National Oceanic and Atmospheric Administration, "Storm Events Database - Event Details | National Centers for Environmental Information: Event Map." [Online]. Available: <https://www.ncdc.noaa.gov/stormevents/eventdetails.jsp?id=451572>. [Accessed: Sep. 8, 2024].
9. National Oceanic and Atmospheric Administration's National Weather Service, "The Tornado Outbreak of May 20, 2013." [Online]. Available: <https://www.weather.gov/oun/events-20130520>. [Accessed: Sep. 8, 2024].
10. National Oceanic and Atmospheric Administration, "Storm Events Database - FAQ | National Centers for Environmental Information." [Online]. Available: <https://www.ncdc.noaa.gov/stormevents/faq.jsp>. [Accessed: Sep. 8, 2024].
11. National Oceanic and Atmospheric Administration, National Weather Service Instruction 10-1605: Storm Data Preparation, vol. 10–1605, 2021. [Online]. Available: <https://www.weather.gov/media/directives/010>. [Accessed: Sep. 8, 2024].
12. National Oceanic and Atmospheric Administration, "SPC Severe weather event review for Wednesday April 28, 2021: Hail Reports." [Online]. Available: <https://www.spc.noaa.gov/exper/archive/event.php?date=20210428>. [Accessed: Sep. 8, 2024].
13. National Oceanic and Atmospheric Administration, "SPC Severe weather event review for Tuesday April 04, 2017: Hail Reports." [Online]. Available: <https://www.spc.noaa.gov/exper/archive/event.php?date=20170404>. [Accessed: Sep. 8, 2024].
14. National Oceanic and Atmospheric Administration, "Storm Events Database - FAQ | National Centers for Environmental Information." [Online]. Available: <https://www.ncdc.noaa.gov/stormevents/faq.jsp>. [Accessed: Sep. 8, 2024].